This dissertation has been microfilmed exactly as received

65–10,797

EL–RIFAI, Mustafa, 1934–
DISPERSION AND TRANSPORT IN TURBULENT PIPE FLOW.

The University of Oklahoma, Ph.D., 1965
Engineering, chemical

University Microfilms, Inc., Ann Arbor, Michigan

Downloaded from SHAREOK. Persistent Handle URL: https://hdl.handle.net/11244/1905

THE UNIVERSITY OF OKLAHOMA

GRADUATE COLLEGE

DISPERSION AND TRANSPORT IN TURBULENT PIPE FLOW

A DISSERTATION

SUBMITTED TO THE GRADUATE FACULTY

in partial fulfillment of the requirements for the

degree of

DOCTOR OF PHILOSOPHY

BY

MUSTAFA EL-RIFAI

Norman, Oklahoma

1965

DISPERSION AND TRANSPORT IN TURBULENT PIPE FLOW

APPROVED BY

C. M. Sliepcevich

A. J. Weinheimer

Hsing-Ta Ho

DISSERTATION COMMITTEE

ACKNOWLEDGEMENTS

This work is dedicated to my father for many personal and permanent sacrifices. His ideals and early teachings were motivating and inspiring.

I am grateful to Professor Jon H. Olson, University of Delaware, for his many contributions to this work. Dr. Olson helped me refine, elucidate and shape many of the ideas presented here and was most generous with his time in frequent inspiring discussions.

Thanks are also due to John A. Beutler, Jr., DuPont's Engineering Department, for making it possible to use the I.B.M. 7070 computer. The material presented in Chapter V would not have been possible without this help.

The author wishes to thank his committee for their encouragement. Thanks are due to Professor C. M. Sliepcevich, Committee Chairman, for his advice and guidance throughout my graduate work at Oklahoma University, Professor M. McGuire for reviewing the thesis, Professor R. L. Huntington for his kindness and encouragement. Professors F. M. Townsend and A. J. Weinheimer were very helpful in many ways at various stages of my graduate study.

Dr. William Viavant helped me understand the Statistical Theory of Turbulence. Drs. H. E. Affsprung and J. D. Palmer made many valuable suggestions on the

construction of the experimental set-up of Appendix-B.

This work was initiated at The University of Oklahoma; Dr. J. E. Powers was then its research director. It was completed under the direction of Dr. Jon H. Olson while the author was employed at DuPont's Experimental Station (Wilmington). Thanks are due to the Management of the Pioneering Research Division, particularly, Drs. W. E. Jordan and R. E. Albert for their tolerance and generosity. None of this work is proprietary of DuPont or connected with the author's duties during that period.

The Moncrief Foundation and Continental Oil Company provided fellowships for the author during part of his graduate study.

TABLE OF CONTENTS

	Page
LIST OF TABLES	viii
LIST OF ILLUSTRATIONS	ix
Chapter	
I. INTRODUCTION	1
II. EDDY DIFFUSIVITY AND EDDY VISCOSITY IN THE TURBULENT CORE	7
Problem Review	7
Eddy Diffusivity	7
Eddy Diffusivity Equations	10
Analysis and Treatment of Data	12
Eddy Diffusion Data	12
A Generalized Eddy Diffusivity Correlation	14
Empirical Expression of the Mixing Length	16
Peclet Number	26
Contribution of Molecular Diffusion to Eddy Diffusion	29
Eddy Viscosity in the Core	31
Turbulent Schmidt and Prandtl Numbers over the Core	39
Summary of Conclusions and Results	40

Chapter Page

III. RELATING TURBULENT DIFFUSION IN THE CORE TO EULERIAN TURBULENCE PARAMETERS. 42

Introduction to Turbulence Theory. 42

Review of the Problem. 53

Previous Mixing Length and Turbulent Diffusion Theories. 54

Previous Attempts to relate Eulerian and Lagrangian Statistical Properties . 65

Proposed Theory and Model-Turbulent Diffusion by Microscopic Deformation . . . 68

Physical Considerations 68

Development of Microscopic Deformation Theory by Extension of Prandtl's Theory 73

Comparison of Theory with Experimental Data. 80

Discussion 90

Summary of Conclusions 97

IV. TURBULENT DIFFUSION IN NONISOTROPIC PIPE FLOW. 100

Review of Pertinent Equations. 101

Mean Velocity Distribution. 101

Eddy Viscosity. 105

Point Eddy Diffusivity. 106

A Proposed Equation for Nonisotropic Eddy Diffusivity in the Turbulent Region . 114

V. COMPUTATION OF AXIAL MIXING FROM NONISOTROPIC TURBULENT DIFFUSION AND VELOCITY DISTRIBUTION CORRELATIONS 124

Problem Review 124

Chapter Page

Analysis of Problem. 129

Summary of Velocity and Eddy Diffusivity Distributions. 133

Interpretation and Discussion of Results. 134

Summary of Conclusions 148

VI. CONCLUSIONS. 151

BIBLIOGRAPHY. 154

NOMENCLATURE. 163

APPENDICES

A. DETERMINATION OF TURBULENT DEFORMATION FROM TURBULENCE MEASUREMENTS 169

B. EXPERIMENTAL DETERMINATION OF AXIAL MIXING IN TRANSITION FLOW. 175

Problem Review 175

Apparatus and Procedure. 177

Results. 186

Treatment and Discussion of Experimental Mixing Results. 187

C. EFFECTS OF PULSE THICKNESS AND SLIT THICKNESS ON PULSE RESPONSE IN LAMINAR FLOW 194

Review and Statement of Problem. . . 194

Developments and Computations . . . 196

Derivations 196

Computational Results 203

Discussion of Results. 205

D. TEST OF DEPENDENCE OF TURBULENT DIFFUSIVITY ON MOLECULAR DIFFUSIVITY . . 212

LIST OF TABLES

Table		Page
I.	Eddy Diffusivity Data.	18
II.	Experimental Conditions of Eddy Diffusivity Data of Table I.	20
III.	Data of Sherwood and Woertz.	23
IV.	Average Peclet Number Data	28
V.	Molecular Properties of the Systems of Table I.	34
VI.	Eddy Viscosity Data.	38
VII.	Mean Square Deformations Computed from Turbulence Data.	83
VIII.	Dimensionless Turbulent Deformation versus Eddy Diffusivity Number.	89
IX.	Turbulent Dissipation Data	99
X.	Mean Velocity Distributions.	102
XI.	Eddy Viscosity Distributions	106
XII.	Test for Functional Form of Isotropy Data. . .	117
XIII.	Diffusivity and Velocity Equations Used in Different Programs.	136
XIV.	Summary of Experimental Conditions	189
XV.	Pulse Response Data.	190
XVI.	Values of Parameters Used in Different Computational Runs	204

LIST OF ILLUSTRATIONS

Figure		Page
1.	Correlation of Eddy Diffusivity Data.	17
2.	Correlation of Selected Eddy Diffusivity Data .	21
3.	Eddy Diffusivity Number Calculated from Woertz's Equation and Compared with Present Correlation of Diffusivity Data	22
4.	Peclet Number vs. Reynolds Number	27
5.	A Plot of Reynolds Number vs. Dimensionless Diffusivity, α_c/D^m_{12}	32
6.	A Plot of Turbulent Peclet Number vs. Molecular Schmidt Number.	33
7.	Correlation of Eddy Viscosity Data.	37
8.	Turbulent Velocity Spectrum	43
9.	Longitudinal and Lateral Eulerian Correlation Coefficients.	48
10.	Eulerian Correlation Coefficient and Microscale.	48
11.	Oscilloscope Traces of Two Anemometer Signals Showing Varying Degrees of Correlation.	49
12.	Determination of the Expected Number of Zero Velocities per Second from Sandborn's Spectrum Data	84
13.	Eddy Diffusivity Number vs. Dimensionless Turbulent Deformation	88
14.	Application of Local Isotropy Theory to Turbulent Diffusion	98

Figure Page

15. Comparison of Nunner's Equation with Laufer's Data. 103

16. Ratio of Bulk Average Velocity to Axial Velocity as a Function of Reynolds Number. . . . 104

17. Turbulent Viscosity over the Turbulent Region Calculated from Different Velocity Distributions. 108

18. Turbulent Viscosity Distribution Near the Wall at Re = 5000 109

19. Turbulent Viscosity Distribution Near the Wall at Re = 20000. 110

20. Degree of Isotropy at Different Radial Positions. 116

21. Radial Distribution of Eddy Diffusivity (Equation 4-27). 121

22. Distribution of Radial Eddy Diffusivities and Turbulent Viscosity at Re= 3000 for Water Flow 122

23. Distribution of Radial Eddy Diffusivities and Turbulent Viscosity at Re= 5000 for Water Flow 123

24. Computed Longitudinal Dispersion Number for Water Flow at Re= 3770 139

25. Radial Contributions to Axial Mixing at Re = 3770. 140

26. Radial Contributions to Axial Mixing at Different Reynolds Numbers (Program 506) 141

27. Radial Contributions to Axial Mixing at Different Reynolds Numbers (Program 506) 142

28. Computed Longitudinal Dispersion Number at Different Reynolds Numbers 143

29. Radial Contributions to Axial Mixing - Lin's Equations. 144

Figure Page

30. Variation of $\frac{\partial C}{\partial x}$ with Radial Position. 150

31. Improved Pulse Injection Device 182

32. Piston-Type Pulse Injector. 183

33. Photomultiplier Circuit 184

34. Photometer Calibration Curves 185

35. Pulse Response Data 188

36. Axial Mixing Data for Liquid Flow in Straight Smooth Pipes 193

37. Illustration of Slug Passage through the Slit at Different Stages. 197

38. Computed Pulse Response Diagrams. 206

39. Effect of Pulse Thickness on Pulse Response . . 207

40. Effect of Slit Thickness on Pulse Response. . . 208

DISPERSION AND TRANSPORT IN TURBULENT PIPE FLOW

CHAPTER I

INTRODUCTION

According to the kinetic theory of gases, molecules move in straight lines in an erratic discontinuous motion with sudden changes in direction caused by frictionless collisions that do not involve the dissipation of kinetic energy into heat. The molecular diffusion coefficient can be expressed in terms of the statistical mean velocity and the mean free path. The molecular velocity obeys a certain statistical distribution.

Ever since Reynolds made his well known visual observation of the irregular motion of a colored tracer injected in a turbulent stream, which he called "sinusoidal motion," many scientists have been intrigued by the nature of turbulence and the similarity between turbulent motion and molecular motion. In contrast to the Brownian motion of molecules, turbulent motion is continuous, nonparticulate, and dissipative in nature. That is, the kinetic energy is partly transformed into heat due to the viscosity of the fluid. The parameters of molecular motion and turbulent

motion are widely different in their order of magnitude. For instance, the size of the smallest turbulent eddy is not likely to be less than one millimeter compared to a mean free path of gases under atmospheric conditions of the order of 10^{-4} mm. Turbulent fluctuating velocities are normally less than 30 f.p.s. as opposed to 1500 f.p.s. for the mean molecular velocity of air. For gas flow, the turbulent diffusivity is about twenty times the molecular diffusivity.

The mixing length theory or momentum transfer theory was first proposed by Prandtl. By analogy to molecular diffusion theory, Prandtl expressed the turbulent diffusivity as a product of velocity and a mixing length that corresponds to the mean free path. He then assumed that the mixing length may be expressed as a function of the mean velocity gradient. Prandtl, intuitively, described physically the mixing length in terms of the identity and composition of a fluid particle. Later on, G. I. Taylor (84) advanced his theory of diffusion by continuous movement in which turbulent diffusion was expressed in terms of Lagrangian mixing length and velocity parameters. Lagrangian turbulent parameters express the motion of a hypothetical fluid particle as it travels through the flow field while retaining its identity, except for possible changes caused by molecular diffusion. The main shortcoming of Taylor's theory is that Lagrangian variables are not directly measurable and

can be only evaluated from actual turbulent diffusion data.

In the Eulerian domain, the variation of some property is considered with respect to a fixed space coordinate system. Eulerian turbulence variables can be directly determined by means of hot wire equipment or from the turbulence spectrum. Several empirical attempts have been made recently to bridge this gap by relating Lagrangian variables to Eulerian turbulence variables (3,4,55,58). In view of the complexity of the problem and our limited knowledge of the statistical functions describing the turbulent motion, the problem of expressing the rate of turbulent transport of a transferable quantity in terms of the turbulent velocity field remains unsolved.

This work deals with eddy diffusion and axial mixing in fully developed turbulent pipe flow which is incompressible and nondecaying (steady). The central core approximates the simpler case of stationary isotropic turbulence that is homogeneous in two directions. Turbulence in the outer region is nonisotropic which is considerably more difficult to treat.

The results obtained here apply to mass, heat, or momentum transfer in any gas or liquid flow satisfying the above conditions. Turbulent diffusion and convective mixing are often encountered in many chemical engineering applications such as tubular chemical reactors, pipe line flow, mixing vessels, gas absorption and solvent extraction columns, etc.

The principal objectives of this work were:

- To relate material and thermal turbulent diffusivities for isotropic turbulent pipe flow to measurable Eulerian turbulence parameters. This would also relate the Eulerian and Lagrangian domains since turbulent diffusion is a Lagrangian property.

- To find a more general nonisotropic relationship between turbulent diffusion and Eulerian turbulence parameters; turbulence is nonisotropic over most of the pipe (outer and wall regions).

- To find a generalized eddy diffusivity correlation for the central core of gas or liquid pipe flow.

- To investigate the contributions of various radial elements to overall axial mixing in turbulent pipe flow using Taylor's numerical analysis (88).

The presentation deals with turbulent diffusion in the isotropic core and the nonisotropic outer and wall regions in this order. It then extends to include the convective effect in a study of axial mixing that applies various nonisotropic radial distributions. Despite their apparent relationship, these topics do not share the same theoretical background and require different methods of analysis. Each topic is, therefore, presented in a separate chapter containing a problem review, developments and analyses, and discussion of results.

In Chapter II, a useful generalized eddy diffusivity

correlation is obtained from available core eddy diffusion data. Some interesting results are reported on the nature of the mixing length, the mutual independence of turbulent and molecular diffusion, the dependence of Peclet number on Reynolds number, and other empirical core equations for eddy viscosity and turbulent Prandtl number.

Chapter III deals with relating turbulent diffusion to measurable Eulerian turbulence parameters. This chapter's findings are believed the most important of all the results reported in the thesis. An equation is obtained, on the basis of a postulated physical deformation model, that relates isotropic turbulent diffusivity to energy dissipation rate and pipe diameter.

Nonisotropic turbulent diffusion is treated briefly in Chapter IV. An equation is proposed for eddy diffusivity as a function of radial position over the entire pipe cross section.

The contribution of different radial elements to axial mixing is investigated in Chapter V using various eddy diffusivity, eddy viscosity, and velocity distributions discussed in Chapter IV.

Finally, additional results and developments that are not necessarily part of the thesis are included as appendices. Appendix B reports some experimental results obtained here on axial mixing in transition flow. Appendix C deals with the effects of pulse thickness and slit thickness

on pulse response obtained by determining the average concentration across the exit plane, for laminar flow having negligible diffusion effect.

CHAPTER II

EDDY DIFFUSIVITY AND EDDY VISCOSITY IN THE TURBULENT CORE

Problem Review

Eddy Diffusivity

Determination of Eddy Diffusivity from Point Source Data

The turbulent diffusion of a tracer from a steady point source of negligible size is described by the following equation:

$$\frac{1}{r}\frac{\partial}{\partial r}\left(\alpha_r r \frac{\partial C}{\partial r}\right)+\alpha_x \frac{\partial^2 C}{\partial x^2} - U\frac{\partial C}{\partial x} = 0 \qquad (2\text{-}1)$$

Where:

C = tracer concentration at position r

α_r = radial eddy diffusivity

α_x = axial eddy diffusivity

r = radial distance from pipe axis

U = mean velocity at a distance r from pipe axis

x = axial distance from source

In order to solve this equation analytically, the following simplifying assumptions are usually made:

(a) At sufficiently high Reynolds numbers, the velocity profile across the central third of the pipe is flat, i.e., $U = U_o \neq f(r)$.

(b) Since the concentration gradient in the axial direction is much smaller than the radial gradient, turbulent diffusion in the axial direction is ignored.

(c) Isotropy and two dimensional homogeneity are assumed to apply throughout the core in view of the flat velocity profile.[1] The radial diffusion coefficient across the core is, therefore, considered independent of r.

By making these assumptions, Equation (2-1) reduces to:

$$\alpha_c \frac{\partial^2 C}{\partial r^2} + \frac{\alpha_c}{r} \frac{\partial C}{\partial r} = U_o \frac{\partial C}{\partial x} \qquad (2\text{-}2)$$

α_c is the average eddy diffusivity in the core calculated assuming negligible axial diffusion. The boundary conditions which apply are:

$$C = 0 \qquad \text{at } s = \infty$$

$$\text{as } s \to 0 \qquad Q = -4\pi s^2 \alpha_c \frac{\partial C}{\partial s}$$

$$\text{at } r = 0 \quad \frac{\partial C}{\partial r} = 0$$
$$r = a$$

The above equation has the following known analytical solution,

$$C = \frac{Q}{4\pi \alpha_c s} e^{-\frac{U_o(s-x)}{2\alpha_c}} \qquad (2\text{-}3)$$

Where:

Q = flow rate of injected tracer

U_o = axial mean velocity

$s = \sqrt{r^2 + x^2}$

Towle and Sherwood (92) made the following

---

[1]The degree of isotropy was as low as 75% in some core investigations.

simplification for large values of x:

since $r^2 = s^2 - x^2$

and $s-x = \frac{r^2}{s+x}$

For large values of x, $s \cong x$

It follows that:

$$C = \frac{Q}{4\pi\alpha_c s} e^{-\left(\frac{U_o}{2\alpha_c}\right)\left(\frac{r^2}{2x}\right)} \qquad (2\text{-}4)$$

This equation represents very well the actual experimental concentration profile over most of the turbulent region. Near the wall, the conditions of isotropy and flat profile do not hold and the actual concentrations are greater than those predicted by Equation(2-4).

The eddy diffusivity, α_c, is determined from the asymptotic slope of a plot of the variance of the Gaussian distribution as a function of x. The variance, $\overline{Y^2}$, becomes a linear function of x after a short distance from the source.

$$\overline{Y^2} = \frac{2\alpha_c x}{U_o}$$

$$\alpha_c = \frac{U_o}{2}\frac{d\overline{Y^2}}{dx} \qquad (2\text{-}5)$$

The eddy diffusion coefficient determined by this method is the sum of turbulent and molecular diffusivities. Molecular diffusivity, however, makes a negligible contribution to eddy diffusivity since it is much smaller than turbulent diffusivity in the core. For gases, the molecular diffusivity is about 3-5 per cent of the eddy diffusivity

and is even much smaller for liquids. Considering the accuracy of eddy diffusivity data and the errors introduced due to the simplifying assumptions, eddy and turbulent diffusivities in the core can be considered to be approximately the same. In case of liquid mercury data (38), corrected turbulent diffusivities were used.

Eddy Diffusivity Equations

Sherwood and Woertz (78) proposed an eddy diffusivity correlation and compared it with their data on the diffusion of water vapor in air, CO_2, or helium flow in a narrow rectangular duct:

$$\alpha_c = 0.04\ V\ a_o\sqrt{f} \qquad (2\text{-}6)$$

Where:

V = The average bulk velocity

a_o = Width of duct or distance between parallel plates

f = Fanning friction factor

This equation was obtained by writing

$$\alpha_c = v'\ell$$

v' = the root mean square fluctuating velocity

ℓ = the mixing length

ℓ was obtained using Prandtl's definition,

$$u' = \ell \frac{dU}{dy} \qquad (2\text{-}7)$$

Sherwood and Woertz tried various ways of evaluating v' and ℓ

and finally chose the one that agreed best with their data; $\frac{dU}{dy}$ was obtained from a Von Karman velocity equation and u' was taken equal to $\sqrt{\frac{\tau}{\rho}}$, where τ is the shear stress and ρ is the density; i.e.

$$\tau = \rho \overline{uv} \tag{2-8}$$

$$R_{uv} = \frac{\overline{uv}}{\overline{u'v'}} \tag{2-9}$$

= the cross correlation coefficient

For isotropic turbulence u' = v', so v' can be written as

$$v' = \sqrt{\frac{\tau}{\rho R_{uv}}} \tag{2-10}$$

Up to this point, this is essentially another way of determining the distribution of the eddy viscosity, ϵ. This approach has always led to zero eddy viscosity at the pipe axis which is known to be untrue, (τ, R_{uv} and $\frac{dU}{dy}$ vanish at the axis). Sherwood and Woertz were able to obtain Equation (2-6) by assuming R_{uv} constant over the core (equal to one) and by taking α_c equal to the maximum $v'l$ value attained as calculated from Equations (2-7) and (2-10), thus, disregarding the dip in $v'l$ near the center. These maximum $v'l$ values were still lower than experimental α_c values determined in their work. Sherwood's equation is essentially an eddy viscosity equation. Although some of the assumptions are disputable, their analysis was not claimed to be fundamental and the equation is a surprisingly good correlation of eddy diffusivity (See Figure 3).

Emmert and Pigford (22) recently fitted Sherwood and Woertz's data for gases by the following approximate equation:

$$3600\alpha_c = 6.6\times10^{-5}Re+0.2 \qquad (2\text{-}11)$$

Analysis and Treatment of Data

Eddy Diffusion Data

The eddy diffusion data considered here are for the transfer of mass or heat in the core of fully-developed turbulent Newtonian pipe or duct flow. Turbulent diffusion of momentum (eddy viscosity) is treated separately later in this chapter. The term eddy diffusivity is reserved for mass and heat transfer. Throughout this chapter α_c is considered independent of radial position, θ, in the "isotropic" turbulent core (taken one third of the pipe cross section). When dealing with point eddy diffusivity data, α_c was taken here equal to α at $\theta = 0.15$ or 0.16. The data treated here are for gas, water and liquid metal flow over a range of Reynolds number between 5,000 and 684,000 (Tables I and II).

Baldwin (3) reported thermal eddy diffusion data obtained by the turbulent diffusion of heat from a hot wire point-source. Sherwood and Woertz (78) obtained their data from the eddy diffusion of water vapor, from a water film falling along the walls of a narrow rectangular duct, in gas flow. Roley and Fahien (67) reported point-source data for the eddy diffusion of carbon dioxide in air. The value listed in Table I is an average core value of data reported

farthest from the source (90 inches). Their data at Re = 10,000 were not used here because of steep variations in α near the center.

Isakoff studied heat transfer from a hot wall to turbulent liquid mercury flow (38); the turbulent diffusion data listed in Table I were corrected for molecular thermal diffusivity and were taken at an L/d ratio of 138 and $\theta = 0.15$ ($\nu = 1.2 \times 10^{-6}$ ft^2/sec.). Johnk and Hanratty (39) reported "constant" eddy diffusivity data for heat transfer in the turbulent core from the pipe wall. Their data are included in Table I, ν was calculated for an air temperature of 105°F.

Some of the point-source data reported in the literature were left out since they were not taken under conditions that permit accurate determination of the turbulent diffusion coefficient. For example, Mickelsen (58) reported $\overline{Y^2}$ data near the source that did not extend far enough to where the asymptotic slope may be accurately determined. McCarter et al. (56) reported eddy conductivity data under conditions that gave nonhomogeneous flow in the x direction due to entry effect (entry length was six diameters). As these authors pointed out, the variation of α_c with x was of the order of 50 per cent of the lower value. Data reported by Frandolig and Fahien (27) on the diffusion of carbon dioxide in air were also x dependent indicating the presence of entry effect. Data reported by Flint, Kada and Hanratty (25) fell

about 60 per cent lower than the data of other investigators which was recognized by these authors.

A Generalized Eddy Diffusivity Correlation

A generalized eddy diffusivity correlation is developed in this section. It is based on all mass and heat transfer data of Table I for gas, water and liquid mercury flow. It should apply to the turbulent core of fully developed Newtonian flow (gases or liquids) in smooth pipes at low mass transfer rates (negligible effect on the mean velocity distribution). Some of the data used to obtain this correlation are for flow between parallel plates (or in narrow rectangular ducts). The same correlation was found to agree with open channel eddy diffusivity data such as those of Kalinske and Van Driest (40); these data were not included, however, when deriving the correlation.

The best correlation developed in this work was obtained when plotting $\frac{\alpha_c}{\nu}$, referred to here as The Eddy Diffusivity Number, versus Reynolds number on logarithmic coordinates. None of the various dimensionless quantities examined, which involved α_c, ν, Re and D_m, showed any correlation.

The correlation line of all the data plotted in Figure 1 was obtained by the least square method:

$$\frac{\alpha_c}{\nu} = 0.0098\ Re^{0.8423} \qquad (2\text{-}12)$$

Correlation coefficient = 0.9963

The 95% confidence limits are also shown in Figure 1. On the basis of confidence limits computations, the significant decimals are only those given in Equation (2-13):

$$\frac{\alpha_c}{\nu} = 0.01 \quad Re^{0.84} \qquad (2\text{-}13)$$

Despite some scatter due to Isakoff's data, the data of Figure 1 correlate remarkably well. One should bear in mind that the data are for widely different systems of mass and heat transfer and for both circular and rectangular conduits.

Another correlation is reported here that is based on selected data (Figure 2). In view of the experimental scatter in Isakoff's liquid metal data and since the molecular properties of mercury change markedly with the very slight contaminations commonly encountered in heat transfer experiments, this set of data was not included. Baldwin's highest point was also excluded.[1] Data of Becker et al. (8), Johnk and Hanratty, and Roley and Fahien were not included either because the author was not aware of their existence or because they appeared after this work was completed.[2] The rest of the data of Table I were fitted by the least square method:

$$\frac{\alpha_c}{\nu} = 0.012 \quad Re^{0.82} \qquad (2\text{-}14)$$

Correlation coefficient = 0.9995

---

[1]According to Baldwin (private communication), this was the first point determined and may not have been as accurate as later measurements. Also, errors caused by instrument's resolution time are larger for higher flow velocities.

[2]See footnote, page 16.

The number of decimals shown in Equation (2-14) is based on 95% confidence limits computations.

Equation (2-14) is recommended here as the most reliable equation for evaluating material and thermal eddy diffusivities in the turbulent core of pipe flow.[1]

Comparison with Sherwood and Woertz's Equation

Figure 3 compares the smoothed experimental data reported by Sherwood and Woertz (Table III) with the same diffusivities calculated from their proposed Equation (2-7), and the correlation line representing Equation (2-14). The proposed Equation (2-14) fits Woertz's data as well as all the data of Table II better than Equation (2-7).

Empirical Expression of the Mixing Length

The eddy diffusivity is often written as the product of the root mean square (r.m.s.) fluctuating velocity, v', and the mixing length, which is also called sometimes the Lagrangian integral scale. A new expression for the mixing length can be obtained from Equation (2-14) and by using Sandborn's proposed correlation for v' (70).

Sandborn's equation is a correlation of experimental data taken by him and others over a wide range of

---

[1]After including data by Roley and Fahien, and Johnk and Hanratty, the same "significant" correlation was obtained:

$$\frac{\alpha_c}{\nu} = 0.012 \ Re^{0.82}$$

Correlation coefficient = 0.9989

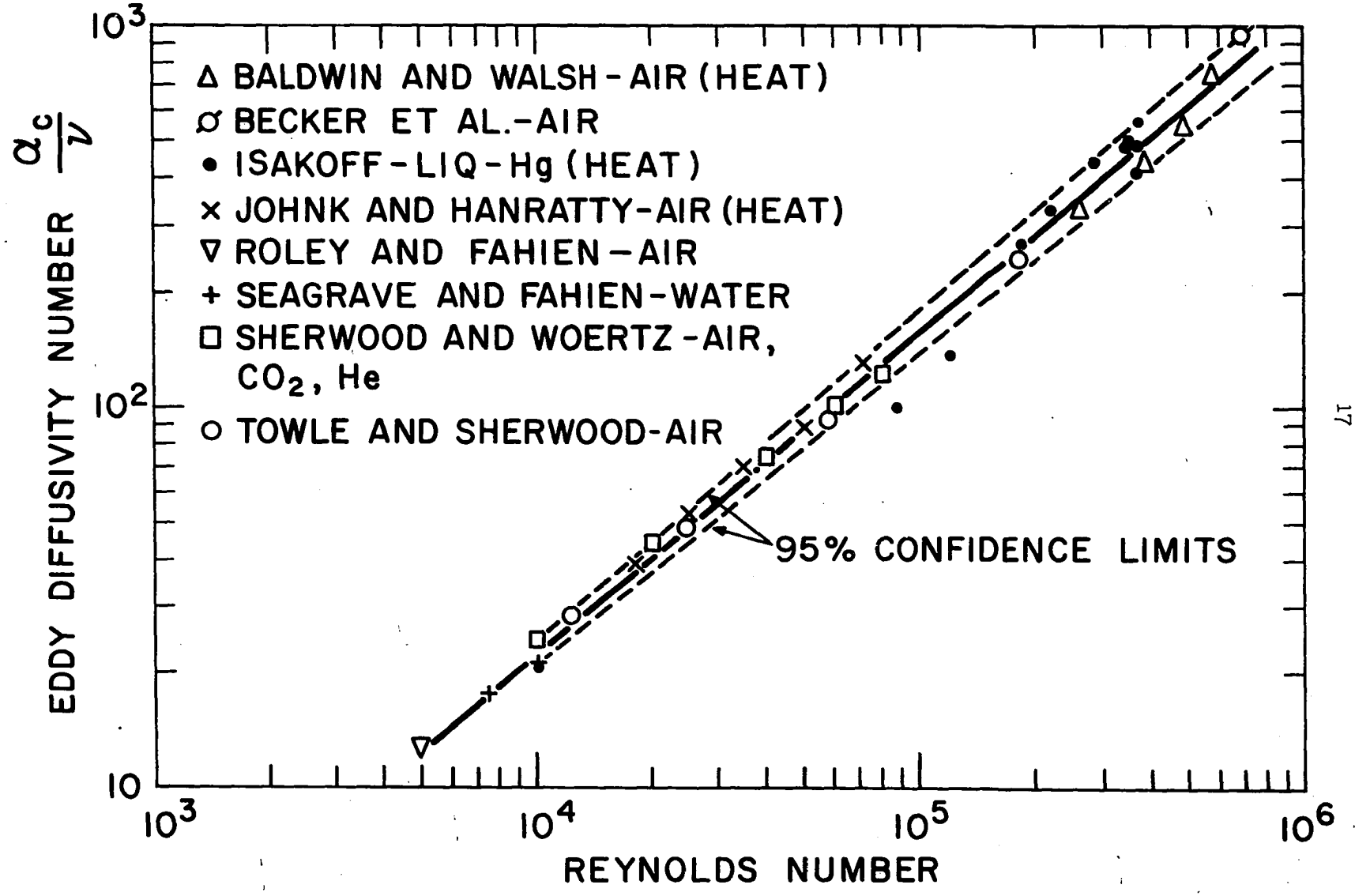


Fig. 1 CORRELATION OF EDDY DIFFUSIVITY DATA

TABLE I

EDDY DIFFUSIVITY DATA

Re	α_c ft^2/sec.	$\frac{\alpha_c}{\nu}$	Source of Data
12,200	0.0045	28.1	Towle and Sherwood (92)
24,600	0.0079	48.8	
57,400	0.0150	92.9	
180,000	0.0393	244.0	
241,000-257,000[1]	0.054	335.4	Baldwin and Walsh (4)
354,000-376,500	0.072	447.2	
451,000-480,000	0.088	546.6	
570,000	0.120	740.0	
10,000	0.0039[2]	24.1	Sherwood and Woertz (78)
20,000	0.0070	43.5	
40,000	0.0122	75.5	
60,000	0.0162	100.9	
80,000	0.0196	121.7	
5,000	0.00014	13.3	Seagrave and Fahien (75)
7,500	0.00019	17.4	
10,000	0.00023	21.3	
684,000	0.155	945.1	Becker et al. (8)
18,000	0.0075	39.4	Johnk and Hanratty (39)
25,000	0.0102	53.7	
35,000	0.0134	70.5	
50,000	0.0169	89.0	
71,000	0.0249	131.0	
5,000	0.0021	13.0	Roley and Fahien (67)
364,000	0.00050	413	Isakoff (38)
373,000	0.00067	560	
350,000	0.00059	500	
346,000	0.00058	480	
368,000	0.00058	484	

[1]Reynolds values were calculated by two different methods from the maximum mean velocities given by the author.

[2]Data obtained by plotting Woertz's diffusivity data for all gases versus a modified Reynolds number in which the kinematic viscosity of the gas is corrected to that of air and reading off the smoothed curve.

TABLE I - continued

Re	α_c ft2/sec.	$\frac{\alpha_c}{\nu}$	Source of Data
285,000	0.00052	436	Isakoff (continued)
219,000	0.00039	329	
185,000	0.00033	267	
119,000	0.00017	137.5	
87,300	0.00012	100	

TABLE II

EXPERIMENTAL CONDITIONS OF EDDY DIFFUSIVITY DATA OF TABLE I

Source of Data	Main-stream	Tracer or Source	Duct Shape	Duct Inside Diameter, in.	Duct Wall Material	Remarks
Towle and Sherwood (92)	Air	CO_2	Pipe	12	Steel	
Sherwood and Woertz (78)	Air	Water vapor	Rectan-gular duct	2.08 x 24	Galvan-ized iron	Re based on equivalent diameter
	CO_2	Ditto				
	He	Ditto				
Baldwin (4)	Air	Heat source	Pipe	8**	Steel	
Seagrave and Fahien (75)	Water	Fluores-cein dye	Pipe	4	Copper	α_c taken at $\frac{r}{a} = 0.16$
Becker et al. (8)	Air	Oilfog	Pipe	7.91	Aluminum	
Johnk and Hanratty (39)	Air	Heat*	Pipe	3.08	Stainless steel	
Roley and Fahien (67)	Air	CO_2	Pipe	4**	Galvan-ized steel	
Isakoff (38)	Mercury	Heat*	Pipe	1.5	Stainless steel	α_c taken at $\frac{r}{a} = 0.15$ @ $\frac{L}{d} = 138$

*Heat transferred through pipe walls.

**Nominal

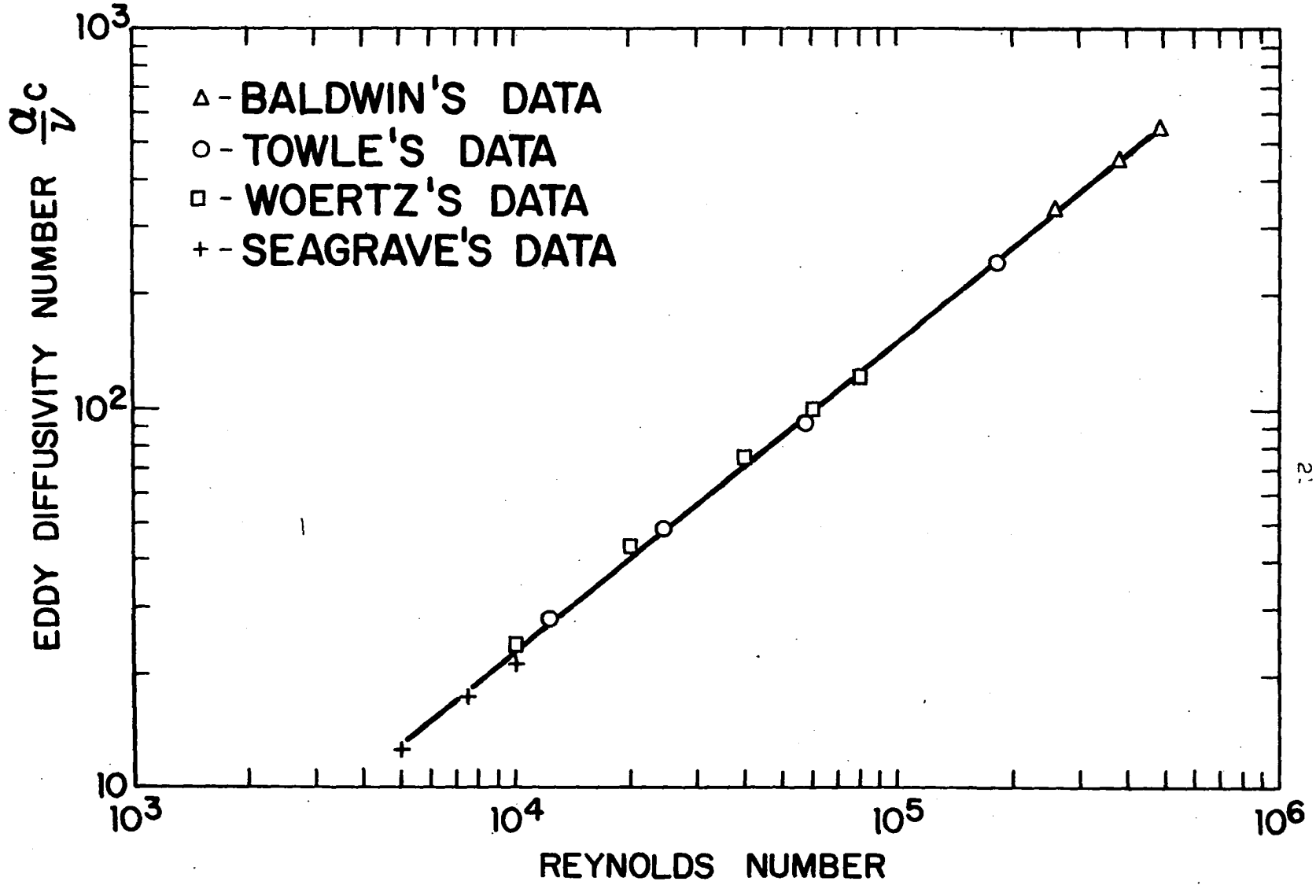


Fig. 2 CORRELATION OF SELECTED EDDY DIFFUSIVITY DATA

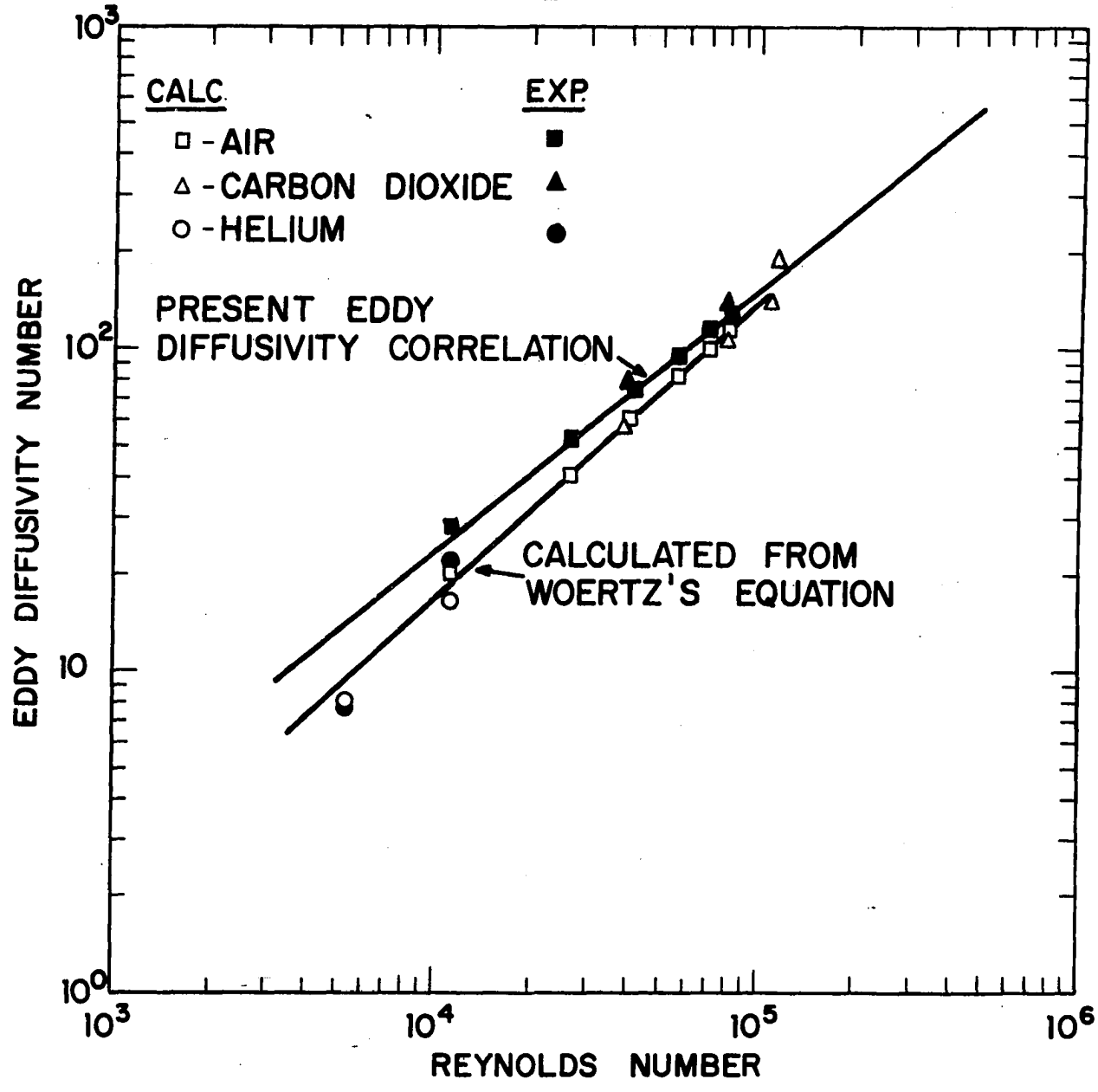


Fig. 3 EDDY DIFFUSIVITY NUMBER CALCULATED FROM WOERTZ'S EQUATION AND COMPARED WITH PRESENT CORRELATION OF DIFFUSIVITY DATA

TABLE III

DATA OF SHERWOOD AND WOERTZ

Main Stream	Re[1]	α_c $cm^2/sec.$	α_c/ν
Air	11,100	3.1	20.22
	25,800	6.3	41.10
	40,200	9.4	61.32
	56,200	12.6	82.19
	69,000	15.3	99.80
	79,900	17.5	114.16
CO_2	38,300	5.1	57.28
	79,000	9.5	106.7
	108,000	12.5	140.38
He	5,300	10.1	8.05
	11,100	20.6	16.43

[1]Reynolds number was calculated by the authors assuming the characteristic dimension, d, to be equal to twice the width a_o. This is a reasonable approximation when the breadth is much greater than a_o. These two dimensions were 61 and 5.3 cms respectively.

Reynolds number,

$$\frac{u'}{U_o} = 0.144 \left(\frac{U_o a}{\nu}\right)^{-0.146} \qquad (2\text{-}15)$$

Where:

u' = The r.m.s. fluctuating velocity in the flow direction at the pipe axis

U_o = The maximum velocity at pipe axis

a = Radius

ν = Kinematic viscosity

Assuming isotropic turbulence at the pipe axis, one can write (see Chapter III)

$$v' = u'$$

This condition was closely approached though not completely satisfied in Sandborn's set-up. It is also customary to assume that the Lagrangian and Eulerian mean square velocities are equal. The mixing length or Lagrangian integral scale, ℓ_L, can be written as follows:

$$\ell_L = \frac{\alpha_c}{v'} = \frac{0.012\,\nu\,Re^{0.82}}{0.144\left(\frac{a}{\nu}\right)^{-0.146} U_o^{0.854}} \qquad (2\text{-}16)$$

The bulk average velocity, V, is related to the axial velocity by applying Nunner's power law (61) as described in Chapter IV.

$$U = U_o \left(1 - \frac{r}{a}\right)^{1/n}$$

Where:

U = Mean velocity at position r

$n = 1/\sqrt{\lambda}$

λ = Moody friction factor

It can be readily seen that

$$\frac{V}{U_o} = \frac{2n^2}{(1+n)(1+2n)}$$

where V is the average bulk velocity.

Equation (2-16) can then be expressed in terms of V, Re and n:

$$\ell_L = 0.0772\ Re^{-0.036}\ d\left(\frac{(1+n)(1+2n)}{2n^2}\right)^{-0.854}$$

$$\ell_L = 0.0772\ d\ Re^{-0.036}/(0.5\ \lambda + 1.5\sqrt{\lambda}+1)^{0.854} \qquad (2\text{-}17)$$

The denominator is roughly equal to unity since λ ranges usually between 0.01 and 0.03. Also the exponent of Re is very close to zero which indicates that the mixing length is practically independent of Re and is directly proportional to the pipe diameter, d. In other words, the mixing length is practically independent of all flow variables and is mainly a function of the characteristic geometric dimension of the pipe. This interesting result supports earlier indications that the mixing length is proportional to the Eulerian integral scale or eddy size which in turn is dependent on the size of the vessel. The ratio of the mixing length at the pipe axis to pipe diameter was calculated by Nikuradse (60) from smooth open pipe velocity distribution data and was found to be approximately 0.07 over a range of Reynolds number between 110,000 and 3,200,000. This value compares well with Equation (2-17) which is based on eddy diffusivity rather than eddy viscosity data.

Peclet Number

It is well known that Peclet number reaches a constant asymptotic value of 2 in packed beds at Reynolds numbers higher than 3,000 (both Pe and Re are based on particle diameter in this case). Seagrave and Fahien (75) suggested that the average Pe should reach a constant value in case of open pipe flow at Reynolds numbers greater than 10,000. This was based on the following postulation:

$\alpha_c = v' \ell$

ℓ is proportional to tube diameter d

v' is proportional to U or V, constant intensity at high Re (70).

It follows that $\frac{Vd}{\alpha_c} = Pe = \text{constant}$.

One may test the above postulation by making use of the proposed Equation (2-14).

$$\text{If } \frac{Vd}{\alpha_c} = Pe = \text{constant}$$

$$\text{then } \frac{\alpha_c Pe}{\nu} = Re$$

$$\text{or } \frac{\alpha_c}{\nu} = \frac{Re}{Pe}$$

and since Pe is assumed constant at high Re, then $\frac{\alpha_c}{\nu}$ should be directly proportional to Re which is not in agreement with Equation (2-14) because the exponent of Re is 0.82 and not 1.0. The average Peclet number remains a function of Re up to values of the latter as high as 480,000. Figure 4 and Table IV show Peclet number as a function of Re.

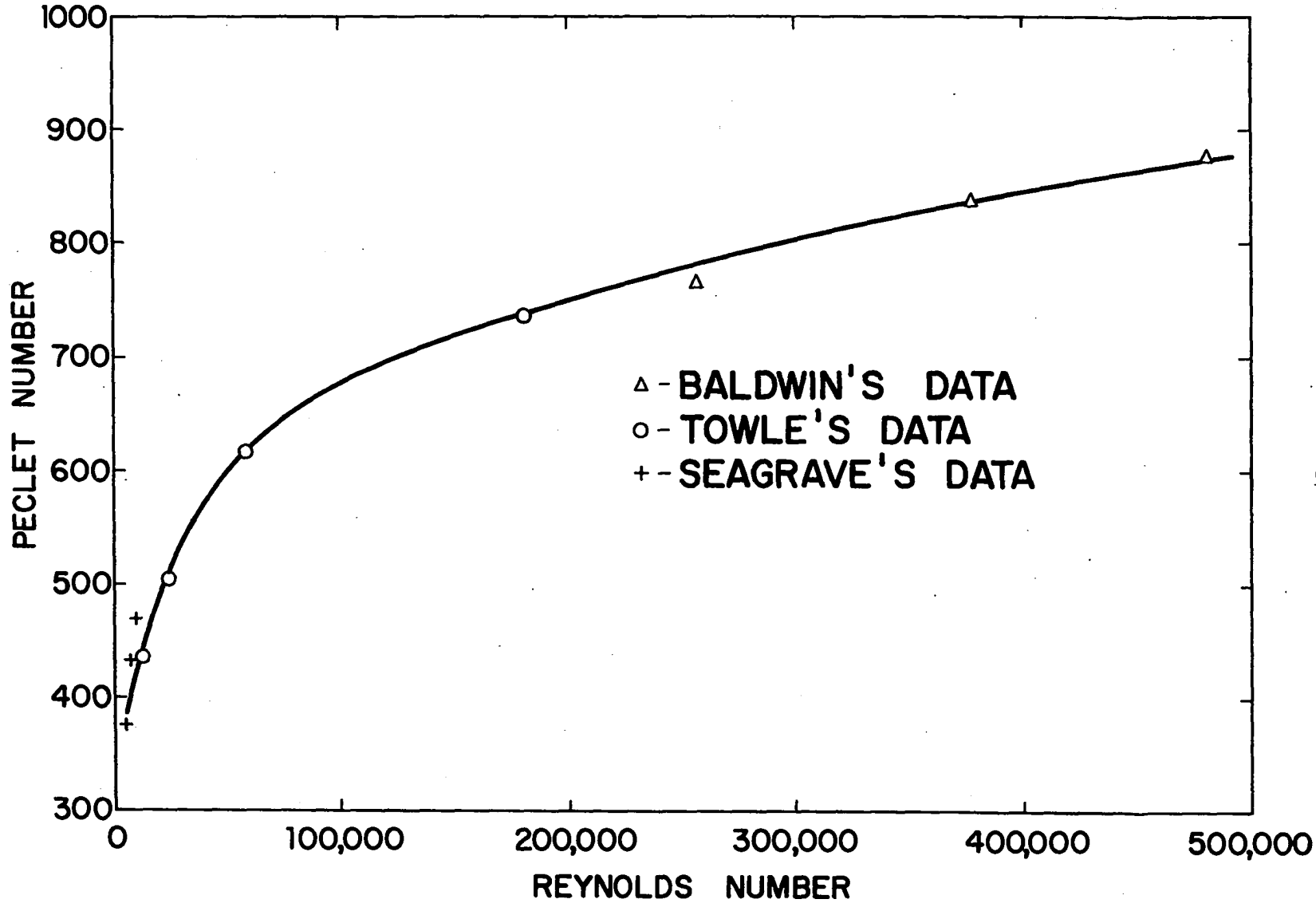


Fig. 4 PECLET NUMBER vs. REYNOLDS NUMBER

TABLE IV

AVERAGE PECLET NUMBER DATA

Re	Pe	Source of Data
12,200	434.5	Towle and Sherwood (92)
24,600	503.9	
57,400	617.7	
180,000	737.6	
257,000	766.2	Baldwin (3)
376,500	839.5	
480,000	876.2	
20,000	564.9	Sherwood and Woertz (78)
40,000	623.4	
60,000	634.9	
5,000	375	Seagrave and Fahien (75)
7,500	431	
10,000	469.6	

It is conceivable, however, that for smooth pipes, Pe would attain a constant value at Reynolds numbers in excess of 10^7. This is based purely on the form of Equation (2-23) which expresses the eddy viscosity as directly proportional to the product of Re and $\sqrt{f}$ (Reynolds analogy assumed). For perfectly smooth pipes, the friction factor is a function of Re up to Reynolds numbers of about 10^7, beyond which f remains constant.

Contribution of Molecular Diffusion to Eddy Diffusion

Molecular and turbulent variances are normally assumed to be additive which implies that the two diffusion mechanisms are mutually independent.

i.e., $$\overline{Y^2} = \overline{Y_t^2} + \overline{Y_m^2} \qquad (2\text{-}18)$$

$$= \overline{Y_t^2} + 2D_m t$$

where $\overline{Y^2}$ = observed total variance

$\overline{Y_t^2}$ = variance due to turbulent diffusion.

The interaction between turbulent and molecular diffusivities has become lately a controversial issue in the literature. Batchelor and Townsend (7) suggested that turbulent vorticity is likely to increase the rate of molecular diffusion by the rotation and strain of a diffusion wake. A third term was added to account for such interaction which Townsend termed "accelerated diffusion":

i.e., $$\overline{Y^2} = \overline{Y_t^2} + 2D_m t + \frac{28}{45} D_m \overline{\omega^2}\, t^3 \qquad (2\text{-}19)$$

$\overline{\omega^2}$ = the mean square vorticity defined by these authors.

Saffman (69) argued that this additional term should be $(-\frac{1}{9}D_m\overline{\omega^2}t^3)$. Both developments were made for decaying isotropic grid turbulence.

Mickelsen (59) determined experimentally the lateral dispersion or variance $\overline{Y^2}$ downstream from a point source in decaying isotropic grid turbulence for the dispersion of helium and carbon dioxide in air. His data showed that, for long diffusion times, accelerated molecular diffusion is negligible and that molecular diffusion makes only its own independent contribution to the total dispersion. Townsend's argument that turbulent and molecular diffusion are mutually dependent has not been tested for nondecaying steady turbulent pipe flow.

Pipe flow data treated here (long diffusion times) showed no accelerated diffusion effect. The data given in Table I and Figure 1 afford a dramatic test of the accelerated diffusion conception because they are for gas and liquid systems that differ in their molecular diffusivities by a factor of 10^5 (as opposed to a factor of 5 for the CO_2-air, He-air systems studied by Mickelsen). The fact that Equation (2-12) represents the eddy diffusivity data so well despite very large differences in the molecular diffusivities of gases and liquids, is in itself an evidence that α_c is a function of ν and Re only. The lack of correlation between dimensionless quantities

including molecular diffusivity, and Reynolds number or Peclet number is demonstrated by Figures 5 and 6. Although some of the eddy diffusivity data are really turbulent diffusivity data, the molecular diffusivity was not always subtracted from eddy diffusivity. The correction was made only in those cases where D_m is $> 3\%$ of α_c. The experimental error in eddy diffusivity is normally greater than 3% , (See Appendix D).

Table V lists the molecular properties of some of the systems plotted in Figures 1, 5 and 6. The molecular diffusivities of the gases have been calculated at 20° C using Hirschfelder equation and collision integrals based on the Lennard-Jones potential (64). For the diffusivity of fluorescein dye in water, the listed value is that calculated by Seagrave (74) as an average of two estimates obtained by two different methods (1,101). The term D_{12}^m is used here to indicate the molecular diffusivity of tracer 1 in the main stream 2.

Eddy Viscosity in the Core

Eddy viscosity is the coefficient of eddy diffusion of momentum. Figure 1 indicates that eddy diffusivity applies to the transfer of heat or mass in the core. The purpose of this section is to determine if the same correlation applies to momentum transfer. The distribution of eddy viscosity across the pipe cross section is dealt with in greater detail in Chapter IV.

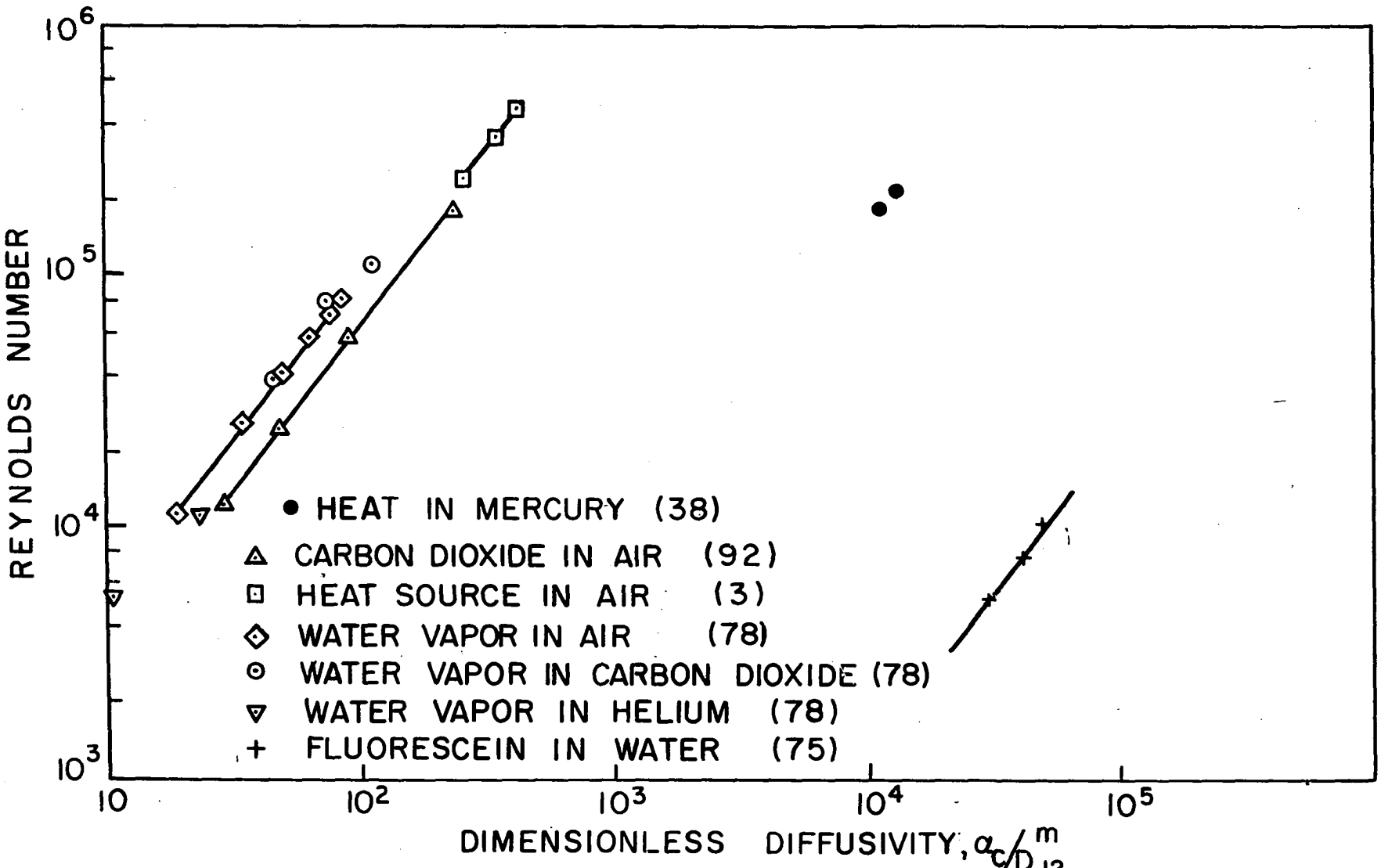


Fig. 5 A PLOT OF REYNOLDS NUMBER vs DIMENSIONLESS DIFFUSIVITY, α_c/D_{12}^m

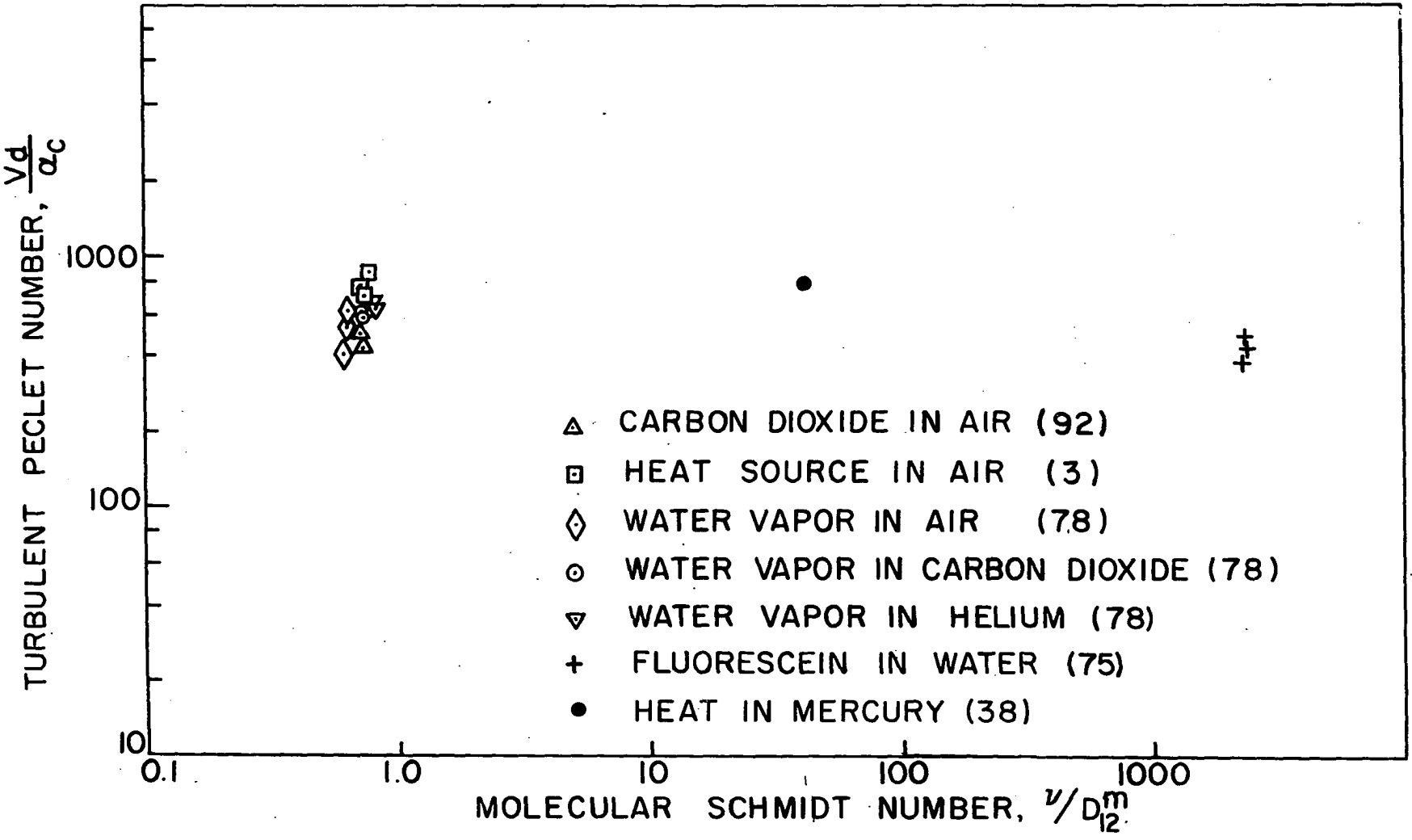


Fig. 6 A PLOT OF TURBULENT PECLET NUMBER vs MOLECULAR SCHMIDT NUMBER

TABLE V

MOLECULAR PROPERTIES OF THE SYSTEMS OF TABLE I

System		D_{12}^m	ν_{12}	Sc_{12}
Diffusing Medium	Main Stream	ft^2/sec	ft^2/sec	
Hydrogen	Air	$(8.06)(10^{-4})$	$(6.48)(10^{-4})$	0.80
Carbon Dioxide	Air	$(1.63)(10^{-4})$	$(1.23)(10^{-4})$	0.75
Water Vapor	Air	$(2.40)(10^{-4})$	$(1.52)(10^{-4})$	0.63
Water Vapor	Carbon Dioxide	$(1.59)(10^{-4})$	$(1.15)(10^{-4})$	0.72
Water Vapor	Helium	$(9.59)(10^{-4})$	$(6.87)(10^{-4})$	0.72
Heat	Air	$(2.06)(10^{-4})$*	$(1.61)(10^{-4})$	0.78
Fluorescein Dye	Water	$(4.6)\ (10^{-9})$	$(1.08)(10^{-5})$	2341
Heat	Mercury	$(2.9)\ (10^{-8})$*	$(1.2)\ (10^{-6})$	41.8

*This is thermal diffusivity = $\frac{\text{Thermal conductivity}}{\text{Density x specific heat}}$

The eddy viscosity, ϵ, is defined by Equation (2-20):

$$\tau_{rx} = -\epsilon \rho \frac{dU}{dr} \qquad (2\text{-}20)$$

τ_{rx} = shear stress

ρ = density

A linear shear distribution applies across the turbulent region; ϵ can be determined if U is known as a function of r. Assuming Von Karman's universal logarithmic velocity distribution:

$$u^+ = 5.5 + 2.5 \ln y^+ \qquad (2\text{-}21)$$

$u^+ = \frac{U}{U_*}$ = dimensionless velocity parameter

$U_* = \sqrt{\frac{\tau_w}{\rho}}$ = friction velocity

τ_w = shear stress at the wall

$\tau_w = \frac{\rho f v^2}{2}$

$y^+ = \frac{y\, U_*}{\nu}$ = dimensionless friction distance

f = Fanning friction factor

ρ = density

Substituting for τ and $\frac{dU}{dr}$ in Equation (2-21), we get:

$$\epsilon = 0.4\, V \sqrt{\frac{f}{2}}\, \theta\, (1-\theta)\, a \qquad (2\text{-}22)$$

$\theta = r/a$

a = Pipe radius

This can also be written as

$$\frac{\epsilon}{\nu} = 0.2\, Re \sqrt{\frac{f}{2}}\, \theta\, (1-\theta) \qquad (2\text{-}23)$$

The main drawback of Equation (2-23) is that the eddy viscosity reaches a maximum value somewhere between the pipe wall and axis and then dips to zero at $\theta = 0$ where it should have a non-zero finite value.

Schlinger et al. (73) compared eddy conductivity values obtained for the case of parallel plates with the eddy viscosities obtained from Equation (2-22). They found that for $\theta < 0.3$, the eddy conductivity remains fairly constant at Reynolds numbers greater than 20,000. That is, ϵ does not vanish at the pipe axis. Connell, Schlinger and Sage (14) computed ϵ at different values of θ and Re for both round pipes and parallel plates. The eddy viscosity across the core, ϵ_c, was assumed to remain constant for all values of θ less than 0.3. Table VI lists values of $\frac{\epsilon_c}{\nu}$ computed by these authors at $\theta = 0.3$ using Equation (2-23). Also listed is the eddy viscosity of air over the center core at Re = 425,000 as determined from Laufer's pipe flow data (46,47). Laufer's data showed also a fairly constant eddy viscosity over the turbulent core.

Figure 7 is a plotting of the data of Table VI. Laufer's data point agrees very well with Connell's data. The eddy viscosity number or relative viscosity correlates well with Reynolds number, a computed correlation coefficient of 0.998. Equation (2-24) is a least square fitting of these data.

$$\frac{\epsilon_c}{\nu} = (9)\ (10^{-3})\ Re^{0.86} \qquad (2\text{-}24)$$

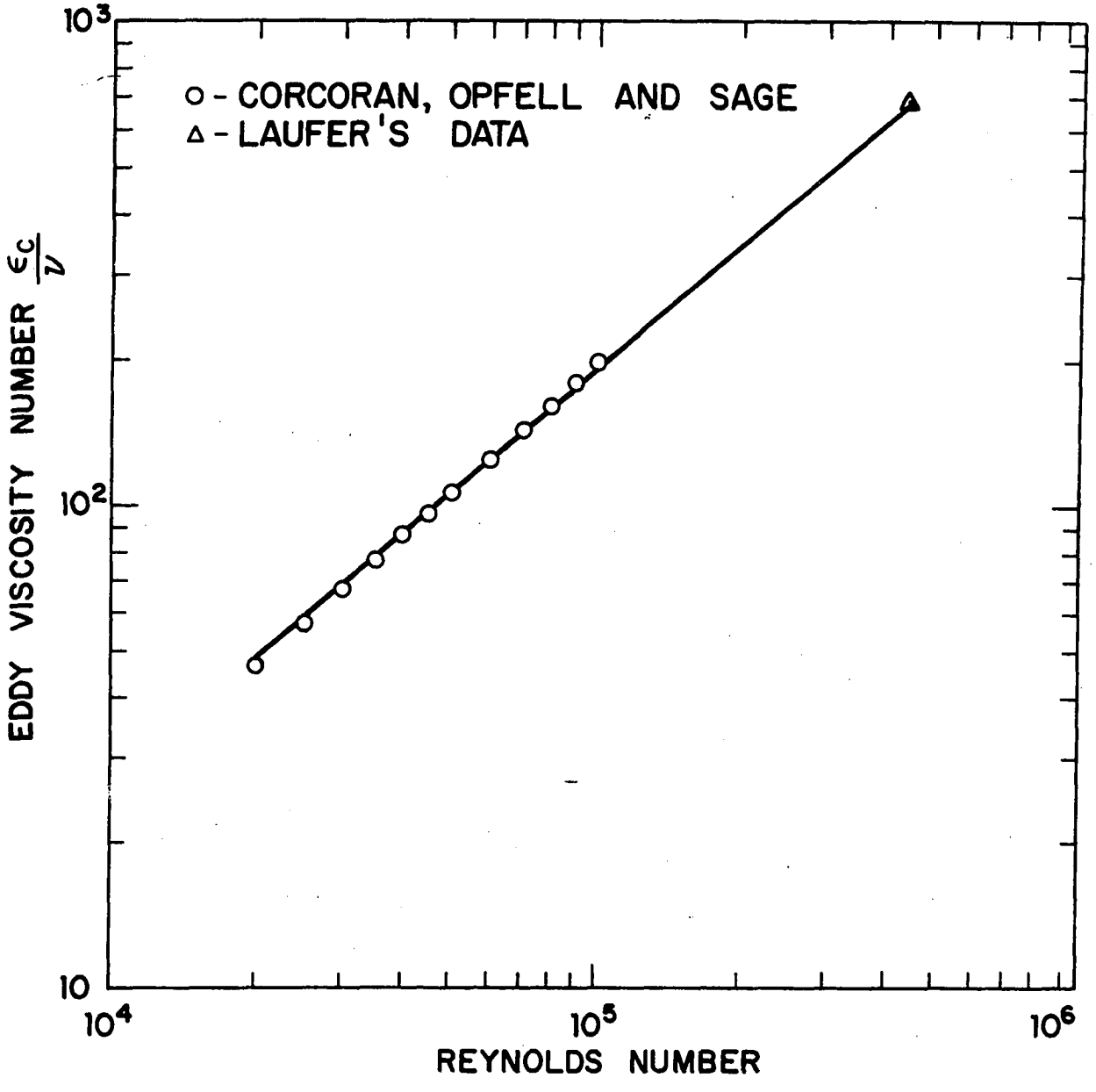


Fig. 7 CORRELATION OF EDDY VISCOSITY DATA

TABLE VI

EDDY VISCOSITY DATA

Reynolds Number	Eddy Viscosity Number ϵ_c/ν	Source of Data
20,000	46.31	Corcoran, Opfell and Sage (15)
25,000	56.64	
30,000	66.67	
35,000	76.52	
40,000	86.32	
45,000	96.00	
50,000	105.42	
60,000	124.48	
70,000	142.83	
80,000	161.14	
90,000	179.30	
100,000	197.00	
425,000	667.00	Laufer (46)

Turbulent Schmidt and Prandtl Numbers over the Core

An empirical expression for turbulent Schmidt and Prandtl numbers can be readily obtained from Equations (2-14) and (2-24).

$$(Pr)_t = (Sc)_t = \frac{\epsilon_c}{\alpha_c} = 0.74\ Re^{0.04} \qquad (2\text{-}25)$$

Comparison of Equation (2-22) with Sherwood's Equation

Equation (2-6) due to Sherwood and Woertz (78) and Equation (2-22) are eddy viscosity equations obtained using Von Karman's mean velocity distribution. The main difference between these two procedures is that Sherwood used Prandtl's mixing length theory which required the estimation of the intensity of turbulence.

$$\alpha_c = 0.04 V a_o \sqrt{f} \qquad (2\text{-}6)$$

For parallel plates, Equation (2-22) can be written as:

$$\epsilon_c = 0.2 V \sqrt{\frac{f}{2}}\, \theta(1-\theta) a_o \qquad (2\text{-}26)$$

a_o = the spacing between the plates

θ = relative position from the center of the duct.

One may now substitute in Equation (2-26) for θ with $\frac{5}{9}$ which, according to Sherwood and Woertz, corresponds to the position at which α attained its maximum value and which they used to obtain Equation (2-6); Equation (2-26) becomes:

$$\epsilon_c = 0.035 V a_o \sqrt{f} \qquad (2\text{-}27)$$

Equation (2-27) is essentially the same as Woertz's equation and is arrived at here without resorting to the mixing length concept and without determining v' and ℓ independently or making any assumptions regarding the correlation coefficient and the intensity of turbulence.

Summary of Conclusions and Results

1. An excellent correlation of core eddy diffusivity data was obtained by plotting $\frac{\alpha_c}{\nu}$ as a function of Reynolds number. The data are for mass and heat transfer for gas and liquid flow in pipes or parallel plates over a Reynolds number range between 5000 and 684000,

$$\frac{\alpha_c}{\nu} = 0.012 \ \mathrm{Re}^{0.82} \qquad (2\text{-}14)$$

2. Material and thermal eddy diffusivity data uphold the validity of Reynolds analogy for mass and heat transfer.
3. For long diffusion times in fully developed nondecaying turbulent pipe flow, turbulent diffusion is independent of molecular diffusivity. This result disagrees with Townsend's accelerated diffusion theory. The molecular diffusivities of the systems examined here differ by a factor of as much as 10^5 versus a maximum of 5 in Mickelsen's earlier investigation. The same result applied to liquid metal systems of high thermal conductivity.
4. An expression for the mixing length, ℓ_L, was obtained from the eddy diffusivity correlation and Sandborn's empirical relation for the intensity of turbulence at

the pipe axis:

$$\ell_L = 0.077\ d\ Re^{-0.036} / (0.5\ \lambda + 1.5\sqrt{\lambda}+1)^{0.854} \quad (2\text{-}17)$$

λ is Moody friction factor

d is pipe diameter

i.e. $\ell_L/d \cong 0.077$

Nikuradse (60) reported a similar result for momentum transfer, $\ell/d = 0.07$

5. Peclet number is a function of Reynolds number up to Re = 480000. An asymptotic constant Peclet number is probably greater than 900. It is conceivable that Pe attains its asymptotic value when the friction factor is independent of Re ($Re > 10^7$ for perfectly smooth pipes).

6. Core eddy viscosity, ϵ_c, was found to be represented by:

$$\frac{\epsilon_c}{\nu} = 0.009\ Re^{0.86} \quad (2\text{-}24)$$

7. Reynolds analogy does not apply to the turbulent diffusion of momentum. Turbulent Prandtl and Schmidt numbers for the core can be written as:

$$Pr_t = Sc_t = 0.74\ Re^{0.04} \quad (2\text{-}25)$$

CHAPTER III

RELATING TURBULENT DIFFUSION IN THE CORE TO EULERIAN TURBULENCE PARAMETERS

Introduction to Turbulence Theory

The main objective of this introduction is to define and describe some of the basic turbulence parameters that characterize a field of turbulence and that are used in the developments presented in this chapter. A more detailed treatment of the theory of turbulence can be found in Hinze (31), a very valuable reference on this subject. Taylor's statistical theory of turbulence (85) is the backbone of today's turbulence theory; the energy dissipation rate, correlation coefficient, and micro and macro scales of turbulence were all introduced by Taylor.

The components of the instantaneous velocity at a certain point in a turbulent field can be recorded continuously using instruments that are sensitive to velocity fluctuations such as the hot wire anemometer. Figure 8 illustrates a typical signal of the velocity spectrum showing the random fluctuation of the instantaneous

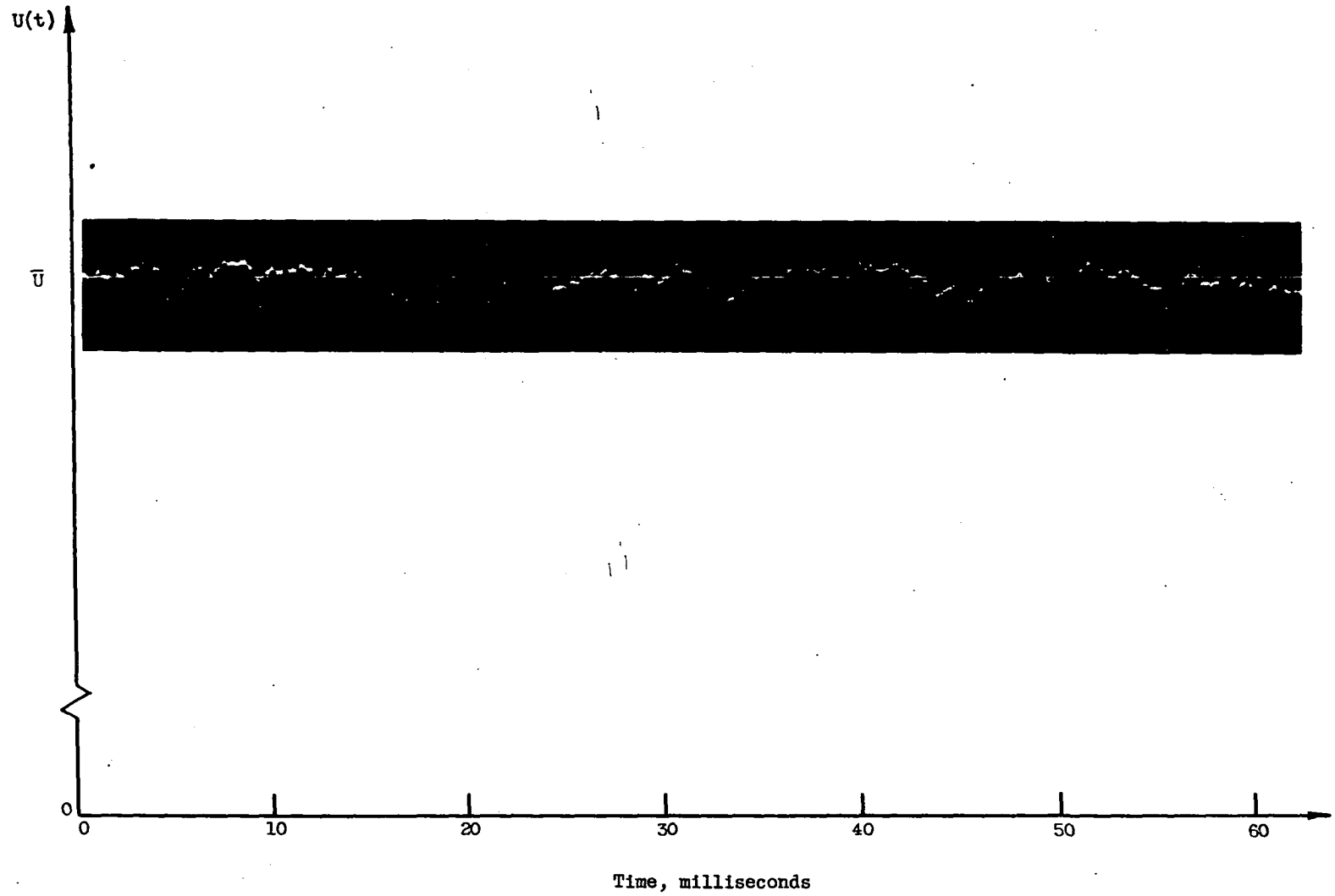


Figure 8 - Turbulent Velocity Spectrum

(Taken by L. V. Baldwin)

velocity about a mean value.

The mean velocity at any radial position in a pipe, U, is a time average of the instantaneous axial velocity at that point. It is independent of time but a function of the radial position θ.

$$U = \lim_{T_1 \to \infty} \frac{1}{T_1} \int_0^{T_1} U(t)\, dt \qquad (3\text{-}1)$$

Where U(t) is the instantaneous velocity that is normally recorded as the velocity spectrum, and which may be considered as the sum of the mean velocity U and the instantaneous fluctuating velocity u.

$$U(t) = U + u \qquad (3\text{-}2)$$

In case of pipe flow, since there is no net flow in the radial and tangential directions; the instantaneous velocities in these directions are the same as the fluctuating velocities and the mean velocities are zero. For isotropic flow, the statistical distribution of the instantaneous fluctuating velocities was found to be well represented by a Gaussian distribution function (79, 93). The mean square velocity, $\overline{u^2}$, $\overline{v^2}$, or $\overline{w^2}$ for x, y, or z directions respectively, is an important turbulence parameter that can be defined as the variance of the distribution of the fluctuating velocity.

$$\overline{u^2} = u'^2 = \int_{-\infty}^{+\infty} u^2 f(u)\, du \qquad (3\text{-}3)$$

Where f(u) is the frequency distribution function of u. The root-mean-square value (r.m.s.) or the standard deviation, u', is used to characterize the intensity of turbulence or degree of turbulence in the x direction which is $\frac{u'}{U}$.

Turbulence is said to be isotropic when the distribution function for the fluctuating velocity components is not a function of orientation. As a consequence

$$\overline{u^2} = \overline{v^2} = \overline{w^2}$$

Changes in the direction and magnitude of velocity fluctuations are wholly random, and there is no correlation between the velocity components in different directions.

i.e., $\overline{uv} = \overline{vw} = \overline{uw} = 0$

The condition of isotropy is approached over the central core of pipe flow where the velocity profile is flat. Turbulence is assumed to be isotropic in all "core" developments. The relative values of u', v' and w' can be used as a measure of the degree of isotropy. Turbulence outside the core, where appreciable mean velocity gradients exist, is nonisotropic or anisotropic $\overline{u^2} \neq \overline{v^2} \neq \overline{w^2}$.

The condition of homogeneity implies that turbulence has the same structure in all parts of the flow field.

That is, the fluctuating velocity distribution function and its mean do not change by translating the axes. Turbulence in fully developed pipe flow is homogeneous in the axial and tangential directions. Turbulence is not homogeneous in case of decaying grid turbulence or insufficient entry length since it is not independent of x.

The third assumption made in this chapter is that the turbulence is stationary which implies that the mean values at any point are not time dependent. That is, the mechanism underlying the generation of turbulence does not change with time. Stationarity here does not mean that the fluid is at rest.

The degree of correlation between the fluctuating velocities at two points is expressed by the spatial Eulerian correlation coefficient. The correlation function is defined as the time mean of the product of the instantaneous fluctuating velocities; it is normally obtained by analog computing techniques. Several correlation coefficients can be defined for the different velocity components. Subscripts are used here to identify any particular correlation coefficient as illustrated in Figure 9 (the super-bar means a time average).

e.g., $$R_{xu} = \frac{\overline{u_1 u_2}}{\overline{u^2}} \qquad (3\text{-}4)$$

As shown in Figure 10, the spatial correlation

coefficient varies with the separation distance between the two points. It attains a maximum value of 1.0 when the two points coincide and decreases gradually as the separating distance increases. The correlation coefficient R_{xu} vanishes when x reaches a certain value, indicating no correlation (Figures 10 and 11).

The area under the correlation coefficient curve is the macro-scale of turbulence

$$L_{yu} = \int_0^\infty R_{yu}\, dy \qquad (3\text{-}5)$$

L_{yu} = Eulerian scale of turbulence.

For each correlation coefficient a corresponding scale of turbulence may be defined by an equation similar to (3-5). The scale of turbulence derives its name from the old notion that turbulence is composed of eddies and that some velocity correlation is maintained within an eddy. The average size of an eddy may be then represented by the scale of turbulence. Of course, a fluid eddy is a three dimensional body that requires more than one dimension for its complete definition. The concept of fluid eddies remains a descriptive curiosity that has had limited functional utility in the theory of turbulence. It is noteworthy, however, that the scale of turbulence was found to be proportional to the size of mesh opening in case of grid generated isotropic turbulence. In case of open pipe

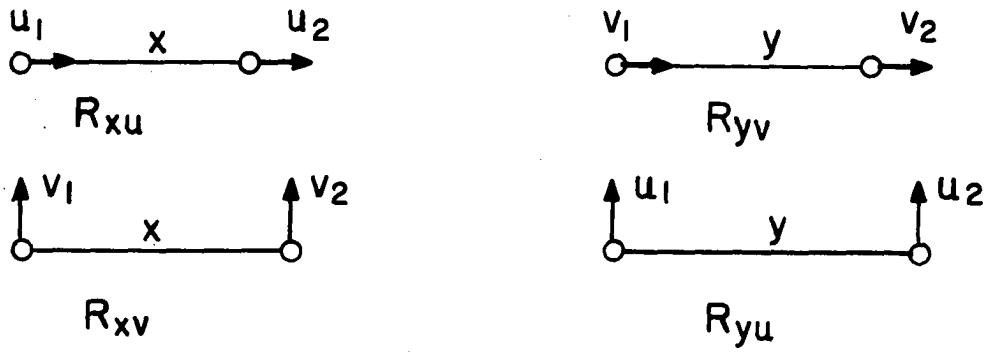


Fig. 9 LONGITUDINAL AND LATERAL EULERIAN CORRELATION COEFFICIENTS

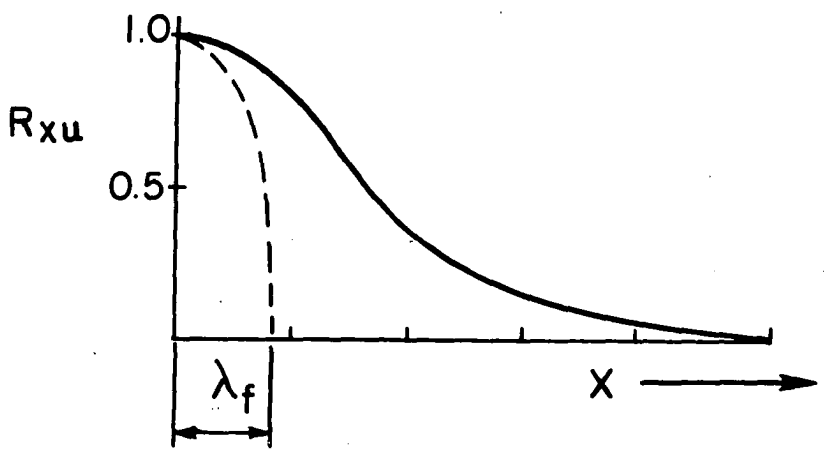
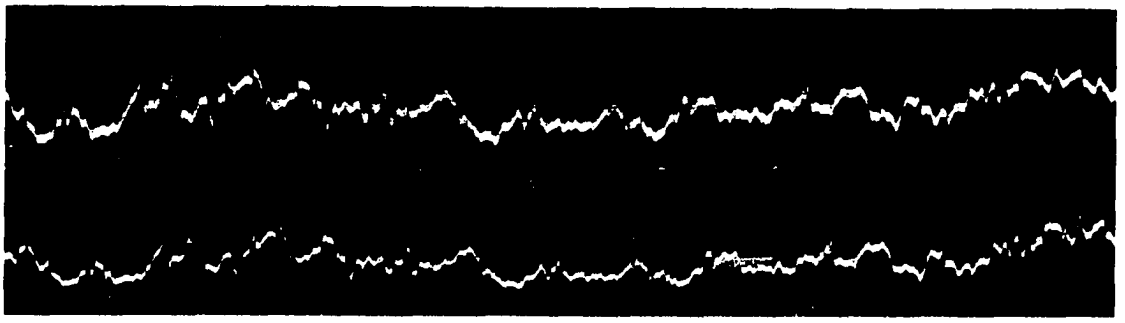


Fig. 10 EULERIAN CORRELATION COEFFICIENT AND MICROSCALE



(a) Perfect correlation, R = 1.0



(b) Moderate correlation, R = 0.5



(c) Low correlation, R = 0

Figure11. - Oscilloscope traces of two anemometer signals showing varying degrees of correlation.

flow, some proportionality would be expected to exist between the pipe diameter and the scale of turbulence. Also the Lagrangian integral scale (Chapter II and Equation (3-35)) was found to increase with the Eulerian macro-scale. (3). The two scales have not been mathematically related.

Another turbulence parameter that was introduced by Taylor (85) is the microscale of turbulence, λ_g, which may be regarded roughly as the characteristic length of the smallest eddies that are responsible for the dissipation of energy. A parabola drawn tangent to the R_{yu} curve at y = o (osculating parabola) intersects the y axis at the point $y = \lambda_g$ (Figure 10). In other words, λ_g is proportional to the radius of curvature of the R_{yu} curve at y = o.

$$\frac{1}{\lambda_g^2} = \lim_{y \to o} \frac{(1 - R_{yu})}{y^2} \qquad (3\text{-}6)$$

A similar microscale can be defined for the longitudinal correlation coefficient R_{xu},

$$\frac{1}{\lambda_f^2} = \lim_{y \to o} \frac{(1 - R_{xu})}{x^2} \qquad (3\text{-}7)$$

λ_f is sometimes called the longitudinal microscale.

Von Karman and Howarth (99) related the lateral and longitudinal correlation coefficients (R_{yu} and R_{xu}) for homogeneous isotropic turbulence and showed also that

$$\lambda_f = \sqrt{2}\,\lambda_g \qquad (3\text{-}8)$$

The rate of energy dissipation per unit mass per unit time, ε', can be related to the microscale of turbulence. Taylor (85) showed that for isotropic turbulence,

$$\varepsilon' = 7.5\,\nu\,\overline{\left(\frac{\partial u}{\partial y}\right)^2} \qquad (3\text{-}9)$$

and that

$$\overline{\left(\frac{\partial v}{\partial x}\right)^2} = \overline{\left(\frac{\partial u}{\partial y}\right)^2} = 2\overline{\left(\frac{\partial u}{\partial x}\right)^2} \qquad (3\text{-}10)$$

$$\varepsilon' = 15\,\nu\overline{\left(\frac{\partial u}{\partial x}\right)^2} \qquad (3\text{-}11)$$

He also proved that:

$$R_{yu} = 1 - \frac{1}{2!}\frac{y^2}{u^2}\overline{\left(\frac{\partial u}{\partial y}\right)^2} + \frac{1}{4!}\frac{y^4}{u^2}\overline{\left(\frac{\partial^2 u}{\partial y^2}\right)^2} - \ldots (3\text{-}12)$$

R_{yu} may be also expressed in the form of an even Taylor series expansion at $y = o$

$$R_{yu} = 1 + \frac{y^2}{2!}\left[\frac{\partial^2 R_{yu}}{\partial y^2}\right]_{y=o} + \frac{y^4}{4!}\left[\frac{\partial^4 R_{yu}}{\partial y^4}\right]_{y=o} + \ldots (3\text{-}13)$$

at $y = o$, all terms of the above series may be ignored except the first two terms. Since the osculating parabolas are described by the following equations:

$$R_{xu} = 1 - \frac{x^2}{\lambda_f^2} \qquad (3\text{-}14)$$

$$R_{yu} = 1 - \frac{y^2}{\lambda_g^2} \tag{3-15}$$

It can be deduced from the above equations that:

$$\frac{2}{\lambda_f^2} = - \left[\frac{\partial^2 R_{xu}}{\partial x^2} \right]_{x = o} \tag{3-16}$$

$$\frac{1}{\lambda_f^2} = - \frac{1}{2 \overline{u^2}} \overline{\left(\frac{\partial u}{\partial x} \right)^2} \tag{3-17}$$

$$\varepsilon' = 30 \nu \frac{\overline{u^2}}{\lambda_f^2} \tag{3-18}$$

Another important turbulence parameter is the one-dimensional <u>energy spectrum function</u>, F(n). Simmons and Salter (80) showed that the mean value $\overline{u^2}$ may be regarded as the sum of contributions of energy from all frequencies obtained by resolving the random instantaneous velocity signal into its harmonic components. The spectral density or the energy spectrum function F(n) is the relative contribution from frequencies between n and n + dn to the turbulent kinetic energy per unit mass.

$$\overline{u^2} = \int_o^\infty \overline{u^2}(n) \, F(n) \, dn \tag{3-19}$$

$$\int_o^\infty F(n) \, dn = 1$$

n = frequency, sec^{-1}

The one-dimensional spectrum function is obtained by plotting F(n) as a function of n. The wave number is more commonly used when describing the spatial structure at any instant; the wave number and the frequency are related by:

$$\text{wave number} = \frac{2\pi n}{U}$$

Taylor (86) showed that the spectrum function and the Eulerian correlation coefficient are related by Fourier transforms.

Review of the Problem

This Chapter deals with the very complex problem of relating turbulent diffusion to fundamental Eulerian turbulence variables characterizing the turbulent field. A microscopic deformation theory is proposed which suggests that turbulent diffusion is a function of both microscopic turbulent deformation and macroscopic deformation (or velocity gradient).

It was established in Chapter II that $\frac{\alpha_c}{\nu}$ is a function of Reynolds number. This result is explained fundamentally in this chapter; in particular, why the Eddy Diffusivity Number is used rather than $\frac{\alpha_c}{D_m}$ or other dimensionless quantities containing variables such as u', V, d, λ_f ... etc. The lack of correlation between eddy diffusivity and molecular diffusivity was demonstrated in Chapter II and is further discussed and explained in this chapter.

Previous Mixing Length and Turbulent Diffusion Theories

Phenomenological Mixing Length Theories

The concept of "apparent" or "eddy" viscosity was first introduced by Boussinesq (10) who assumed that turbulent shear stresses are directly proportional to the velocity gradient.

$$\tau_{yx} = - (\rho \epsilon) \frac{dU}{dy} \qquad (3\text{-}20)$$

This equation is similar to Newton's law for viscous flow which states that viscous stresses are directly proportional to the velocity gradient with the dynamic viscosity, μ, as the proportionality constant. Boussinesq assumed ϵ a scalar quantity.

Prandtl's theory was the earliest attempt to define a turbulent mixing length analogous to the mean free path in the kinetic theory of gases. Prandtl made the hypothesis that:

$$\tau_{yx} = - \rho \ell^2 \left|\frac{dU}{dy}\right| \left(\frac{dU}{dy}\right) \qquad (3\text{-}21)$$

Where

τ_{yx} = Shear stress in the x direction on a fluid surface of constant y.

ρ = Density

ℓ = Prandtl mixing length (for momentum transfer).

U = Time average axial velocity at y.

The turbulent shear stress is related to the velocity gradient by Equation (3-20); this defines the eddy viscosity, ϵ, as:

$$\epsilon = \ell^2 \left| \frac{dU}{dy} \right| \tag{3-22}$$

From a dimensional argument, ϵ can be written as

$$\epsilon = u' \ell \tag{3-23}$$

u' = the root mean square fluctuating velocity

That is, for isotropic turbulence

$$v' = u' = \ell \frac{dU}{dy} \tag{3-24}$$

Prandtl's mixing length, ℓ, is physically described as the distance a fluid particle travels, in a direction normal to the direction of flow, before it loses its identity and becomes imbedded in a fluid layer at a distance ℓ. Fluid lumps are assumed to preserve their identity till some definite point in their path where they mix with the surroundings and attain the same velocity and other transferable properties as those of the corresponding neighborhood.

Prandtl assumed in wall turbulence that ℓ changes linearly with distance from the wall,

i.e., $$\ell = hy' \tag{3-25}$$

y' = distance from the wall

h = a constant

i.e., $$\tau_{yx} = \rho h^2 y^2 \left|\frac{dU}{dy}\right| \frac{dU}{dy}, \qquad (3\text{-}26)$$

Another hypothesis for estimating ℓ is that of Von Karman in which ℓ is assumed a function of the derivatives of the mean velocity rather than merely a function of distance from the wall.

$$\ell = K \frac{\left(\frac{dU}{dy}\right)}{\left(\frac{d^2U}{dy^2}\right)} \qquad (3\text{-}27)$$

K = a "universal" constant whose value was reported as 0.4 or 0.36.

Von Karman's assumption gives

$$\tau_{yx} = K^2 \rho \frac{(dU/dy)^4}{(d^2U/dy^2)^2} \qquad (3\text{-}28)$$

The solution of the above equations gives a logarithmic expression for the radial distribution of the mean velocity U. A more detailed discussion of velocity correlations is given in Chapter IV.

Discussion of Prandtl mixing length theory. - The mixing length, as defined by Prandtl, depends only on the dynamical conditions of the fluid, namely the velocity gradient and the shear stress. Taylor (85) commented that

the only way by which a small volume of fluid can lose heat or change composition is conduction or molecular diffusion to the surroundings; a decrease in molecular diffusivity would, therefore, lead to an increasing time during which the small volume would retain its composition distinct from that of the surroundings and, therefore, should result in increasing the mixing length. The mixing length, as defined by Prandtl, is independent of such physical constants as thermal conductivity and molecular diffusion. He later reiterated this criticism (90)

> The chief difficulty with a mixture length theory is to form a physical picture of the process by which a body of fluid carrying some transferable property (heat, mass, or momentum), discharges its load into the surrounding fluid. Taken literally, the original mixture length theories would envisage the unrealistic conception that a mass of fluid retains its load unchanged till at a certain instant it meets with a sudden catastrophe and disintegrates into fine threads or drops which then discharge their load by molecular processes.

Taylor also remarked that fluctuating pressure gradients should affect the mixing length in some way and that the Momentum Transport Theory does not take such effects into consideration.

The contribution of molecular diffusion to eddy diffusivity was discussed in Chapter II; the data examined for gases and liquids indicate that molecular diffusion makes an independent contribution to eddy diffusivity. That is, the latter can be expressed as the sum of molecular

and turbulent diffusion coefficients. This implies that the transfer or exchange of transferable properties between a fluid lump and its surroundings occurs predominantly by mechanical means since molecular diffusion is too slow to be solely responsible for the mixing process. Also, fluid lumps do not have well defined rigid boundaries across which diffusion exchange may be expected to take place strictly by molecular means.

The mixing length conception represents a desire to draw some analogy between the kinetic theory of gases or molecular motion and turbulent motion by expressing the eddy diffusivity in terms of a mixing length corresponding to the mean free path and a velocity that corresponds to the mean molecular velocity. Until a method becomes available for predicting the mixing length from measurable Eulerian parameters that characterize the turbulent field, the mixing length concept remains merely another way of writing the eddy viscosity and can be only determined from eddy viscosity data.

Another shortcoming of Prandtl Mixing Length Theory is that a zero eddy viscosity is given at the pipe axis where the velocity gradient is zero

$$\epsilon = \ell^2 \left| \frac{dU}{dy} \right|$$

The eddy viscosity, ϵ, is known to have finite non-zero values at the center of the pipe that are slightly lower

than its maximum value (35, 73).

Theory of Diffusion by Continuous Movement

This classical theory was presented by G. I. Taylor in 1921 (84). A homogeneous turbulent field is considered in which the fluid is both turbulent and stagnant ($V = o$). Turbulence is conceived to be generated by the movement of a grid in the fluid. We are interested in the turbulent diffusion of fluid particles in the y direction from a point source that is taken as the origin of a cartesian coordinate system. At time t, a marked fluid particle would be moving with an instantaneous Lagrangian velocity $v_L(t)$. The average conditions, however, are the same at every point because turbulence is assumed to be uniformly distributed throughout the field.

Assuming this model, Taylor arrived at Equation (3-31) by the following steps. A Lagrangian double velocity correlation coefficient was defined as

$$R_L = \frac{\overline{v_L(t)\ v_L\ (t-\xi)}}{\overline{v_L^2}} \qquad (3\text{-}39)$$

Where $\overline{v_L(t)\ v_L\ (t-\xi)}$ is the average, over a large number of particle motions, of the product of instantaneous particle velocities at time t and $t - \xi$; $\overline{v_L^2}$ is the mean square value of the instantaneous particle velocity averaged with respect to time; ξ is a time increment. By

integrating over ξ and taking into consideration that $v_L(t) \neq f(\xi)$.

$$v_L(t) \int_0^t v_L\,(t - \xi)\, d\xi = \overline{v_L^2} \int_0^t R_L\, d\xi \qquad (3\text{-}30)$$

The displacement variable Y at time t can be defined as $Y = \int_0^t v_L\,(t - \xi)\, d\xi$. The R.H.S. of Equation (3-30) can be then written as:

$$\overline{Y\, v_L(t)} = \overline{Y \frac{dY}{dt}} = \frac{1}{2}\left(\overline{\frac{dY^2}{dt}}\right) = \frac{1}{2}\frac{\overline{dY^2}}{dt}$$

i.e., $$\frac{1}{2}\frac{\overline{dY^2}}{dt} = \overline{v_L^2} \int_0^t R_L\, d\xi \qquad (3\text{-}31)$$

$\overline{Y^2}$ = the variance of temperature or concentration distribution curve. At values of t very close to zero, R_L is approximately equal to 1, so that at points very close to the source,

$$\overline{Y^2} = \overline{v_L^2}\, t^2 \qquad (3\text{-}32)$$

Equation (3-32) is used for determining the mean square Lagrangian velocity from $\overline{Y^2}$ data near the source.

Since $R_L \rightarrow 0$ as $t \rightarrow \infty$,

$$\int_0^\infty R_L\, d\xi = \text{constant} = T \qquad (3\text{-}33)$$

At points sufficiently far from the source, $R_L = 0$, $(t \ggg T)$

$$\frac{1}{2}\frac{d\overline{Y^2}}{dt} = \overline{v_L^2}\, T \qquad (3\text{-}34)$$

T is described as the effective average time required for a fluid particle to lose any correlation with its initial velocity.

A Lagrangian integral scale, ℓ_L, was defined by Taylor as:

$$\ell_L = \sqrt{\overline{v_L^2}} \int_0^\infty R_L \, d\xi \qquad (3\text{-}35)$$

In other words, at a sufficiently large distance from the source,

$$\frac{1}{2}\frac{d\overline{Y^2}}{dt} = \sqrt{\overline{v_L^2}}\, \ell_L$$

ℓ_L = Taylor's mixing length or Lagrangian integral scale.

$\sqrt{\overline{v_L^2}} = v'_L$ = the r.m.s. fluctuating particle velocity.

$$\overline{Y^2} = 2\, v'_L\, \ell_L\, t + \text{constant} \qquad (3\text{-}36)$$

That is, for large values of t, $\overline{Y^2}$ is directly proportional to the diffusion time. Experimental $\overline{Y^2}$ data agree with Equations (3-33) and (3-36) in that $\overline{Y^2}$ is proportional to t^2 at the source and is linearly related to t at some distance from the source. The determination of v'_L from $\overline{Y^2}$ data at the source involves some errors due to

disturbances caused by the finite size of the source. More accurate v'_L results could be obtained from heat source measurements since a hot wire can be made much smaller in size than a tracer injector.

The eddy diffusion coefficient, α_c, is determined from the asymptotic slope of $\overline{Y^2}$ as a function of t. The same result is obtained in the previous chapter by a different method when discussing the determination of α_c from point source data.

$$\frac{1}{2}\frac{d\overline{Y^2}}{dt} = \alpha_c = v'_L \ell_L \qquad (3\text{-}37)$$

For a flow system with a maximum axial fluid velocity, U_o,

$$t = \frac{x}{U_o}$$

$$\alpha_c = \frac{U_o}{2}\frac{d\,\overline{Y^2}}{dx} \qquad (3\text{-}38)$$

In a recent paper (90), Taylor spelled out the physical conception underlying his turbulent diffusion theory. This may be best presented by quoting him. After citing his criticism of the Mixing Length Theory, he said:

> To devise a more realistic description of turbulent diffusion I had to base it on the Lagrangian conception in which attention is fixed on a particle of the diffusing matter which preserves its identity as it moves in the turbulent field of flow. I therefore tried to describe the diffusive properties

> of turbulence by defining the correlation between the velocity of a particle at one instant and that of the same particle at a later time. I found in fact that the diffusion from a fixed point-source can be described when only this Lagrangian time-correlation function and the mean square velocity are known. I found that this correlation vanishes after an interval of time, the diffusion for much longer periods proceeds as though it were due to a constant virtual coefficient of eddy diffusivity. Since as I have already mentioned, a mixture length can be formally defined without reference to the physical process of mixture, the time correlation function makes it possible to think of a mixture length roughly proportional to the average length of path which a particle traverses before its velocity becomes uncorrelated with that which it had at the beginning of the path. This method of describing diffusion makes it possible to define a mixture length without considering any physical process, but it involves the assumption that the particles of the diffusing substance are indistinguishable so far as their motion is concerned from those of the transporting fluid. Since turbulent diffusion is mostly due to eddies of the large sizes and the large part of the Lagrangian correlation-time curve is also due to them, one would only expect molecular diffusion to affect turbulent diffusion if the amount of material which could diffuse by molecular processes from a large-scale eddy were appreciable during the period over which its velocity preserves appreciable correlation with its initial velocity.

Discussion of Taylor's Turbulent Diffusion Theory.

Lagrangian theory of Diffusion by Continuous Movement predicts correctly a linear relationship between $\overline{Y^2}$ and time for all periods of time greater than that of $R_L = o$ (Equation 3-36). It also offers means of determining the Lagrangian r.m.s. fluctuating velocity from

the initial slope of the $\overline{Y^2}$ curve. The eddy diffusion coefficient is expressed in terms of a Lagrangian r.m.s. velocity and an integral scale which can be determined from the Lagrangian correlation function.

What Taylor conceived of is a fluid molecule that retains its identity while wandering in the turbulent field. His theory does not tell us the functional form of the correlation coefficient. The determination of R_L from actual diffusion data is also very difficult and inaccurate since it involves a double differentiation technique (Equation 3-31). Flint, Kada, and Hanratty (25) found that the form of the $\overline{Y^2}$ vs. t curve is not sensitive to the form of the correlation coefficient and that very accurate measurements at small diffusion times would be needed to discern which function describes R_L best.

The effectiveness and utility of Taylor's theory would have been considerably enhanced had the theory related the Eulerian and Lagrangian correlation coefficients or integral scales. This would bridge the present gap between two important fields, the Eulerian statistical theory of turbulence and another area of greater interest to the chemical engineer which is mass, heat, and momentum transfer in turbulent single phase flow. Until the Lagrangian and Eulerian domains are related so that turbulent diffusion mixing data may be predicted from hot

wire anemometer measurements, the Lagrangian conception remains an interesting curiosity and the eddy diffusion coefficient would still have to be determined from actual mass transfer data.

Taylor's Lagrangian model proposes a fluid particle or molecule that is so small that it may only exchange its contents with the surroundings by molecular mechanisms. Turbulent diffusion is then assumed to occur by the Lagrangian motion of the particle itself rather than by mechanical shear effects.

Previous Attempts to Relate Eulerian and Lagrangian Statistical Properties

Recent work has been aimed at relating the Lagrangian and Eulerian integral scales (3, 4, 55, 58). Mickelsen (58) made turbulent diffusion measurements over the central core of open pipe flow for the purpose of comparing them with Eulerian correlation hot wire data taken under the same conditions. The data were taken close to the source mostly over the region where $\overline{Y^2}$ is not a linear function of x. Since the Eulerian and Lagrangian correlation coefficients appear to be similar in shape, Mickelsen assumed both to have the same functional form, and that their space and time coordinates can be related by a linear proportionality.

i.e., $$R_{yv} = R_L\left(\frac{y}{B\left(\overline{v^2}\right)^{\frac{1}{2}}}\right) \qquad (3\text{-}39)$$

R_{yv} is the Eulerian correlation coefficient defined as:

$$R_{yv} = \frac{\overline{v_1 \, v_2}}{\overline{v^2}}$$

Where $\overline{v_1 \, v_2}$ is the time average of the instantaneous product $v_1 \, v_2$. v_1 and v_2 are the instantaneous fluctuating velocities at points 1 and 2 spaced apart by a distance y. B is a numerical factor of proportionality which was determined by the cross plotting of the independent variables of Equation (3-39) corresponding to the same values of the Eulerian and Lagrangian spreading coefficients ω_f and ω_T respectively.

$$\omega_T = \overline{v^2} \int_0^t \int_0^t R_L \, dt \, dt \qquad (3\text{-}40)$$

$$\omega_f = \int_0^y \int_0^y R_{yv} \, dy \, dy \qquad (3\text{-}41)$$

Spreading coefficients were used in order to avoid a severe double differentiation of experimental $\overline{Y^2}$ data at points near the source and to use a double integration of R_{yv} instead. The proportionality constant, B, determined by this method varied between 0.55 and 0.72 over a range of turbulent intensities from 1.8 to 14 f.p.s.; Mickelsen suggested that B is roughly equal to 0.6.

The assumption that R_L and R_{yv} have the same functional form is an approximation since R_{yv} is known to attain negative values whereas R_L remains always positive.

Also, R_{yv} was assumed equal to R_{xu} which is valid only in homogeneous isotropic turbulence. Mickelsen reported a 20 per cent deviation in homogeneity and 13 per cent deviation in isotropy over the central core.

Baldwin (3, 4) used an empirical approach similar to that of Mickelsen for relating the Eulerian and Lagrangian domains. The assumptions made here are essentially the same as those mentioned above except that the empirical factor defined by Baldwin is a function of distance or time rather than an absolute numerical constant.

$$\int_0^{kx} \int_0^{kx'} R_{xu}\, dkx''\, dkx' = \frac{1}{2}\overline{Y^2} = v_L^2 \int_0^{t} \int_0^{t'} R_L\, dt''\, dt' \qquad (3\text{-}42)$$

$$x = \frac{v'_L t}{k} \qquad (3\text{-}43)$$

t = Lagrangian time variable

k = Baldwin's empirical factor defined by Equations (3-42) and (3-43).

$v'_L = \sqrt{\overline{v_L^2}}$ = r.m.s. Lagrangian fluctuating velocity.

The method is a refinement over Mickelsen's in that k is a function of distance though it was treated as a constant over any numerical increment and also in that actual v'_L values determined from the initial slope of the $\overline{Y^2}$ curve were used. The empirical factor k transforms the distance axis x or y of the Eulerian

correlation coefficient. For each flow condition, k was found to be approximately constant over the entire range of x and t but varied from about 0.28 to 0.14 and u' varied from 2.1 to 4.8. As in Mickelsen's work, R_{xu} was measured and assumed to be equal to R_{yv}. The ratio $\frac{v'}{u'}$ varied over the central core between 0.7 and 0.8 instead of 1.0 for perfect isotropy.

Baldwin also reanalyzed Mickelsen's data using this method and obtained values of k ranging from 0.2 to 0.5 (4). Although this may be considered to be in qualitative agreement with Baldwin's k data, the results obtained showed no evidence of the existence of a simple relationship between k and turbulence parameters characterizing the field.

Proposed Theory and Model
Turbulent Diffusion by Microscopic Deformation

This treatment deals with the unsolved problem of relating the turbulent diffusivity, or Lagrangian properties, to Eulerian turbulence quantities. As shown below, this is done without employing Taylor's turbulent diffusion theory or making use of the Lagrangian system.

Physical Considerations

Instead of dealing with infinitesimal fluid particles as Taylor did, consider finite fluid plumes or lumps. The smallest size of these lumps is of the

same order as the smallest scale of turbulent motion which is roughly a hundred times that of a fluid particle. The fluid occupying a fixed Eulerian volume moving with the mean local velocity, U, is subjected to instantaneous fluctuating stresses that cause its deformation and strain. This should result into continued material exchange and flux across the boundaries of this fixed volume which is referred to here as turbulent diffusion by microscopic deformation. The fluctuating turbulent motion causing microscopic deformation would produce also concentration or temperature fluctuations if such gradients exist across the field.

Microscopic turbulent deformation is a mechanical shear phenomena that is associated with turbulent energy dissipation into heat (fluid lumps, unlike molecules, are neither rigid nor elastic; also the motion of such real viscous fluids is not frictionless).

An Eulerian analysis of this sort is based on total deformation and differs from earlier models in that a fluid lump does not retain its identity and is constantly exchanging its transferable properties with its surroundings. The exchange is predominantly mechanical and is not limited to molecular diffusion or conduction. Unlike Boussinesq, Prandtl and Von Karman theories, the degree of mixing or dispersion is assumed here not only dependent on the velocity gradient, or macroscopic

deformation, but also on the microscopic turbulent deformation and its intensity or the frequency and intensity of velocity fluctuation. The turbulent diffusion coefficient assumes, therefore, a finite value at the pipe axis, where a zero velocity gradient exists, since turbulent deformation is finite. It may be recalled that one of the difficulties with the Mixing Length Theory is that it predicts incorrectly a zero eddy viscosity at the tube axis.

Another way of explaining turbulent diffusion by microscopic deformation is that large eddies are strained and deformed until they finally break down into smaller and smaller eddies. These eddies are dispersed in the turbulent stream and consequently transport all transferable properties such as kinetic energy, mass or heat. Townsend (96) and Hinze (36) suggest that larger eddies attached to the wall absorb energy from the mean velocity gradient, break away from the wall, and become free, detached eddies that orient themselves according to the applying strains. These free eddies diffuse by turbulence toward the inner regions of the pipe section (the center), thereby transporting their kinetic energy but at the same time decaying into smaller eddies that dissipate energy. As these fine eddies dissipate their kinetic energy, they turn into energy poor fluid lumps that flow back to the

wall where they are sheared again by the mean motion into smaller high intensity eddies.

According to the Similarity and Local Isotropy theories, at high Reynolds numbers the motion of the smallest eddies of the highest wave numbers is uniquely determined by the local rate of energy dissipation, ε', and the kinematic viscosity ν. These eddies behave like similar eddies in free turbulence and are independent of external conditions causing anisotropy such as the finite pipe diameter and wall effects. They dissipate their energy by viscous effects and are isotropic despite the anisotropy of the flow.

All evidences available indicate that the larger eddies in pipe or channel flow are anisotropic. That is their size and motion are not independent of the characteristic conduit dimension (or pipe diameter). Kolmogoroff's second hypothesis concerning the larger eddies of the inertial subrange (45) is not believed to apply to the larger eddies in pipe flow. In other words their motion is not solely determined by the rate of energy dissipation, and the average size of these eddies would not be properly expressed by an inherent length scale obtained from u' and ε'. The assumption of isotropy over the pipe core is a simplifying assumption that is only approached at the pipe center. It is normally made because it simplifies the treatment of

turbulence measurements considerably. However, a certain degree of anisotropy prevails over the core; in fact, the wall effect is felt all the way to the pipe axis. Correlation functions are known to fall off much more rapidly in the traversal direction than in the axial direction (96). Laufer's spatial correlation measurements in a two-dimensional channel showed that longitudinal correlation in the axial direction extends over much larger distances than transverse correlations. Seagrave and Fahien (76) reported the axial eddy diffusivity at pipe axis which was 210 times α_r at Re = 7500 and 460 α_r at Re = 5000. All these evidences show that the large eddies in the core region are anisotropic and are elongated in the axial direction (36, 96). Their diameter as determined from the scale of turbulence is said to be roughly equal to one-quarter to one-half the radius of the pipe and is nearly constant in the core region (36).

The above qualitative account suggests that one could write:

$$\alpha_c = f\,(D'_{xy},\ d,\ \nu) \qquad (3\text{-}44)$$

where

D'_{xy} = the intensity of turbulent deformation (see below)

d = pipe diameter

ν = kinematic viscosity

A Lagrangian analysis of lump deformation deals with the relative motion of two fluid particles that are initially very close to each other. Dispersion or turbulent diffusion in this case may be considered a function of the rate of separation of these two particles which will be affected by turbulent motions of all wave numbers. The result showed that a small spherical element is ultimately drawn into a long thin ribbon and that the rate of dimensional change or deformation is an exponential function of time. We are interested here in an Eulerian rather than Lagrangian deformation analysis.

Development of Microscopic Deformation Theory by Extension of Prandtl's Theory

This development is limited to isotropic fields in orthogonal coordinate systems. A general eddy diffusivity equation for mass transfer is

$$\underline{J} = - \underset{\sim}{\alpha} \cdot \nabla \underline{C}$$

where

$\underline{J}$ = mass flux

$\underset{\sim}{\alpha}$ = eddy diffusivity tensor

All nondiagonal elements of $\underset{\sim}{\alpha}$ are zero; also

because of isotropy,

$$\alpha_{11} = \alpha_{22} = \alpha_{33} = \alpha_c$$

In this Eulerian treatment it is postulated that α_{ij} is a function of the deformation rate tensor, D_{ij}. For isotropic turbulence, α_c is related to the contraction or double dot product of D_{ij} which is a scalar quantity that is henceforth treated as such.

$$\overline{D_{ij}D_{ij}} = b\,\overline{D_{xy}^2} \tag{3-45}$$

or

$$\overline{\underset{\sim}{D} : \underset{\sim}{D}} = b\,\overline{D_{xy}^2}$$

b is a scalar constant that is not a factor in the analysis.

The deformation rate tensor, D_{ij}, can be obtained from the spatial variation of the velocity U_i due to the stress tensor τ_{ij} in cartesian tensors as follows:

$$\frac{\partial}{\partial x_j} U_i = \frac{1}{2}\left(\frac{\partial U_i}{\partial x_j} + \frac{\partial U_j}{\partial x_i}\right) + \frac{1}{2}\left(\frac{\partial U_i}{\partial x_j} - \frac{\partial U_j}{\partial x_i}\right) \tag{3-46}$$

The symmetrical part of this second order tensor D_{ij} determines the deformation of the fluid and is called the deformation tensor

$$D_{ij} = \frac{\partial U_i}{\partial x_j} + \frac{\partial U_j}{\partial x_i} \tag{3-47}$$

The second term in Equation (3-46) is the antisymmetrical part which determines rotation without deformation and is identified with vorticity.

For incompressible laminar flow D_{ij} is a steady nonfluctuating quantity that is related to the stress tensor by

$$\sigma_{ij} = \mu D_{ij} \tag{3-48}$$

In case of turbulent flow both the stress and deformation tensors are fluctuating quantities. One could therefore express these variables in the form of time averaged mean square values. The xy tensor element of the deformation tensor is representative of $D_{ij}D_{ij}$ for isotropic turbulence and is written as:

$$D_{xy}(t) = \frac{\partial U(t)}{dy} + \frac{\partial v}{\partial x} \tag{3-49}$$

where $U(t) = U + u$

U being the time mean velocity and u the fluctuating component.

i.e., $$D_{xy}(t) = \frac{\partial U}{\partial y} + \frac{\partial u}{\partial y} + \frac{\partial v}{\partial x} \tag{3-50}$$

The first term accounts for the <u>macroscopic deformation</u> or velocity gradient effect. The total deformation thus is expressed in terms of mean and fluctuating deformations.

$$D_{xy}(t) = \overline{D_{xy}} + D_{xy} \tag{3-51}$$

Equation (3-44) which is based on the postulated physical model can be now written more clearly in this general form:

$$\alpha_{ij} = f\,(d, \nu, D'_{ij})$$

or

$$\alpha = f\left(d, \nu, \left[\overline{D_{xy}^{2}(t)}\right]^{\frac{1}{2}}\right) \tag{3-52}$$

This may be regarded as an extension of Prandtl's theory which expressed the eddy viscosity, ϵ, for nonisotropic turbulent flow in terms of the mixing length, ℓ, and the velocity gradient:

$$\epsilon = \ell^2 \left|\frac{\partial U}{\partial y}\right| \tag{3-22}$$

A similar equation can be written for eddy diffusivity,

$$\alpha = \ell_L^2 \left|\frac{\partial U}{\partial y}\right|$$

Where ℓ_L is the mixing length for mass or heat transfer which has been referred to as the Lagrangian integral scale and is normally related to α by:

$$\alpha = v' \ell_L$$

Prandtl's theory is extended here by making the hypothesis

that turbulent diffusion is a function of the total instantaneous velocity spectrum and fluctuations. That is α is written here as a function of total instantaneous deformation rather than macroscopic deformation or mean velocity gradient only. One may now proceed to express $\left[\overline{D_{xy}^2(t)}\right]^{\frac{1}{2}}$ in terms of the mean squares of the turbulent velocity gradients or the local dissipation terms. The assumptions of isotropy and flat velocity profile over the core imply a zero velocity gradient or a zero mean deformation so that the total instantaneous deformation is equal to the turbulent deformation:

$$D_{xy} = \frac{\partial u}{\partial y} + \frac{\partial v}{\partial x} \tag{3-53}$$

The mean square turbulent deformation $\overline{D_{xy}^2}$ is

$$\overline{D_{xy}^2} = \overline{\left(\frac{\partial u}{\partial y}\right)^2} + 2\,\overline{\frac{\partial v}{\partial x}\frac{\partial u}{\partial y}} + \overline{\left(\frac{\partial v}{\partial x}\right)^2}$$

For isotropic turbulence,

$$\overline{\left(\frac{\partial v}{\partial x}\right)^2} = \overline{\left(\frac{\partial u}{\partial y}\right)^2}$$

i.e.,
$$\overline{D_{xy}^2} = 2\,\overline{\left(\frac{\partial u}{\partial y}\right)^2} + 2\,\overline{\frac{\partial v}{\partial x}\frac{\partial u}{\partial y}} \tag{3-54}$$

Hinze (32) showed that:

$$\overline{\left(\frac{\partial v}{\partial x}\right)\left(\frac{\partial u}{\partial y}\right)} = \frac{u'^2}{2}\left[\frac{\partial^2 R_{xu}}{\partial x^2}\right]_{x=0}$$

By substituting for $\left[\frac{\partial^2 R_{xu}}{\partial x^2}\right]_{x=0}$ from Equation (3-16)

Equation (3-50) is obtained:

$$\overline{\left(\frac{\partial v}{\partial x}\right)\left(\frac{\partial u}{\partial y}\right)} = -\frac{u'^2}{\lambda_f^2} \qquad (3\text{-}55)$$

But according to Equation (3-17)

$$\frac{\overline{u^2}}{\lambda_f^2} = \frac{1}{2}\overline{\left(\frac{\partial u}{\partial x}\right)^2} \qquad (3\text{-}17)$$

Also for isotropic turbulence,

$$\overline{\left(\frac{\partial u}{\partial y}\right)^2} = 2\overline{\left(\frac{\partial u}{\partial x}\right)^2} \qquad (3\text{-}10)$$

Therefore

$$\overline{\left(\frac{\partial v}{\partial x}\right)\left(\frac{\partial u}{\partial y}\right)} = -\frac{1}{4}\overline{\left(\frac{\partial u}{\partial y}\right)^2} \qquad (3\text{-}56)$$

From Equations (3-54) and (3-55), the mean square turbulent deformation $\overline{D_{xy}^2}$ can be written as:

$$\overline{D_{xy}^2} = 1.5\overline{\left(\frac{\partial u}{\partial y}\right)^2} = 3\overline{\left(\frac{\partial u}{\partial x}\right)^2} \qquad (3\text{-}57)$$

or

$$D'_{xy} = \sqrt{\overline{D_{xy}^2}} = \sqrt{3}\left[\overline{\left(\frac{\partial u}{\partial x}\right)^2}\right]^{\frac{1}{2}} \qquad (3\text{-}58)$$

D'_{xy} may be regarded as a measure of the intensity of microscopic turbulent deformation and will be referred to here as such.

For the more general case of homogeneous nonisotropic turbulence, $\overline{D_{xy}(t)^2}$ can be obtained by averaging, with respect to time, the square of Equation (3-50):

$$\overline{D_{xy}(t)^2} = \left(\frac{\partial U}{\partial y}\right)^2 + 2\,\overline{\frac{\partial U}{\partial y}\frac{\partial u}{\partial y}} + 2\,\overline{\frac{\partial v}{\partial x}\frac{\partial U}{\partial y}} + \overline{\left(\frac{\partial u}{\partial y}\right)^2} +$$

$$2\,\overline{\frac{\partial v}{\partial x}\frac{\partial u}{\partial y}} + \overline{\left(\frac{\partial v}{\partial x}\right)^2} \qquad (3\text{-}59)$$

Since U is not a function of time

$$\overline{\frac{\partial U}{\partial y}\frac{\partial u}{\partial y}} = \frac{\partial U}{\partial y}\left(\overline{\frac{\partial u}{\partial y}}\right) \qquad (3\text{-}60)$$

Also for homogeneous turbulence,

$$\overline{\frac{\partial u}{\partial y}} = 0 \text{ and } \overline{\frac{\partial v}{\partial x}} = 0$$

The second and third terms of Equation (3-59) drop out and we get the following equation for nonisotropic flow.

$$\overline{D_{xy}(t)^2} = \left(\frac{\partial U}{\partial y}\right)^2 + 2\,\overline{\frac{\partial v}{\partial x}\frac{\partial u}{\partial y}} + \overline{\left(\frac{\partial u}{\partial y}\right)^2} + \overline{\left(\frac{\partial v}{\partial x}\right)^2} \qquad (3\text{-}61)$$

i.e.,

$$\overline{D_{xy}(t)^2} = \overline{D_{xy}}^2 + D'^2_{xy} \tag{3-62}$$

$$\overline{D_{xy}} = \frac{\partial U}{\partial y}$$

$$D'^2_{xy} = \overline{\left(\frac{\partial u}{\partial y}\right)^2} + \overline{\left(\frac{\partial v}{\partial x}\right)^2} + 2\,\overline{\frac{\partial v}{\partial x}\frac{\partial u}{\partial y}} \tag{3-63}$$

Equation (3-63) reduces to (3-57) upon making the appropriate substitutions for isotropic turbulence.

Since for the isotropic turbulent core $\overline{D_{xy}} = 0$, Equation (3-62) becomes,

$$\overline{D_{xy}(t)^2} = D'^2_{xy} \tag{3-64}$$

Equation (3-52) is then written as

$$\alpha_c = f\,(D'_{xy},\ d,\ \nu) \tag{3-44}$$

where

$$D'_{xy} = \sqrt{3}\left[\overline{\left(\frac{\partial u}{\partial x}\right)^2}\right]^{\frac{1}{2}} \tag{3-58}$$

Equation (3-44) may be written in dimensionless form:

$$\frac{\alpha_c}{\nu} = f\left(\frac{D'_{xy}\ d^2}{\nu}\right) \tag{3-65}$$

Turbulent Diffusion by Microscopic Deformation Comparison of Theory with Experimental Data

Turbulent deformation intensities are calculated in this section from available turbulence measurements for

pipe flow by applying the equations given in Appendix A. The deformation data are then treated to determine if the turbulent diffusion coefficient and the Eulerian intensity of deformation are directly related.

The condition of isotropy was only approached but not fulfilled in the different sets of data treated here. Even at the center line appreciable departures from isotropy were reported. The deviation was more pronounced at lower Reynolds numbers and for smaller diameter pipes. All the deformation data presented below were computed from turbulence data measured at the pipe axis. Positional variations in D'_{xy}, λ_f or ξ' were found to be small and are perhaps of the same size as radial variations in α within the core. Directional variations in D'_{xy} due to the lack of true isotropy are believed responsible for the scatter shown in Figure 13. The lowest and highest D'_{xy} values were calculated from actual u', v' and w' data and plotted in this figure; the same procedure was followed for calculating ξ' data of Figure 14.

All Reynolds numbers used here are average Reynolds numbers based on the average bulk velocity, V, rather than axial Reynolds numbers, Re_c, based on the maximum velocity U_o. Since some authors reported U_o data only, the average bulk velocity was calculated from U_o by means of Nunner's velocity correlation (61)

or the modified correlation suggested by Senecal (77) and Rothfus and Monrad (68). The relationship between U_o and V is discussed in detail in Chapter IV.

Baldwin (3) reported microscale data computed from energy spectrum measurements. The intensity of turbulence, $\frac{u'}{U_o}$, over the entire range of velocities was checked by Sandborn and found to be 0.035. This value was later reported by Baldwin (4) who feels that it is more accurate than the values reported in his dissertation. Isotropy data scattered somewhat; Baldwin felt that $\frac{v'}{u'}$ was approximately 0.7-0.8; a $\frac{v'}{u'}$ ratio of 0.75 was used for computing the data of Table VII. Turbulence measurements made at U_o = 160 f.p.s. are not included here since they are less certain than those at lower velocities. Their deviations could be due to the faster resolution required at higher velocities. This was the earliest set of measurements made by Baldwin.

Laufer (46, 47) kindly made available his actual numerical data on the intensity of turbulence and dissipation terms which were used here for computing deformation and dissipation parameters.

Figure 12 is a plot of the second moment of Taylor's one dimensional energy spectrum function versus the frequency, n, as computed from a smoothed plotting of Sandborn's actual numerical spectrum data which were

TABLE VII

MEAN SQUARE DEFORMATIONS COMPUTED FROM TURBULENCE DATA

Re	242000	360000	460000	41000	425000	41000	186000	201000	41000	85400	78000
Re_c	290400	424000	540000	50000	500000	50000	--	--	50000	100000	80500
Fluid	Air	Air	Air	Air	Air	Air	Air	Air	Water	Water	Water
Source of Data	Baldwin and Walsh (3, 4)			Laufer (46, 47)		Sandborn (70, 71)	Brookshire (11)		Cohen & Brodkey (13)		Kalinske & Van Driest (40)
Type of Measurement	spectrum			velocity differentiation		spectrum	velocity differentiation		velocity differentiation		correlation coefficient
Isotropy $\frac{\overline{v'}}{\overline{u'}}$ or $\frac{\overline{w'}}{\overline{u'}}$	0.75	0.75	0.75	0.96	0.88	0.83	0.57	--	0.93	0.83	0.89
u' f.p.s.	2.54	3.71	4.73	0.32	3.00	0.89	3.22	3.45	0.094	0.22	0.065
λ_f ft.	0.02	0.016	0.014	--	--	--	0.017	0.017	0.0084	0.009	0.0467
$\overline{\left(\frac{\partial u}{\partial x}\right)^2}$	--	--	--	103.3	91556	--	--	--	--	--	--
$\overline{r^2}$	--	--	--	--	--	76065	--	--	--	--	11.2
$\overline{D^2_{xy}}$ based on u	$(9.66)(10^4)$	$(32.27)(10^4)$	$(68.34)(10^4)$	$(3.10)(10^2)$	$(10.51)(10^4)$	11662	$(21.60)(10^4)$	$(25.51)(10^4)$	$(7.44)(10^2)$	$(3.59)(10^3)$	11.6
$\overline{\left(\frac{\partial v'}{\partial x}\right)^2}$	--	--	--	0.307	2.65	0.75	--	--	0.088	0.187	0.058
$\overline{D^2_{xy}}$ based on v	$(5.43)(10^4)$	$(18.15)(10^4)$	$(38.44)(10^4)$	$(3.65)(10^2)$	$(13.70)(10^4)$	8369	--	--	$(6.52)(10^2)$	$(2.50)(10^3)$	9.0
$\overline{\left(\frac{\partial w'}{\partial x}\right)^2}$	--	--	--	--	--	0.73	--	--	0.086	0.181	--
	--	--	--	245.3	35037	--	--	--	--	--	--
$\overline{D^2_{xy}}$ based on w	--	--	--	$(3.68)(10^2)$	$(14.64)(10^4)$	7329	--	--	$(6.23)(10^2)$	$(2.43)(10^3)$	--

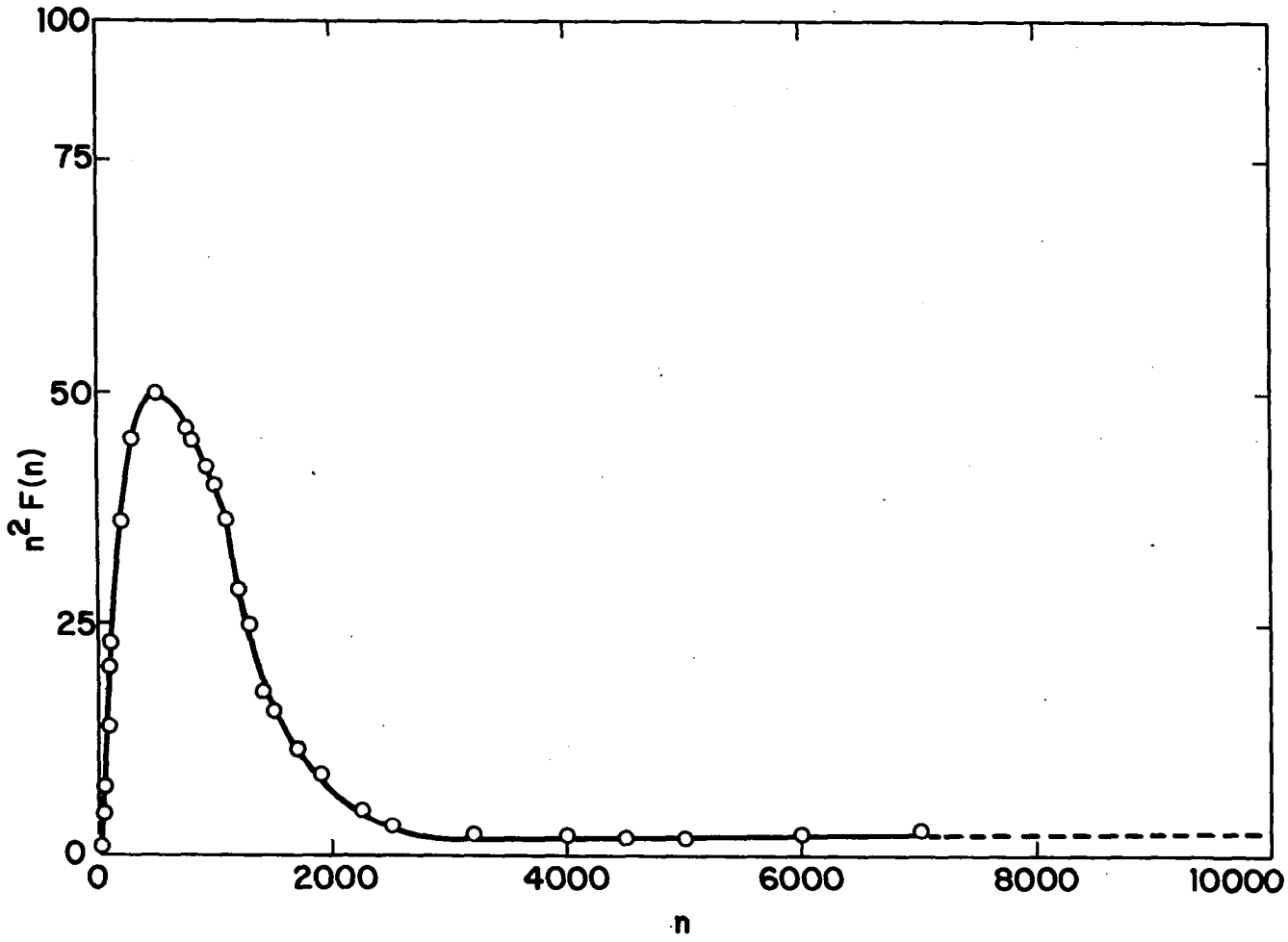


Fig. 12 DETERMINATION OF THE EXPECTED NUMBER OF ZERO VELOCITIES PER SECOND FROM SANDBORN'S SPECTRUM DATA

kindly made available by him (71). These numerical spectrum data are believed to be more correct than Figure 20 of his note (70). The intensity of deformation was calculated here from $\overline{n^2}$ which was determined by the graphical integration of Figure 12.

Brookshire (11) reported open pipe microscale data (λ_g) for air flow over a range of Reynolds number between 81800 and 201000. As he pointed out, the very high noise level made it difficult to obtain accurate λ_f measurements at the lower Reynolds numbers. The noise level was of the same order as the signal itself at Reynolds numbers below 81800. There was no clear pattern for the variation of λ_f with Re which led Brookshire to speculate that λ_f may be independent of Reynolds number. He also indicated that u' values measured in his work were considerably more accurate and reliable than the w' intensities. The two points given in Table VII are computed from his u' and λ_g data at the two highest Reynolds numbers.

Cohen (13) determined the intensities of turbulence and dissipation lengths or microscales for turbulent water flow in a pipe. These liquid flow data along with that of Lee and Brodkey (48, 49) were obtained using the highly sensitive constant temperature hot film anemometer. Earlier attempts to make

extensive turbulence measurements in liquid flow had not been very successful due to the lack of reliable sensing devices of high response and sensitivity that are suited for use in liquid flow.

Kalinske and Van Driest (40) made intensity and correlation coefficient measurements in open channel water flow by injecting a colored dye and photographing the fluctuations at the tip of the injector using a high speed motion camera. The data did not agree with Karman-Howarth equation indicating the lack of true isotropy. This visual technique is less accurate than the hot film anemometer method.

Experimental deformation and eddy diffusivity data obtained from Table VII and Equation (2-14) were used for plotting $\frac{\alpha_c}{\nu}$ versus $D'_{xy}\ d^2/\nu$ (Figure 13). The results are also listed in Table VIII. The excellent correlation shown by Figure 13 demonstrates a very good agreement between the proposed theory and available data. The data for air flow were fitted by the least square method using both extreme directional deformation values and the following equation was obtained:

$$\frac{\alpha_c}{\nu} = 0.091 \left(\frac{D'_{xy}\ d^2}{\nu}\right)^{0.605} \qquad (3\text{-}66)$$

Correlation coefficient = 0.9815

Cohen's data for water flow fell on a line parallel to the correlation line of air flow data. The author is inclined to believe that the difference in the coefficient is due to experimental errors rather than a real effect. Water flow data are too meager and sensitive to slight errors in ν and D'_{xy}. Water flow temperature was not given in this work and was assumed 20°C. for calculating ν. Also there are many difficulties associated with the operation of the hot film anemometer in liquid systems. Therefore turbulence measurements are more accurate for air flow than water flow. The authors suggested a probable 10% error in intensity measurements (13). Water flow points fall closer to the air correlation line when ν is introduced as one of the variables.

Taylor (85) showed that for isotropic turbulence, the rate of energy dissipation per unit mass per unit time, ε' is

$$\varepsilon' = 7.5\,\nu\overline{\left(\frac{\partial u}{\partial y}\right)^2} \qquad (3\text{-}9)$$

Other dissipative quantities can be readily related to ε' by the following equations:

$$\varepsilon' = 15\,\nu\overline{\left(\frac{\partial u}{\partial x}\right)^2} \qquad (3\text{-}11)$$

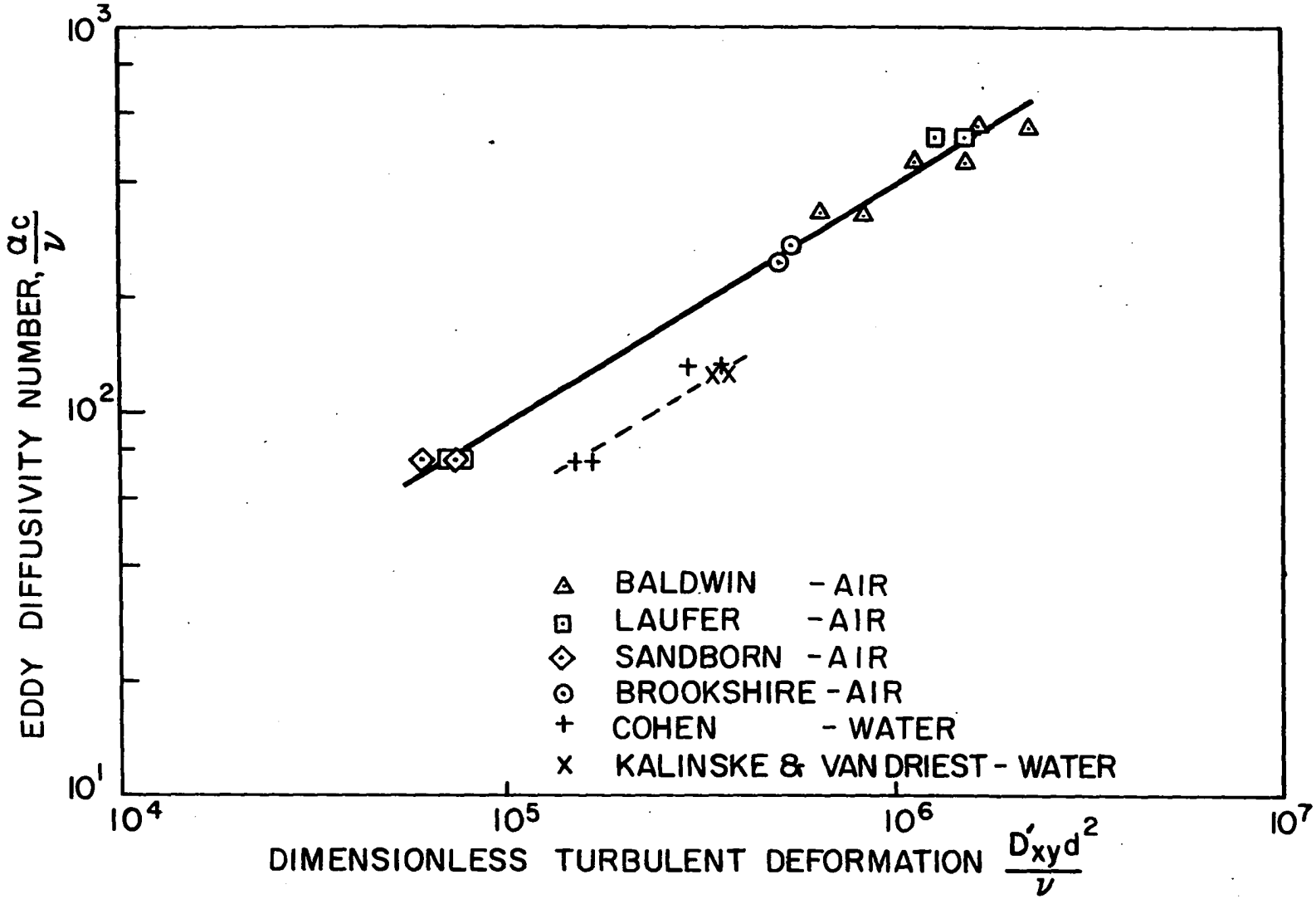


Fig. 13 EDDY DIFFUSIVITY NUMBER vs DIMENSIONLESS TURBULENT DEFORMATION

TABLE VIII

DIMENSIONLESS TURBULENT DEFORMATION VERSUS

EDDY DIFFUSIVITY NUMBER

	$D'_{xy}\ d^2/\nu$			
	Lowest Directional Value	Highest Directional Value	$\frac{\alpha_c}{\nu}$	Fluid
242000	$(62.98)(10^4)$	$(83.98)(10^4)$	328	Air
360000	$(115.07)(10^4)$	$(153.43)(10^4)$	445	Air
460000	$(167.47)(10^4)$	$(223.29)(10^4)$	544	Air
41000	$(5.9800)(10^4)$	$(7.32)(10^4)$	75.6	Air
41000	$(7.04)(10^4)$	$(7.70)(10^4)$	75.6	Air
425000	$(129.62)(10^4)$	$(152.84)(10^4)$	514	Air
186000	---	$(50.73)(10^4)$	250	Air
201000	---	$(55.12)(10^4)$	270	Air
41000	$(15.00)(10^4)$	$(16.39)(10^4)$	75.6	Water
85400	$(29.63)(10^4)$	$(36.02)(10^4)$	132	Water
78000*	$(34.40)(10^4)$	$(37.08)(10^4)$	126	Water

* Open channel

$$\varepsilon' = 30 \nu \frac{\overline{u^2}}{\lambda_f^2} \tag{3-67}$$

$$\varepsilon' = (73.95) \nu \left(\frac{v'}{U}\right) N_v^2 \tag{3-68}$$

$$\varepsilon' = 5 \nu \overline{D_{xy}^2} \tag{3-69}$$

Equation (3-69) relates the local rate of energy dissipation to the mean square deformation. Equation (3-66) could therefore be written in terms of the local rate of energy dissipation ε'.

Discussion

The results obtained in this chapter suggest that turbulent diffusion in pipe flow depends on both microscopic and macroscopic deformations, pipe diameter, and kinematic viscosity. This also means that the turbulent diffusivity and the local rate of energy dissipation are related. That is, the Lagrangian eddy diffusivity is related to measurable Eulerian turbulence quantities. The theory extends Prandtl's original Mixing Length Theory to include the effect of microscopic or turbulent deformations due to turbulent fluctuations.

The turbulent diffusion mechanism proposed here is in harmony with Townsend's (96) and Hinze's (36) explanation of the structure of turbulence in pipe flow.

Larger eddies attached to the wall absorb energy from the mean velocity gradient to break away from the wall as free detached eddies. These large eddies disintegrate into smaller and smaller free eddies. The smallest eddies dissipate energy into heat. The hypothesis made in this chapter is that the larger eddies or lumps deform and strain under the effect of both fluctuating turbulent and steady shear stresses. It is also postulated that material and thermal turbulent diffusivities depend on the intensity of such deformations. Since the intensity of deformation controls the rate of disintegration of lumps* or eddies into very small eddies of the micro-scale size, one could say that turbulent diffusion or dispersion depends on the rate of disintegration of the larger eddies. This microscopic turbulent deformation model differs from Taylor's Lagrangian model in that a lump, unlike a fluid particle, does not retain its identity as it travels in the turbulent field.

The dependence of α on ν follows from its dependence on ξ' (Equations (3-68) and (3-69)). Also, according to the Theory of Local Isotropy, the turbulent motion of the smallest eddies depends on ν and does not depend on external conditions such as vessel dimensions.

---

* Lumps differ from eddies in that a spinning motion is not required; lumps is more generic.

It is commonly understood (36) that the large eddies make a greater contribution to transport in turbulent flow. As pointed out earlier in this chapter, large eddies in pipe flow are believed anisotropic and dependent on pipe diameter. They are elongated in the axial direction.

The dependence of turbulent diffusivity on the local rate of energy dissipation may be further interpreted in the light of Laufer's experimental results on the structure of turbulence in fully developed pipe flow (46). He determined as a function of radial position the various energy terms in the energy equation written in cylindrical coordinates:

$$\overline{uv}\,\frac{dU}{dr} + \frac{1}{r}\frac{d}{dr}\,r\,\overline{v\left(\frac{u^2+u^2+w^2}{2}\right)} + \frac{1}{r}\frac{d}{dr}\left(\frac{\overline{pv}\,r}{\rho}\right) - \frac{\nu}{r}\frac{d}{dr}\,r\frac{d}{dr}\,\overline{\frac{u^2+u^2+w^2}{2}} + \nu\,\overline{\left(\frac{\partial v}{\partial x}\right)^2} = 0 \qquad (3\text{-}70)$$

The first term corresponds to the rate of production of turbulent energy by shearing stresses. The second and third terms represent the rate of energy change due to kinetic energy and potential energy transfer respectively by radial velocity fluctuations; they are usually referred to as diffusion terms. The fourth term expresses a gradient type of energy diffusion that is important only very

near the wall. The last term expresses the rate of energy dissipation into heat by viscosity action (46). Laufer's data showed that near the center, the local rate of energy dissipation equals the rate of energy diffusion (no energy production). The diffusion rate of potential energy was zero near the center and opposed the direction of kinetic energy diffusion over most of the pipe cross section.

Since the dissipation and diffusion rates are equal at the center, one could then say that turbulent diffusion may be a function of the energy diffusion rate. One would have to take the total energy diffusion rate (kinetic and potential) in order to account for the fact that α declines away from the center. This suggests that turbulent diffusion may be a function of the radial gradient of the sum of the Eulerian triple correlation functions and the pressure-velocity correlation function. This should be an interesting area for future experimental investigation.

It was shown in Chapter II that, in pipe flow, turbulent diffusivity is not dependent on molecular diffusivity and that molecular diffusivity makes its own small independent contribution to the total eddy diffusivity. This empirical result was taken into account in this chapter; turbulent diffusivity is not assumed a function of D_m. Several papers appeared in

recent years dealing with the spectrum function of scalar fluctuations such as temperature or concentration (16, 17, 18, 29, 83). Corrsin (17) proposed that the same wave number cascading mechanism of turbulent velocity spectrum could be applied to temperature or concentration fluctuations and that heat or mass would be dissipated at the highest wave number by molecular diffusion. Dissipation means here the smearing out of fluctuations. Later work by Corrsin (16) and Batchelor (5) suggested that, in decaying grid turbulence at $Sc \gg 1$, the rate of time decay of scalar quantities would not be strongly dependent on D_m. Keeler et al. (41) found no difference between the rates of decay of concentration fluctuation in systems differing in their molecular diffusivities by a factor of two. Corrsin proposed a cascade model that showed a sharp cut-off in the transfer rate at high wave numbers in the viscous region (18) which may also explain the lack of dependence on D_m found here and reported also by Keeler et al. (41).

Applicability of Kolmogoroff's Local Isotropy Theory. - The first hypothesis of the Theory of Local Isotropy is that the nonisotropy of the mean flow does not extend down to the motion of the smallest eddies, and that at sufficiently high Reynolds numbers there

is a range of high frequencies where the turbulence is statistically in equilibrium and is uniquely determined by the rate of energy dissipation ξ' and the kinematic viscosity ν (28, 44). The equilibrium is termed universal because the turbulence in this range is independent of external conditions. This first hypothesis would be expected to apply to turbulent pipe flow at high Reynolds numbers. The motion of the large eddies, however, is not universal or isotropic and depends on pipe diameter.

The second hypothesis says that at infinitely large Reynolds numbers, there is an inertial subrange at the lower end of the spectral equilibrium range where the average properties are solely determined by the rate of energy dissipation, ξ', and are independent of ν. That is, it is postulated that the dissipation in the region of frequencies very far below the region of maximum dissipation would be negligibly small compared with the flux of energy transferred by inertial effects (45, 6).

Equation (3-66) indicates that α_c is a function of ξ' and d which suggests that perhaps the major contributions to α_c come from the very large eddies and the intermediate eddies of the inertial subrange. One could write α_c by dimensional reasoning as follows:

$$\alpha_c = (\text{constant})\ (\xi'^{1/3}\ d^{4/3}) \tag{3-71}$$

This form was also proposed by others (97).

Reynolds number should be sufficiently large to fulfill the condition of statistical independence and for the existence of the inertial subrange. Hinze (33) suggested this condition to be:[1]

$$Re_\lambda^{3/4} \gg\gg 1 \tag{3-72}$$

where

$$Re_\lambda = \frac{u'\lambda_g}{\nu} \tag{3-73}$$

The lowest Re_λ for the data listed in Table VII is that of Laufer's data at $Re_c = 50000$; by substituting for λ_g in Equation (3-73), one gets:

$$Re_\lambda = \frac{u'^2}{\nu\left[\overline{\left(\frac{\partial u}{\partial x}\right)^2}\right]^{\frac{1}{2}}} \tag{3-74}$$

which gives $Re_\lambda^{3/4} \cong 22$

In other words $Re_\lambda^{3/4}$ for the data of Table VII is in excess of 22 which is $>> 1$.

The validity of the hypotheses and assumptions leading to Equation (3-71) can be tested by computing ξ' from the above equations using the data of Table VII

---

[1] The exact order of $Re_\lambda^{3/4}$ in this condition is not established.

and plotting α_c versus $\varepsilon'^{1/3} d^{4/3}$. The results are given in Table IX and plotted in Figure 14 which shows the lowest and highest directional $\varepsilon'^{1/3} d^{4/3}$ values. Considering the degree of accuracy of the turbulence data of Figure 14 and the deviation from isotropy, it can be concluded that the experimental data support Equation (3-71).

Summary of Conclusions

Turbulent diffusion in the core was found to be a function of the intensity of lump deformation, pipe diameter, and the kinematic viscosity. This is equivalent to saying that it is a function of the local rate of energy dissipation and pipe diameter.

Turbulent diffusion is postulated to occur by the motion of larger eddies to the inside of the pipe. These eddies or lumps deform and strain under the effect of permanent and fluctuating stresses until they break down into smaller and smaller eddies that disperse. Prandtl's Mixing Length Theory was extended here to include the microscopic deformation effect.

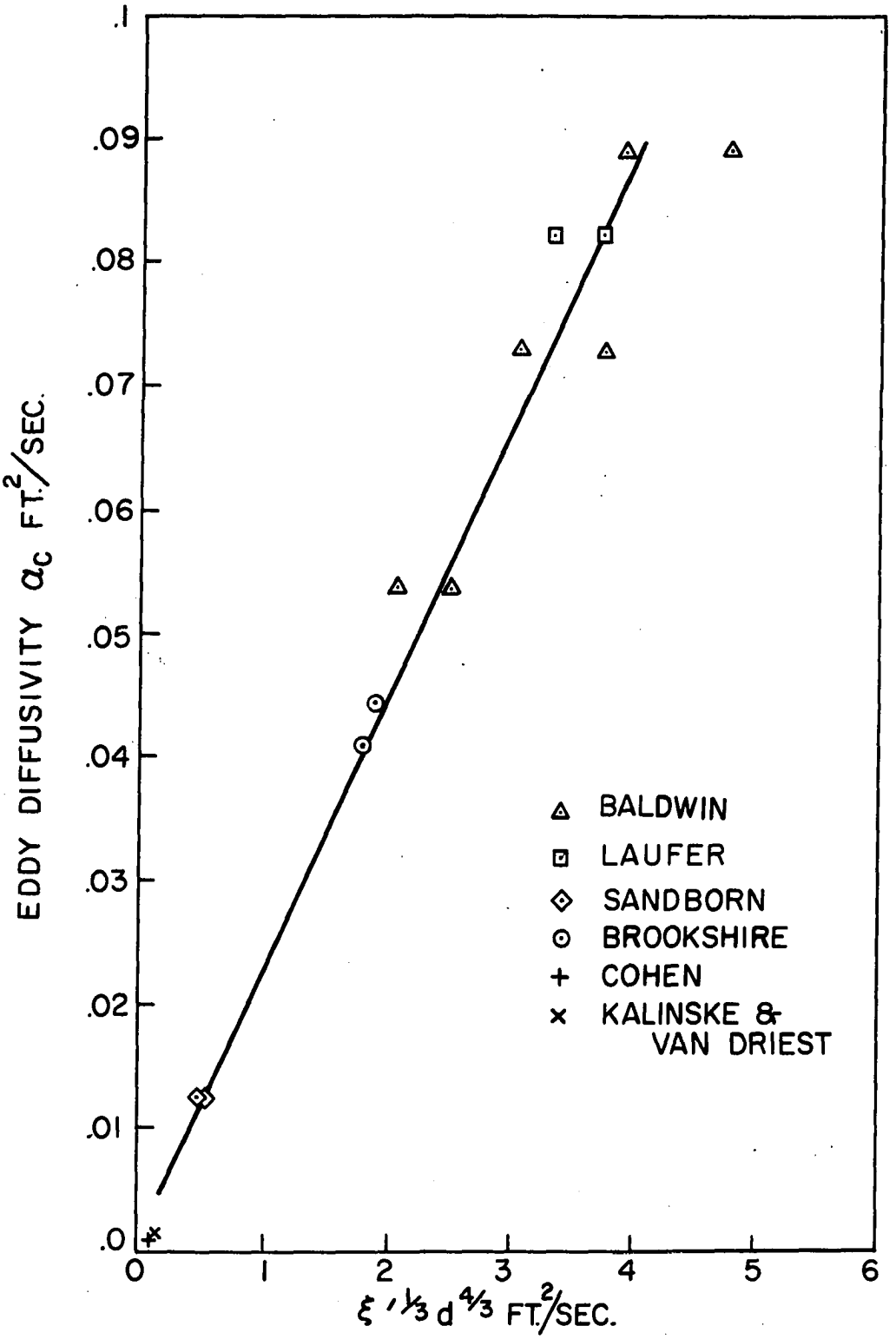


Fig. 14 APPLICATION OF LOCAL ISOTROPY THEORY TO TURBULENT DIFFUSION

TABLE IX

TURBULENT DISSIPATION DATA

Source of Data	Fluid	Re	d-(ft)	α_c* ft^2/sec	ε' Lowest	ε' Highest	$\varepsilon'^{1/3} d^{4/3}$ Lowest Value	$\varepsilon'^{1/3} d^{4/3}$ Highest Value
Baldwin (3)	Air	242000		0.0538	44.02	78.25	2.051	2.484
		360000	0.667	0.0730	148.84	264.6	3.074	3.724
		460000		0.089	311.37	553.55	3.934	4.766
Laufer (46)	Air	41000		0.0124	0.25	0.30	0.476	0.505
		425000	0.810	0.0843	86.2	120	3.33	3.724
Sandborn (70)	Air	41000		0.0124	6.42	9.56	0.429	0.490
Brookshire (11)	Air	186000	0.423	0.0410	--	177.12	--	1.783
		201000		0.0443	--	209.17	--	1.884
Cohen (13)	Water	41000	0.255	0.00082	0.034	0.040	0.052	0.055
		85400		0.001426	0.131	0.194	0.082	0.094
K. and V.**(40)	Water	78000	1.33	0.00136	0.0005	0.00063	0.1162	0.1252

* Obtained from Equation (2-14)

** Open channel

CHAPTER IV

TURBULENT DIFFUSION IN NONISOTROPIC PIPE FLOW

It is important to know the distribution of eddy diffusivity over the entire pipe cross section for the solution of problems dealing with mixing in chemical reactors and pipelines. The preceding two chapters dealt with the isotropic central core. The main purpose of this chapter is to examine the distribution of eddy diffusivity, eddy viscosity and mean velocity over the entire pipe cross section including the boundary layer.

Von Karman's universal velocity distribution is examined and compared with Nunner's power law equation (61). The eddy viscosity results obtained from the differentiation of these velocity equations are discussed and compared with later equations proposed by Lin et al. (52), Wasan, Tien, and Wilke (100), and Taylor (88). It is shown that some of these equations gave sharp discontinuities at the edge of the boundary layer. An equation is proposed for the distribution of eddy diffusivity over the pipe cross section. It is based on the assumption that eddy diffusivity is a function of average core diffusivity and degree of isotropy. The equation is compared with Seagrave's pipe flow data (75) and some of the parallel plate data

reported by Page et al. (62).

Review of Pertinent Equations

Mean Velocity Distribution

Several authors reviewed in detail the origin of different velocity correlations and compared them with experimental velocity profile data (30,34,72). The velocity correlations used in the following chapter for computing the axial mixing results and the average bulk velocity, V, are given in Table X. Nunner's equation (61) is perhaps less known than the logarithmic velocity distribution. He showed using his own data along with those of Nikuradse that n is related to λ by a simple relationship

$$\frac{1}{n} = \sqrt{\lambda} \qquad (4\text{-}8)$$

$$U = U_o\ (1-\theta)^{\frac{1}{n}} \qquad (4\text{-}9)$$

Earlier authors proposed different values of n for various ranges of Reynolds number. Figure 15 shows that the velocity distribution calculated at Re_c = 50,000 from Nunner equation agrees very well with Laufer's results (46) up to θ = 0.96. That is, Nunner equation is not satisfactory for predicting velocity distributions in the boundary layer where the data are in better agreement with Equation (4-2) of the universal logarithmic law.

Often the axial mean velocity is reported only and one has to determine the average bulk velocity. The simplest way to do this is to ignore the sublaminar layer

TABLE X

MEAN VELOCITY DISTRIBUTIONS

1. Von Karman's Universal Logarithmic Velocity distribution:

Sublaminar layer $(0 < y^+ < 5)$ $u^+ = y^+$ (4-1)

Buffer region $(5 < y^+ < 30)$ $u^+ = -3.05 + 5 \ln y^+$ (4-2)

Turbulent region $(y^+ > 30)$ $u^+ = 5.5 + 2.5 \ln y^+$ (4-3)

where:

$$u^+ = \frac{U}{U_*} \tag{4-4}$$

$$y^+ = \frac{y' U_*}{\nu} \tag{4-5}$$

$$U_* = \sqrt{\frac{\tau_w}{\rho}} \tag{4-6}$$

2. Nunner's Velocity distribution:

$$\frac{U}{U_o} = (1 - \theta)^{\sqrt{\lambda}} \tag{4-7}$$

U_o = axial mean velocity

λ = Moody friction factor = $8\left(\frac{U_*}{V}\right)^2$

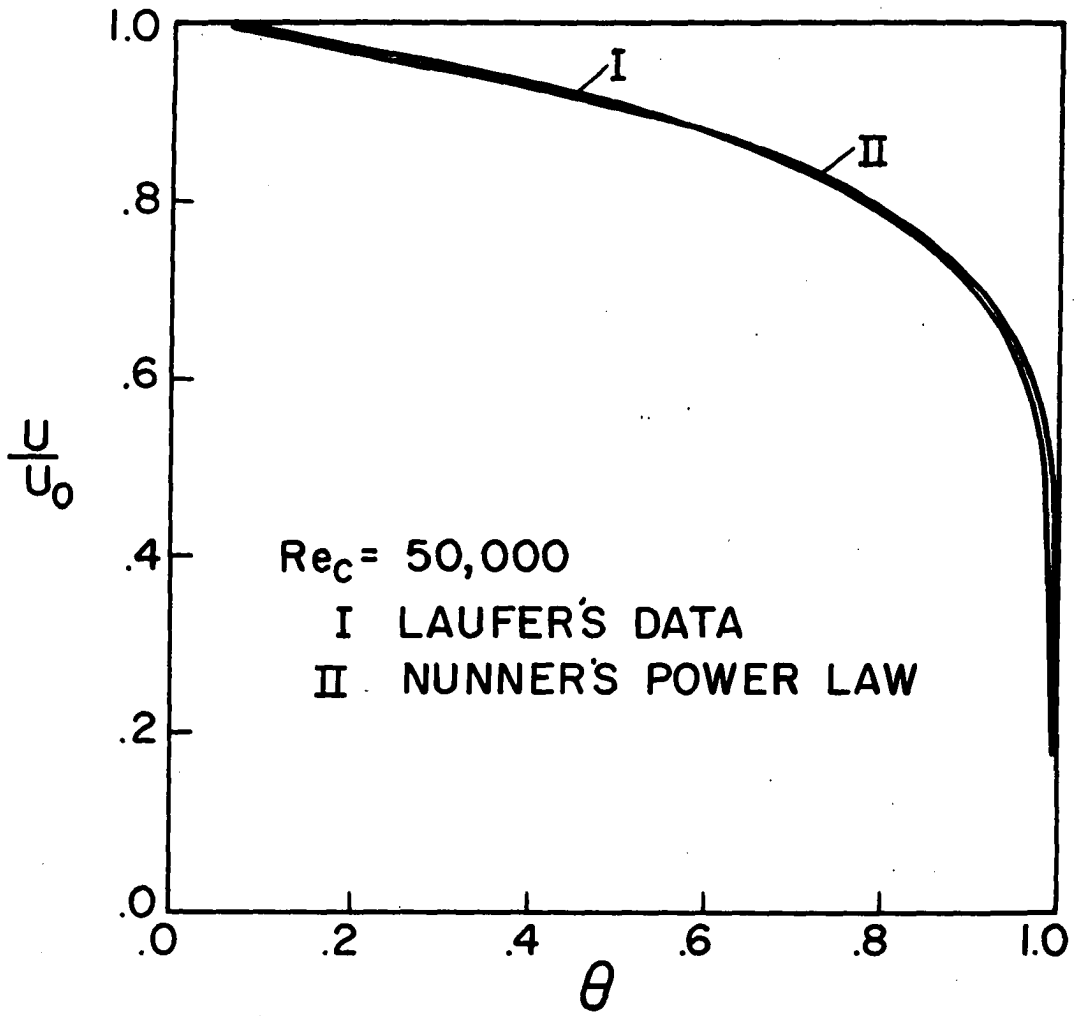


Fig.15 COMPARISON OF NUNNER'S EQN. WITH LAUFER'S DATA

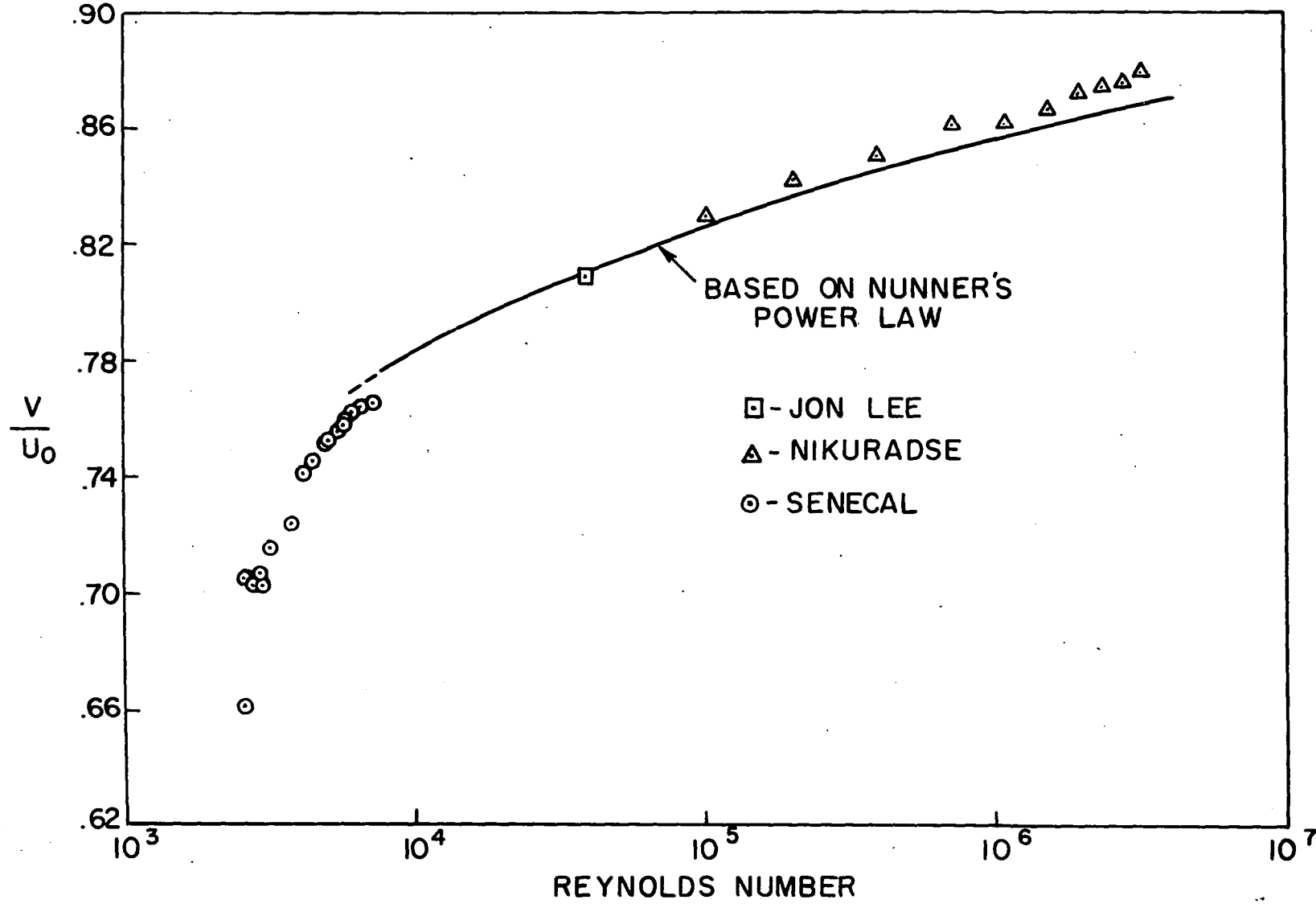


Fig. 16 RATIO OF BULK AVERAGE VELOCITY TO AXIAL VELOCITY AS A FUNCTION OF REYNOLDS NUMBER

and determine the average bulk velocity by integrating Nunner's power law over the entire cross section:

$$\frac{V}{U_o} = \int_o^a \pi d\,(1-\theta)^{\frac{1}{n}}\,dr = \frac{2n^2}{(1+n)\,(1+2n)} \qquad (4\text{-}10)$$

$$n = 1/\sqrt{\lambda}$$

Figure 16 shows a comparison of this equation with integrated profile data by Senecal (77) and Nikuradse (60), and an observed measurement by Jon Lee (48). The agreement is satisfactory for turbulent flow.

Eddy Viscosity

Eddy viscosity distribution equations can be obtained from shear stress and velocity gradient. The shear stress is assumed the product of radial position θ and shear stress at the wall, τ_w. Equations (4-11) and (4-12) are not valid at the pipe axis since they give a zero eddy viscosity at the axis where it is known to be finite (Table XI); both distributions are compared in Figure 17.

It can be seen from Equations (4-12) and (4-13) that a sharp discontinuity exists in the eddy viscosity curve, since ϵ at $y^+ = 30$, calculated from Equation (4-12), is twice that calculated from Equation (4-13) (Figures 18 and 19). Such a discontinuity is not known to exist and has not been observed experimentally which reflects the inadequacy of these empirical relationships.

TABLE XI

EDDY VISCOSITY DISTRIBUTIONS

Eddy Viscosity Distribution		Corresponding Velocity Distribution
$\epsilon = \frac{aVn\theta\ (1-\theta)^{\frac{n-1}{n}}}{4\ (1+n)\ (1+2n)}$	(4-11)	Nunner
$\epsilon = \frac{\lambda V^2 \theta\ a\ (1-\theta)}{20\ U_*}$	(4-12)	Von Karman-turbulent
$\epsilon = \frac{V^2 \lambda \theta\ a\ (1-\theta)}{40\ U_*}$	(4-13)	Von Karman-buffer

Lin's turbulent viscosity equations:

$$\frac{\epsilon_t}{\nu} = \frac{y^+}{5} - 0.959 \qquad (4\text{-}14) \qquad \text{buffer}$$

$$\frac{\epsilon_t}{\nu} = \left(\frac{y^+}{14.5}\right)^3 \qquad (4\text{-}15) \qquad \text{sublaminar}$$

Wasan's turbulent viscosity equation:

$$\frac{\epsilon_t}{\nu} = \frac{(4.16 \times 10^{-4})\ (y^+)^3 - (15.15 \times 10^{-6})(y^+)^4}{1 - (4.16 \times 10^{-4})\ (y^+)^3 + (15.15 \times 10^{-6})(y^+)^4}$$

for $y^+ \leqslant 20$ (4-16)

Von Karman's equation for the sublaminar assumes purely laminar flow at the wall, or:

$$\epsilon = \nu \qquad y^+ < 5.$$

Lin et al. (52) assumed that turbulent fluctuations and turbulent viscosities exist up to the wall. That is, the concept of the existence of a pure laminar layer is discounted. The shear stress in the buffer and sublaminar layer (S.L.) was assumed constant and equal to τ_w. Lin's equations represent the turbulent contribution to eddy viscosity (Table XI). According to Figures 18 and 19, the predicted turbulent viscosities are too low as evidenced by a sharp discontinuity at the edge of the boundary layer.

Wasan, Tien and Wilke (100) also assumed the existence of turbulent viscosities up to the wall; they proposed a single equation for the boundary region ($y^+ < 20$) which seems to give a continuous transition to the turbulent core (Figures 18 and 19).

G.I. Taylor (88) described the velocity distribution in the boundary layer by a single logarithmic equation. The constant in this equation was determined from Nikuradse's data and so chosen to give a continuous velocity distribution at $\theta = 0.9$. His choice of 0.9 as the edge of the boundary layer was arbitrary.

$$0.9 < \theta < 1, \qquad \frac{U_o - U}{U_*} = 1.35 - 2.5 \ln (1 - \theta) \qquad (4\text{-}17)$$

Assuming a linear shear stress distribution in the bound-

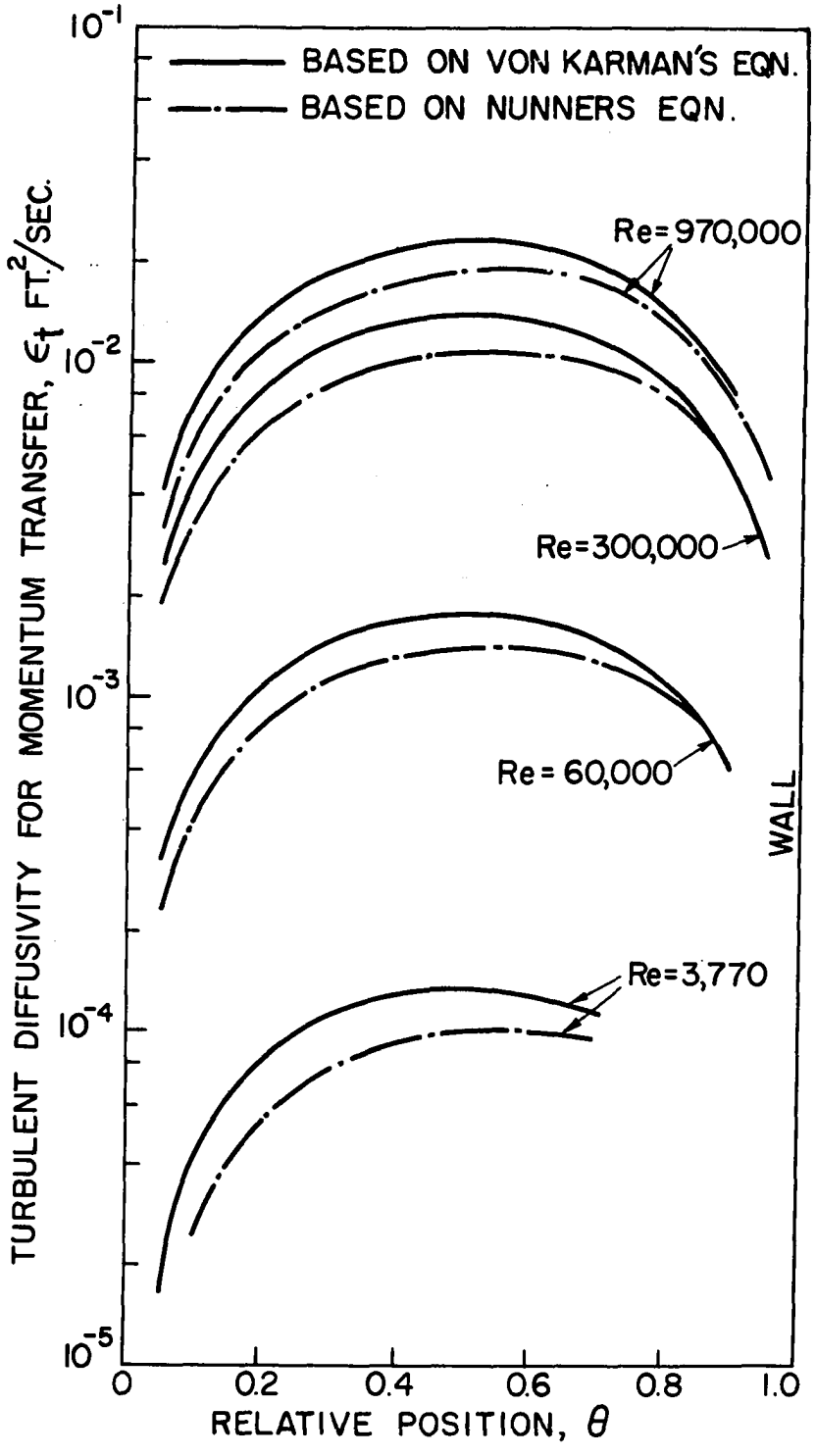


Fig. 17 TURBULENT VISCOSITY OVER THE TURBULENT REGION CALCULATED FROM DIFFERENT VELOCITY DISTRIBUTIONS

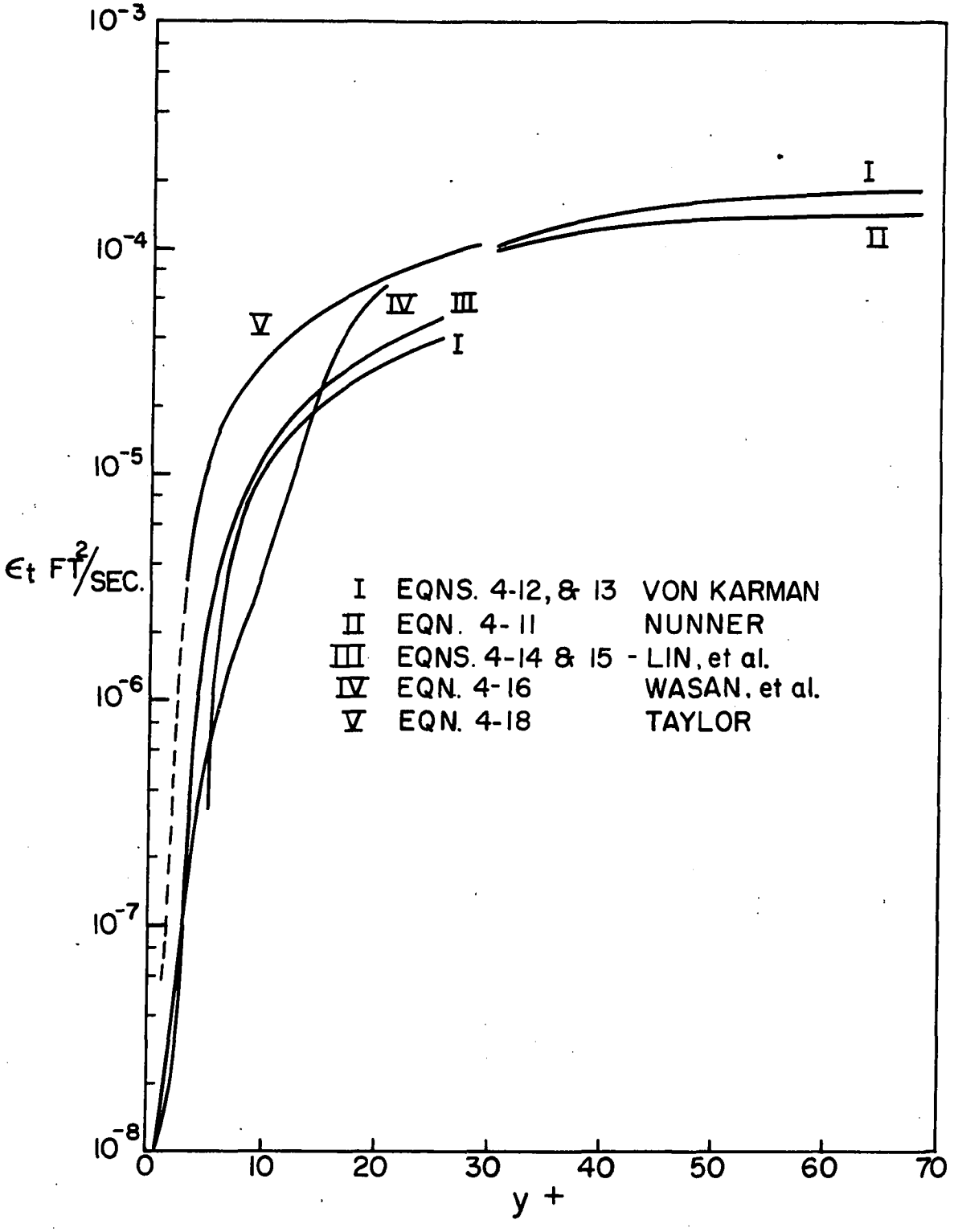


Fig. 18 TURBULENT VISCOSITY DISTRIBUTION NEAR THE WALL @ Re=5000

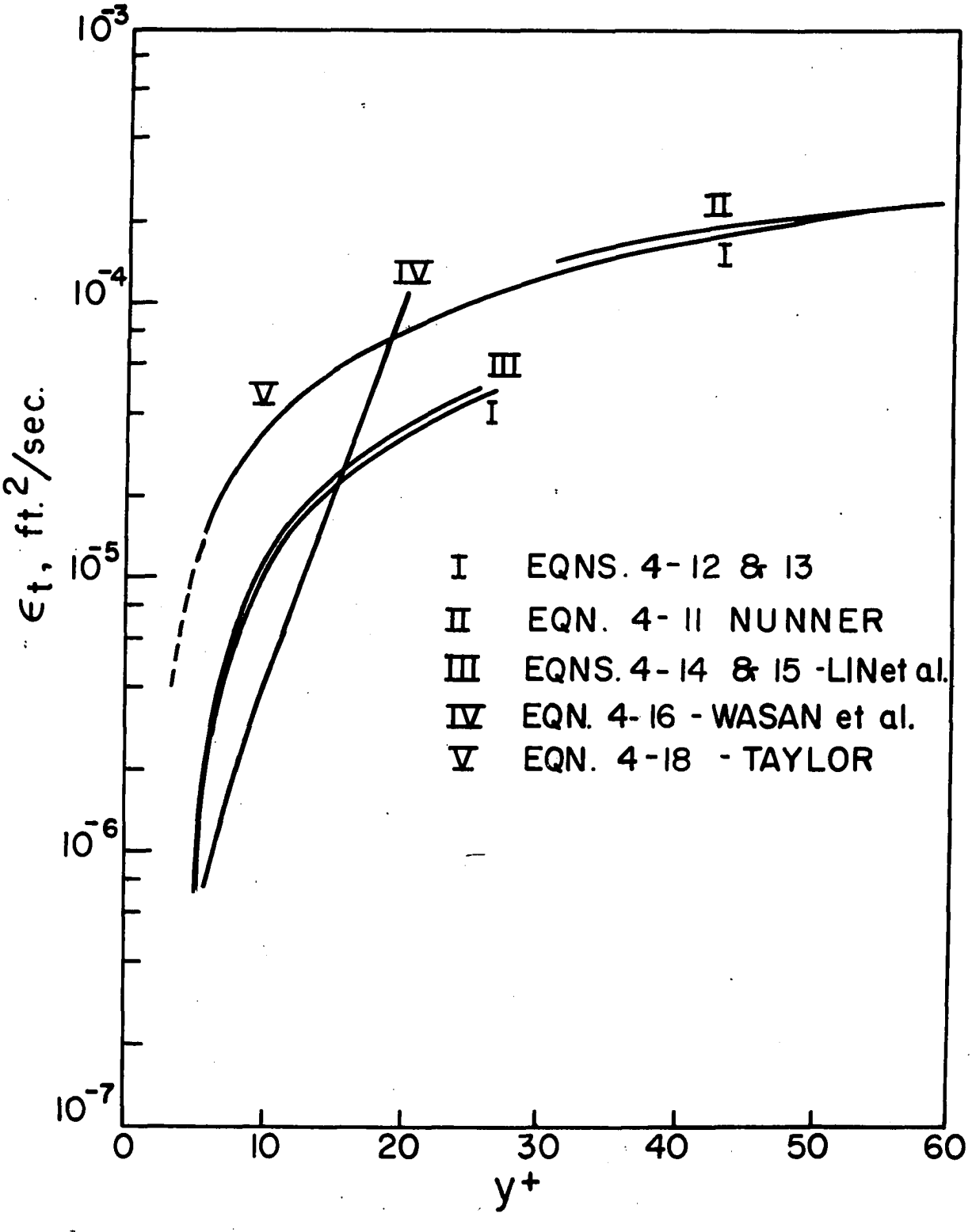


Fig. 19 TURBULENT VISCOSITY DISTRIBUTION NEAR THE WALL @ Re = 20,000

ary layer, ϵ can be expressed as follows.

$$\epsilon = 0.4\, a\, \theta\, U_* (1 - \theta) \qquad (4\text{-}18)$$

$$0.9 < \theta < 1$$

This equation gave also a smooth continuous transition of ϵ_t from the boundary layer to the turbulent region.

Point Eddy Diffusivity

The steady state eddy diffusion of material from a point source into a turbulent field flowing in a circular conduit is described by Equation (2-1).

$$\frac{1}{r}\frac{\partial}{\partial r}\left(r\,\alpha_r\frac{\partial C}{\partial r}\right) + \alpha_x\frac{\partial^2 C}{\partial x^2} - U\frac{\partial C}{\partial x} = 0 \qquad (2\text{-}1)$$

For the turbulent core, α_c is determined from the concentration profiles across the core. The second term is neglected in the treatment of Chapter II where U and α_c are assumed to be independent of r.

For the sake of clarity, the different eddy diffusivity terms referred to here are defined below:

α_c is the average eddy diffusivity across the turbulent core; it is assumed independent of r and has been treated in Chapter II.

α_r is the radial point[1] eddy diffusivity as determined when the effect of axial eddy diffusion is not neglected; α_r is a function

---

[1]The term "point" is used to differentiate this nonisotropic positional variable from average core eddy diffusivity.

of r (α_r is E_r in Seagrave's notations (74)).

α is the radial point eddy diffusivity as determined when the convective mean velocity effect is taken into account but the axial eddy diffusion effect is ignored; it is also a function of r and will be referred to here simply as eddy diffusivity.

The subscript t is used to indicate the contribution of the turbulent effect to eddy diffusivity; for example,

$$\alpha = \alpha_t + D_m \qquad (4\text{-}19)$$

α_t is the radial point turbulent diffusivity. D_m = the molecular diffusion coefficient.

In the turbulent core, D_m is usually very small compared to α_c so that α_c and α_{ct} are usually considered the same. This is not true near the wall where the molecular contribution is not negligible.

Experimental data on α_c are quite abundant as indicated in Chapter II. However, data on point eddy diffusivity (α or α_r) are scarce. Because of our lack of knowledge of α and α_r, it is customary to assume Reynolds analogy, that is turbulent Schmidt and Prandtl numbers equal to 1, and use eddy viscosity data that are much simpler to obtain (88, 91). More α_r data would be needed in order to determine the size of the errors introduced by this assumption. In case of the turbulent core,

α_c and ϵ_c are known to differ by as much as 60 per cent.

Page et al. (62, 63) reported point eddy conductivity data (thermal eddy diffusivity) for air flow between parallel plates. Roley and Fahien (67) reported material point eddy diffusivity for air flow in a pipe. Similar data were reported by Lynn et al. (54) for coaxial air-natural gas flow (turbulent flow was not fully developed).

Seagrave and Fahien (74, 75, 76) reported some data on both α and α_r determined from experimental steady state and transient state point concentration measurements and using one of the mean velocity distribution correlations. Their reported α_r data were for water flow at Reynolds numbers between 3000 and 7500, and did not extend into the boundary layer. The following results were given by Seagrave:

(a) Turbulent Schmidt number, $\frac{\epsilon}{\alpha}$, was found to approach unity at the pipe axis but increased rapidly with θ.

(b) α_x was found to be appreciable in the core region and to vanish near the wall.

(c) Neglecting axial diffusion resulted in eddy diffusivity values that were considerably lower than α_r especially in the core region.

The following equation was proposed by Seagrave to express α_r in terms of θ and Re:

$$\alpha_r = \frac{(Re - 2100)}{10^6}\left[0.193\ (1 - \theta^2) + 1.6\ \theta\right](1-\theta)^3 \qquad (4\text{-}20)$$

Seagrave's data showed considerable scatter in α_r depending on the chosen values of the transformation parameters (Figures 23 and 22). The accuracy of α_r results is also limited by the accuracy of numerical solution techniques and the accuracy of concentration and mean velocity data.

A Proposed Equation for Nonisotropic Eddy Diffusivity in the Turbulent Region

The equation proposed here is based on the premise that the point eddy diffusivity, α, is a function of both the degree of isotropy, v'/u', and eddy diffusivity at the pipe axis. One of the assumptions made in previous chapters is that isotropy reigns over the turbulent core which implies that v' equals u' and that α_c is equal to α at the pipe axis. The assumption is known to be satisfactory at high Reynolds numbers where a flat velocity profile prevails over most of the pipe cross section. As Reynolds number becomes smaller, larger deviations from isotropy would be expected.

If G = the degree of isotropy = $\frac{v'}{u'}$

Then,
$$\alpha = \alpha_c f(G)$$
$$G = f(\theta) \qquad (4\text{-}21)$$

The generalized experimental correlation of eddy diffusivity found in Chapter II represents α_c very well:

$$\frac{\alpha_c}{\nu} = 0.012 \quad Re^{0.82} \qquad (2\text{-}14)$$

Data on the degree of isotropy, G, were obtained from available intensity data (13, 46, 47, 70) and are plotted in Figure 20 at different Reynolds numbers. The data show no dependence of G on Reynolds number since the variations shown in Figure 20 are of the same order as experimental errors involved in taking such data. With the exception of flow at $Re_c = 500000$, all the data fell short of perfect isotropy at the pipe axis.

In order to determine the functional form of G as a function of θ, Laufer's data at $Re_c = 50000$ were fitted by the least square method using the different functions listed in Table X. The computed correlation coefficient indicates how well does any of the listed functions fit the isotropy data. The best fit was obtained with a polynomial; a fourth degree polynomial gave a better fit than a third degree polynomial.

Three air flow data samples were fitted to a fourth degree polynomial by the least square method; the resulting correlations and correlation coefficients are given below:

<u>Data Sample</u>: Laufer, $Re_c = 50000$

$$G = 0.950 - 0.108\,\theta - 4.394\,\theta^2 + 10.598\,\theta^3 - 6.852\,\theta^4 \qquad (4\text{-}22)$$

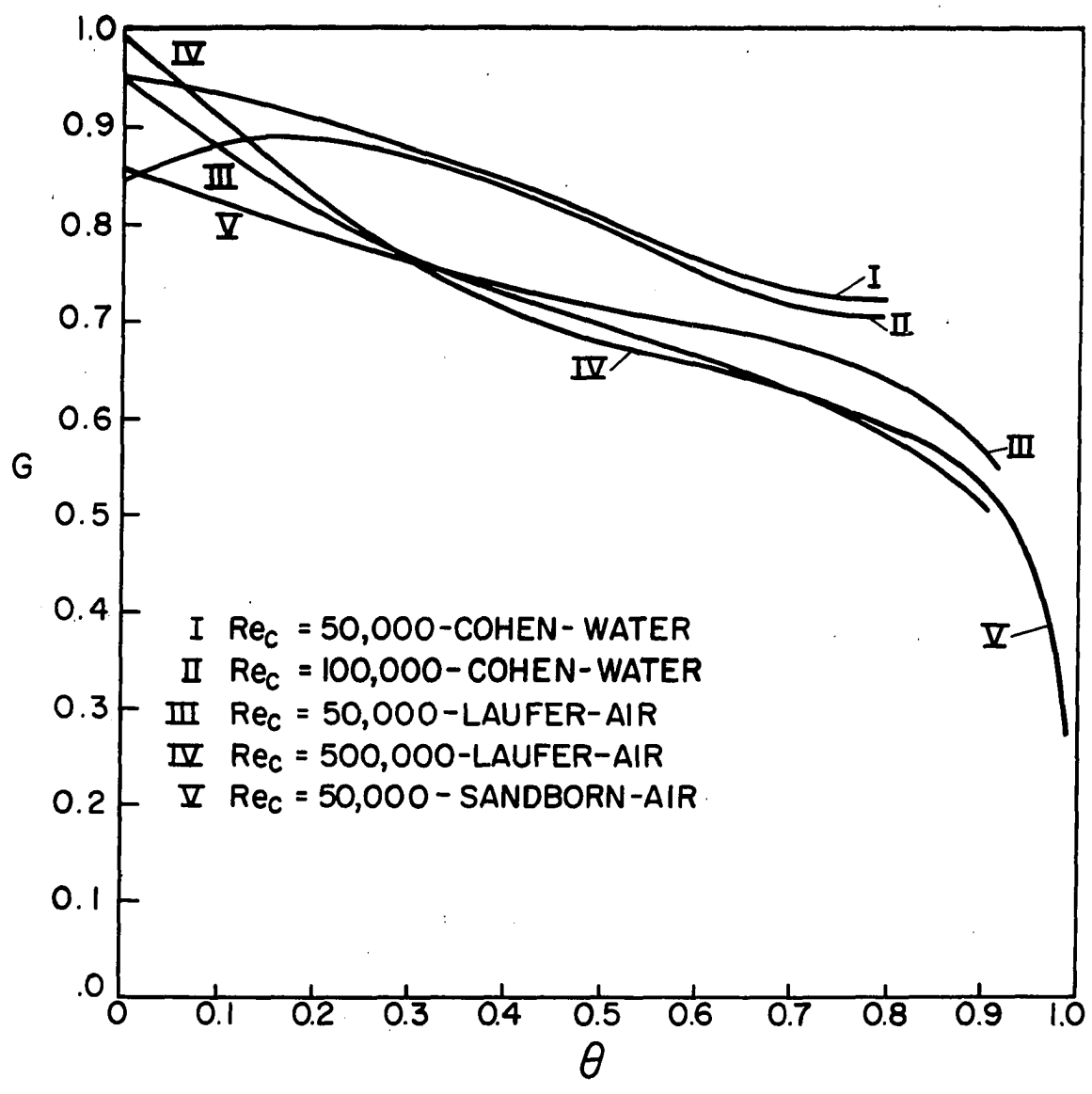


Fig. 20 DEGREE OF ISOTROPY AT DIFFERENT RADIAL POSITIONS

TABLE XII

TEST FOR FUNCTIONAL FORM OF ISOTROPY DATA

Data Sample: Laufer $Re_c = 50000$

Functional Form	Correlation Coefficient
$y = a + bx$	0.909
$y = a + bx + cx^2$	0.935
$y = ax^b$	0.405
$y = \frac{ax}{b+x}$	0.399
$y = ae^{bx}$	0.851
$y = ax^{bx}$	0.448
$y = a(xe^{bx})^x$	0.779
$y = ae^{bx+cx^2}$	0.887
$y = a + \frac{b}{x}$	0.559

correlation coefficient = 0.995

Third degree polynomial, $G = 0.972 - 1.741\ \theta + 4.191\ \theta^2 - 3.178\ \theta^3$ (4-23)

Data Sample: Sandborn - $Re_c = 50000$

$G = 0.844 + 0.575\ \theta - 5.407\ \theta^2 + 10.178\ \theta^3 - 5.940\ \theta^4$ (4-24)

correlation coefficient = 0.991

Data Sample: Laufer - $Re_c = 500000$

$G = 0.987 - 0.548\ \theta - 1.969\ \theta^2 + 5.353\ \theta^3 - 3.503\ \theta^4$ (4-25)

correlation coefficient = 1.0

The above correlations do not provide a unique equation expressing G as a function of θ. The accuracy or reliability of these correlations can not be any better than the accuracy or reliability of the intensity data. It is apparent, however, that a polynomial-type equation gives a very good fit of all data samples. This leads us to suspect that a power law distribution is a good representation of f (G), and α.

In the absence of sufficient experimental data on α or α_r, f (G) may be assumed a power equation whose exponent can be expressed in terms of the friction factor, λ, in the same way as the eddy viscosity equation obtained from Nunner power law (Equation 4-11). The proposed equation, however, is more realistic than (4-11) because it does not give a zero eddy diffusivity at the pipe axis:

$$\alpha = \alpha_c \, (1 - \theta)^{\frac{n-1}{n}} \qquad (4\text{-}26)$$

$$n = 1/\sqrt{\lambda}$$

$$\frac{\alpha}{\nu} = 0.012 \, Re^{0.82} \, (1 - \theta)^{\frac{n-1}{n}} \qquad (4\text{-}27)$$

Equation (4-27) (plotted in Figure 21) assumes that α at $\theta = 0$ is the same as α_c (the core average). It also permits α to vary within the core ($\theta < 0.3$). One could reconcile this with the assumptions made in Chapter II by considering α_c equal to α at $\theta = 0.2$. In other words, by considering the average core value equal to α at $\theta = 0.2$ instead of at $\theta = 0$. This produces these equations

$$\frac{\alpha}{\nu} = 0.012 \, Re^{0.82} \, (1.2 - \theta)^{\frac{n-1}{n}} \qquad (4\text{-}28)$$

and

$$\frac{\alpha}{\nu} \neq f(\theta) \quad \text{at} \quad \theta < 0.2$$

This equation seems to agree with Page's parallel plates data over the turbulent region (Figure 21). The agreement ceases to exist at higher values of θ because Equations (4-27) or (4-28) do not provide for α to go through a maximum away from the pipe axis. There is no reason, however, why the eddy diffusivity distribution should be the same in pipes and parallel plates since they have different geometries. Although the same flow equations apply to flow in round pipes and parallel plates at the center and the wall, the distributions over the cross

section are not the same. It is known that Von Karman's universal velocity distribution for pipe flow does not apply to parallel plates. Incidentally, Figure 21 shows that Page's data abide by the generalized core correlation of Chapter II, (Equation 2-14).

The distributions of radial eddy diffusivities α and α_r and the turbulent viscosity ϵ_t at Re = 3000 to 5000 are shown in Figures 22 and 23; ϵ_t values were computed using Equation (4-11) which does not apply near the pipe axis. Also shown are Seagrave α(75) and α_r (74) data. Equation (4-27) seems to be in reasonably good agreement with Seagrave's data especially at the higher Reynolds number (5000) which is still not high enough for the full development of turbulent flow.

Seagrave's Equation (4-20) is based on his water flow data. Since $\frac{\alpha}{\nu}$ is a function of Re (Equation 2-14), Equation (4-20) was modified here to apply to both gas and liquid flow by dividing both sides by ν for water and writing the equation as follows,

$$\frac{\alpha_r}{\nu} = \frac{(Re - 2100)}{(1 - \theta)^3}\left[0.0179\ (1 - \theta^2) + 0.1481\ \theta\right] \qquad (4\text{-}29)$$

As pointed out earlier, more experimental data are needed to test the applicability of this equation to Reynolds numbers beyond the highest experimental value of 7500.

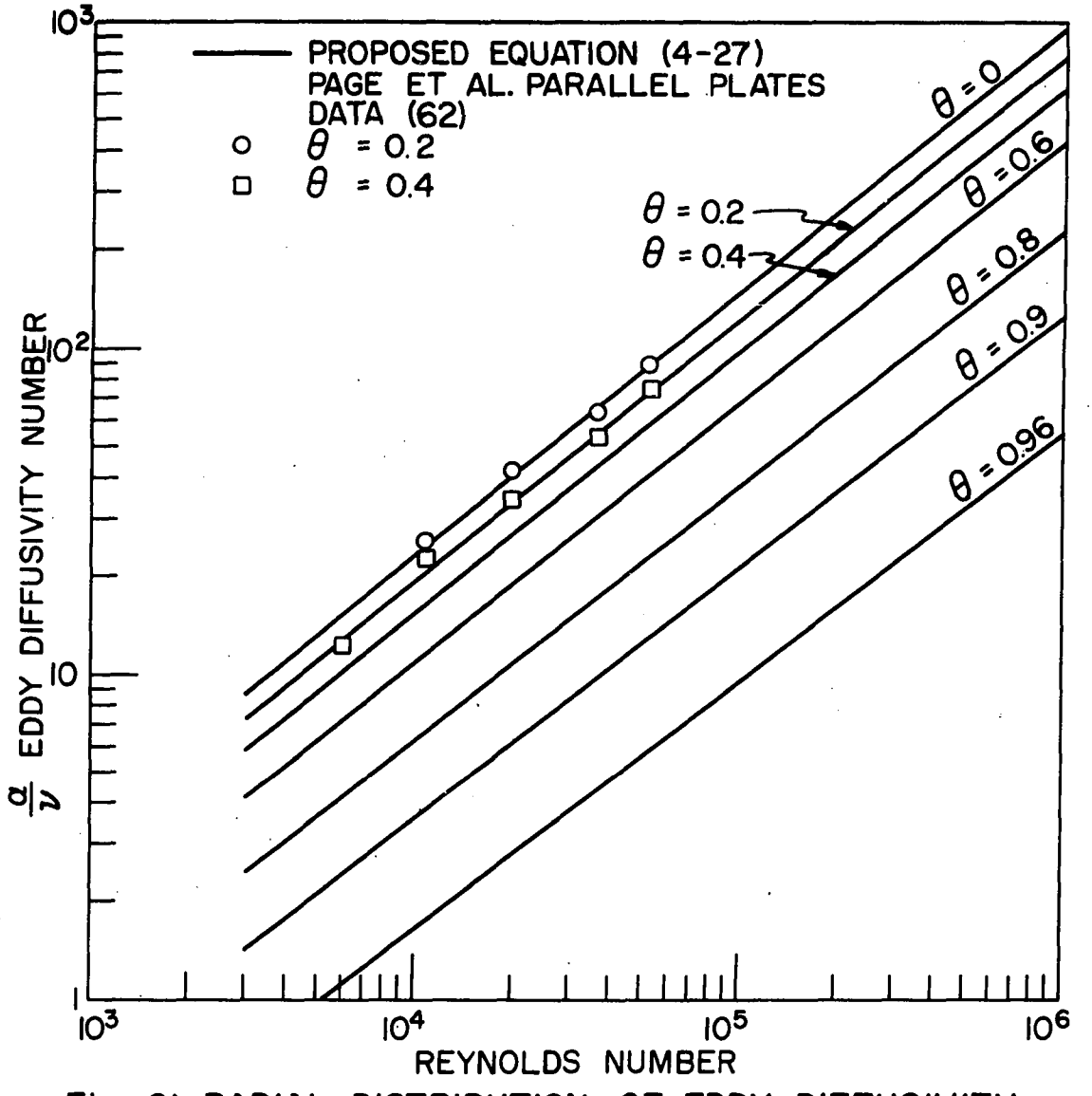


Fig. 21 RADIAL DISTRIBUTION OF EDDY DIFFUSIVITY (EQUATION 4-27)

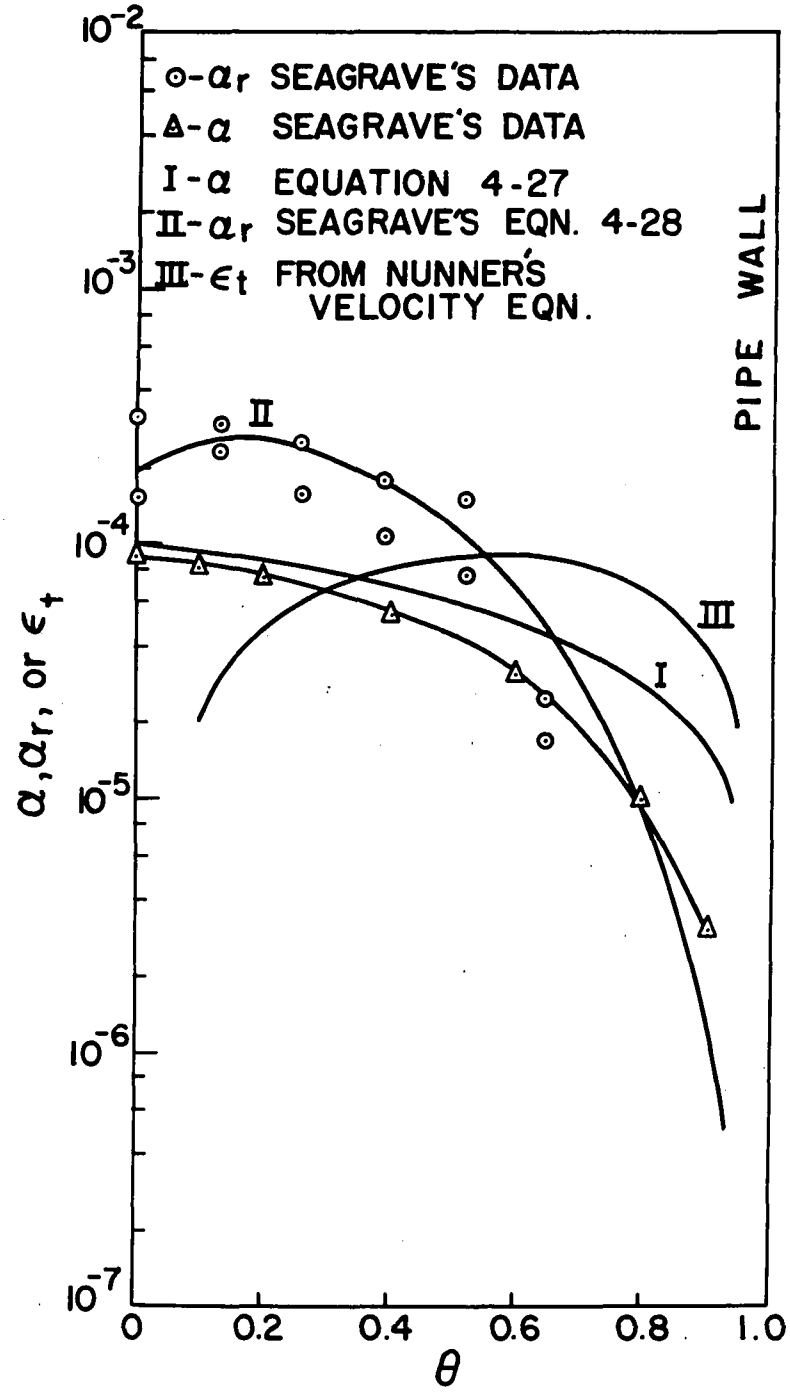


Fig. 22 DISTRIBUTION OF RADIAL EDDY DIFFUSIVITIES & TURBULENT VISCOSITY AT Re = 3000 FOR WATER FLOW

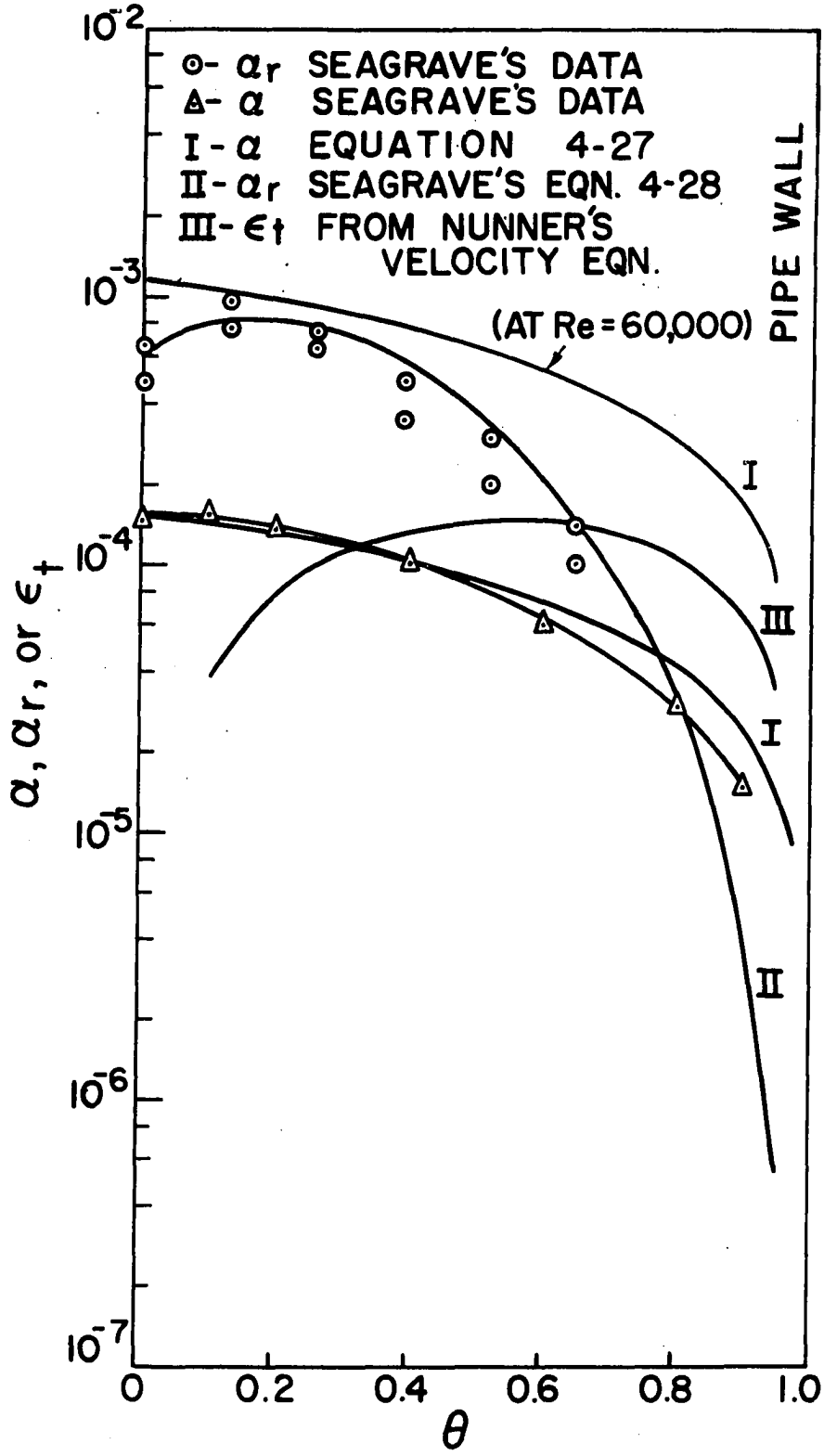


Fig. 23 DISTRIBUTION OF RADIAL EDDY DIFFUSIVITIES & TURBULENT VISCOSITY AT Re = 5000 FOR WATER FLOW

CHAPTER V

COMPUTATION OF AXIAL MIXING FROM NONISOTROPIC TURBULENT DIFFUSION AND VELOCITY DISTRIBUTION CORRELATIONS

Problem Review

One objective of the work presented in this chapter was to determine the relative contributions of the turbulent core and the boundary layer to axial mixing.

Another objective was to compare axial mixing results computed using the various velocity and eddy diffusivity distributions discussed in Chapter IV. Since reliable sublaminar layer diffusivity measurements are almost impossible to make, it was sought to examine the nature of boundary layer diffusion by means of the synthetic method described in this chapter.

Axial mixing in turbulent pipe flow is caused by a convective velocity distribution effect modified by turbulent diffusion. The transport of material from a radial element of a disc moving with the average bulk velocity is described by the following equation:

$$\frac{1}{r}\frac{\partial}{\partial r}\left(\alpha r \frac{\partial C}{\partial r}\right) = (U-V)\frac{\partial C}{\partial x} + \frac{\partial C}{\partial t} \qquad (5\text{-}1)$$

where x = axial distance from reference plane moving with velocity V.

t = time

Mass transfer due to the axial eddy diffusivity is assumed negligible in this equation. The axial mixing coefficient, E, which is also termed the dispersion coefficient, is an empirical coefficient defined by Equation (5-2):

$$\phi = -\pi a^2 E \frac{\partial C_m}{\partial x} \qquad (5\text{-}2)$$

where C_m is the mean concentration across the pipe cross section at x.

ϕ = The rate of material transport in the axial direction across a reference plane moving with velocity V.

a = pipe radius.

G. I. Taylor (88) succeeded in relating the axial mixing coefficient, E, to simple turbulent flow parameters:

$$E = 1.78 \ Vd\sqrt{\lambda} \qquad (5\text{-}3)$$

where d = pipe diameter

λ = Moody friction factor

Taylor arrived at this equation using the same numerical integration technique used in this chapter. As pointed out later, Equation (5-1) was simplified by assuming $\frac{\partial C}{\partial x}$ independent of x and r. By assuming that the turbulent transfer of mass, heat and momentum are exactly analogous (Reynolds analogy), he was able to estimate α at different values of U and r by differentiating Von Karman's universal

velocity distribution. For the boundary layer, which Taylor arbitrarily took as the region $0.9 < \theta < 1$, he chose the constants in the velocity equation so that U was continuous at $\theta = 0.9$:

$$\frac{U_o - U}{U_*} = 1.35 - 2.5 \ln (1-\theta) \qquad 0.9 < \epsilon < 1 \qquad (5\text{-}4)$$

The velocity distribution used over the rest of the pipe was obtained from a mean curve through two different sets of data. As Taylor pointed out, Equation (5-4) is not a satisfactory correlation of velocity as $\theta \longrightarrow 1$.

Sjenitzer (81) showed that most of the available axial mixing data deviate markedly from Taylor's Equation (5-3); he also fitted these data by an empirical correlation.

Tichacek, Barkelew and Baron (91) used Taylor's numerical integration method assuming constant $\frac{\partial C_m}{\partial x}$. They also estimated α from velocity distribution data by assuming Reynold's analogy. The main difference between their method and Taylor's is that they corrected for variations in molecular diffusivity:

i.e. $$\alpha = \alpha_t + D_m$$

$$\epsilon = \epsilon_t + \nu$$

where $$\tau_{rx} = - \epsilon \rho \frac{\partial U}{\partial r}$$

Reynolds analogy says that $\alpha_t = \epsilon_t$

where α_t and ϵ_t are the turbulent diffusivities for material and momentum transfer respectively.

ν is the kinematic viscosity

D_m is the molecular diffusivity

They wrote α in Equation (5-1) as:

$$\alpha = \epsilon - \nu + D_m \qquad (5\text{-}5)$$

while Taylor wrote it as:

$$\alpha = \epsilon \qquad (5\text{-}6)$$

The velocity distribution values used in their computations were obtained by smoothing and averaging velocity profiles taken by several investigators.

Tichacek et al. obtained two different $\frac{E}{Vd}$ curves corresponding to Schmidt numbers of 1 (gases) and 100 (liquids). They also reported that E is very sensitive to slight changes in the velocity profile. For example, two sets of velocity profile data taken at same Reynolds number and differing by less than 3% gave a 50% disagreement in computed $\frac{E}{Vd}$.

One may just point out briefly here that Reynolds analogy does not apply to momentum transfer. Several papers in the literature reported as much as 60% difference between momentum and material (or thermal) turbulent diffusivities (38, 63, 73, 92 . Over the turbulent region, the correction made by Tichacek et al. for molecular diffusivity and viscosity is but a very small fraction of the error introduced by the Reynolds analogy assumption. As shown later in the Discussion of Results, the effect of differences in molecular properties on axial mixing could be pronounced in the boundary layer.

The exact nature of flow at the wall in the so-

called laminar sublayer or sublaminar layer is not clearly understood. The sublaminar thickness is so small that it is very difficult to determine velocity distribution, let alone diffusivity in that region. The presence of a hot wire or a pitot tube disturbs the flow. Various investigators encountered many difficulties and made conflicting statements on the laminar sublayer and some were not able to come to a definite conclusion regarding the existence of a laminar layer.

Equation (4-1) is based on the assumption of laminar motion and constant molecular viscosity:

for $y^+ < 5$. $\quad u^+ = y^+ \quad (4\text{-}1)$

Von Karman suggested that this equation applies up to $y^+ = 5$. Deissler (20) and Laufer (46) obtained velocity data adjacent to the wall of a smooth pipe. Their data extended to y^+ as low as 2 and agreed with Equation (4-1). There are many others who dealt with this problem and this is by no means an exhaustive account.

Reiss and Hanratty (65) reported the presence of fluctuations at $y^+ < 0.5$. Fage and Townend (23) observed the motion of colloidal particles at a distance of 0.000025 inches from the wall using an ultramicroscope. They found that the motion was sinuous; that is, no particles moved in a straight path. Lin et al. (52) proposed a turbulent viscosity equation for the sublaminar layer. Knudsen and Katz (43) said that all investigations near solid

boundaries involved the measurement of temporal-mean velocities. It is likely that the laminar sublayer has its most probable thickness at y^+ in the vicinity of 5.0, and it is reasonable to expect that the thickness, in some instances, would be nearly zero or relatively large (y^+ up to 10.0). Velocity spectra measured at the wall seemed to support this view. The spectrum was intermittently laminar and turbulent.

In summary, the evidence available so far seems to indicate that a parabolic velocity distribution is a satisfactory approximation, and that motion at the wall could be irregular or turbulent. This interesting and controversial question is dealt with in this chapter.

Analysis of Problem

This analysis uses the same numerical integration technique used first by Taylor and later by Tichacek et al.; $\frac{\partial C}{\partial x}$ is also assumed here independent of x and r. It differs from previous work in the following:

- Various velocity and diffusivity correlations are used for computing U and α.
- Computations are made with and without the Reynolds analogy assumption.
- The increment size in the numerical integration is reduced drastically as the wall is approached. This was deemed necessary for obtaining reliable results since both U and α change rapidly near the wall where steep velocity

gradients prevail. The smallest intervals used in previous work were 0.025 in Tichacek's paper and 0.01 in Taylor's work; in this development the size of the interval was cut down to 0.001 near the wall.

- A molecular diffusivity correction was made - (Tichacek did the same).

- Diffusion in the sublaminar layer was assumed molecular at first; later α was taken arbitrarily as the sum of molecular diffusivity and kinematic viscosity. This is dealt with further under the Discussion of Results.

In this analysis the transport of material from a radial element of a disc moving with the average bulk velocity V is described by Equation (5-1)

$$\frac{1}{r}\frac{\partial}{\partial r}\left(\alpha\, r\,\frac{\partial C}{\partial r}\right) = (U-V)\,\frac{\partial C}{\partial x} + \frac{\partial C}{\partial t} \qquad (5\text{-}1)$$

The empirical axial mixing coefficient, E, is defined by Equation (5-2)

$$\phi = -\pi a^2 E\,\frac{\partial C_m}{\partial x} \qquad (5\text{-}2)$$

where ϕ is the rate of axial material flux across the moving reference plane

a = pipe radius

C_m = the average concentration over pipe cross section at point x.

Equation (5-1) is simplified markedly if $\frac{\partial C}{\partial x}$ is assumed independent of x and r, and equal to $\frac{\partial C_m}{\partial x}$; then:

$$\frac{1}{r}\frac{\partial}{\partial r}\left(\alpha\, r\,\frac{\partial C}{\partial r}\right) = (U-V)\,\frac{\partial C_m}{\partial x} \qquad (5\text{-}7)$$

One can then integrate this equation repeatedly from the axis to obtain:

$$C - C_a = \frac{\partial C_m}{\partial x} \int_0^r \frac{1}{\alpha r'} dr' \int_0^r r'' (U-V) dr'' \qquad (5\text{-}8)$$

The axial flux is

$$\phi = 2\pi \int_0^a (C-C_a)(U-V) r\, dr = -\pi a^2 E \frac{\partial C_m}{\partial x} \qquad (5\text{-}9)$$

E is then written in this form:

$$E = -2a^2 \int_0^1 (U-V)\theta\, d\theta \int_0^\theta \frac{1}{\alpha\theta'} d\theta' \int_0^{\theta'} (U-V)\theta''\, d\theta'' \qquad (5\text{-}10)$$

where a = pipe radius

θ = dimensionless radial position = r/a

C_a = concentration at axis

α = radial point eddy diffusivity

V = average bulk velocity

The axial mixing coefficient, E, can be evaluated from Equation (5-10) if U and α are known as functions of θ.

The first integration in Equation (5-10) was performed analytically,

$$Y_1 = \frac{1}{\alpha\theta'} \int_0^{\theta'} (U-V)\theta''\, d\theta'' \qquad (5\text{-}11)$$

Different analytical expressions of Y_1 were obtained for the different velocity correlations. The problem was programmed for the Fortran IBM 7070 computer. Simpson rule was used for the numerical evaluation of the two integrals.

$$SY = \frac{\Delta\theta}{3}(Y_1 + 4Y_2 + Y_3) \qquad (5\text{-}12)$$

$\Delta\theta$ is the interval between θ values corresponding to Y_1 and Y_2 which varied as follows:

$$0 < \theta < 0.90 \qquad \Delta\theta = 0.05$$

$$0.9 < \theta < 0.99 \qquad \Delta\theta = 0.005$$

$$0.99 < \theta < 1.0 \qquad \Delta\theta = 0.001$$

Because of the steep gradients near the wall, the interval was cut down as θ approached unity in order to minimize numerical integration errors. The results obtained using the above $\Delta\theta$ values for $\theta > 0.9$ were in very good agreement with those obtained using intervals that are twice as large.

The last integration in Equation (5-10) was performed the same way as the second integration.

$$Z_1 = (U-V)\ \theta\ SUMSY \tag{5-13}$$

where

$$SUMSY = \sum_{\theta=0}^{\theta=\theta} SY \tag{5-14}$$

$$SZ = \frac{\Delta\theta}{3}(Z_1 + 4Z_2 + Z_3) \tag{5-15}$$

$$SUMSZ = \sum_{\theta=0}^{\theta=\theta} SZ \tag{5-16}$$

The axial mixing coefficient is obtained finally as

$$E = -2a^2 \sum_{\theta=0}^{\theta=1} SZ \tag{5-17}$$

All computed values of U, α, y^+, SY, SUMSY, SZ, and SUMSZ were printed for different values of θ. Also, E and $\frac{E}{Vd}$ were printed for all values of θ larger than 0.99.

Summary of Velocity and Eddy Diffusivity Distributions

The equations given below have been discussed in Chapter IV and were used for computing E.

(a) Mean velocity distribution:

Von Karman logarithmic distribution law,

Sublaminar layer $y^+ < 5 \quad u^+ = y^+$ (4-1)

Buffer region $5 < y^+ < 30, u^+ = 5 \ln y^+ - 3.05$ (4-2)

Turbulent region $y^+ > 30, u^+ = 5.5 + 2.5 \ln y^+$ (4-3)

where: $y^+ = \frac{y' U_*}{\nu}$ (4-5)

$$u^+ = \frac{U}{U_*} \tag{4-4}$$

Nunner's power equation for the turbulent region

$$\frac{U}{U_o} = (1-\theta)^{\sqrt{\lambda}} \tag{4-7}$$

(b) Eddy diffusivity distribution:

Equation proposed in Chapter IV

$$\frac{\alpha}{\nu} = 0.012 \ Re^{0.82} \ (1-\theta)^{\frac{n-1}{n}} \tag{4-27}$$

where $n = 1/\sqrt{\lambda}$

λ = Moody friction factor

Seagrave's equation (4-29)

$$\frac{\alpha_r}{\nu} = (Re-2100)\left[0.0179(1-\theta^2) + 0.1481\ \theta\right](1-\theta)^3$$

(c) Eddy viscosity distribution:

Whenever eddy viscosity equations are used, it is assumed that the turbulent diffusivities of mass and

momentum are equal.

i.e., $\alpha_t = \epsilon_t = \epsilon - \nu$

$$\alpha = \epsilon - \nu + D_m$$

Based on Von Karman's velocity distribution for the turbulent region, the following equation has been obtained:

$$\epsilon = \frac{\lambda V^2 \theta a (1-\theta)}{20 U_*} \qquad (4\text{-}12)$$

Another expression has been deduced from Nunner's velocity distribution,

$$\epsilon = \frac{a\, Vn\, \theta\, (1-\theta)^{\frac{n-1}{n}}}{4\,(1+n)(1+2n)} \qquad (4\text{-}11)$$

which can be also written as:

$$\epsilon = \frac{V^2\, a\, \theta\, (1-\theta)^{\frac{n-1}{n}}}{8\, U_o\, n}$$

Lin's turbulent viscosity equations for the boundary layer (52) were also used in some of the computations;

$$\frac{\epsilon_t}{\nu} = \left(\frac{y^+}{14.5}\right)^3 \qquad 0 < y^+ < 5 \qquad (4\text{-}15)$$

$$\frac{\epsilon_t}{\nu} = \frac{y^+}{5} - 0.959 \,, \quad 5 < y^+ < 30 \qquad (4\text{-}14)$$

Interpretation and Discussion of Results

As pointed out above, the term SZ represents the contribution of any radial element to axial mixing; SUMSZ is a cumulative axial mixing term, or SZ integrated over θ.

Some of the results of the computations are plotted in Figures 31 to 35 for Reynolds numbers from 3000 to 60,000[1] and using the various combinations of velocity and diffusivity equations given in Table XIII. Some of the earlier computational runs differed from those of Table XIII in that:

$$\alpha = D_m \qquad y^+ < 5$$

The results plotted in Figures 24 and 25 were computed for water flow at Re = 3770 using the same conditions as the experimental investigation reported in Appendix B. The molecular diffusivity, D_m, of $KMnO_4$ into water was taken as 7.6×10^{-9} $ft^2/sec.$, and ν was taken as 1.08×10^{-5}.

The Turbulent Region

All the results show that SUMSZ is positive over most of the turbulent region. This could be also deduced from Equation (5-6) when U is greater than V. This result may lead one into believing that the turbulent region makes a negative contribution to overall axial mixing.

---

[1]Unless otherwise stated, the following values were used in the computations:

Pipe diameter = 1 inch

$\nu_{water} = 1.18 \times 10^{-5}$ $ft^2/sec.$

D_m for water flow $= 1.26 \times 10^{-8}$ $ft^2/sec.$

$\nu_{air} = 1.62 \times 10^{-4}$ ft^2/sec

D_m for air flow $= 1.62 \times 10^{-4}$ $ft^2/sec.$

TABLE XIII

DIFFUSIVITY AND VELOCITY EQUATIONS USED IN DIFFERENT PROGRAMS

Region	Turbulent $y^+ > 30$		Buffer $5 < y^+ < 30$		Sublaminar $y^+ < 5$	
Program Number	Velocity Equation	Diffusivity Equation	Velocity Equation	Diffusivity Equation	Velocity Equation	Diffusivity Equation
501	4-3 (Von Karman)	4-12 (Von Karman)	4-2 (Von Karman)	4-12 (Von Karman)	$u^+ = y^+$	$\alpha = \nu + D_m$
502	4-3 (Von Karman)	4-27 (Proposed)	4-2 (Von Karman)	4-27 (Proposed)	$u^+ = y^+$	$\alpha = \nu + D_m$
503	4-3 (Von Karman)	4-29 (Seagrave)	4-2 (Von Karman)	4-29 (Seagrave)	$u^+ = y^+$	$\alpha = \nu + D_m$
506	4-7 (Nunner)	4-27 (Proposed)	4-2 (Von Karman)	4-27 (Proposed)	$u^+ = y^+$	$\alpha = \nu + D_m$
507	4-7 (Nunner)	4-29 (Seagrave)	4-2 (Von Karman)	4-29 (Seagrave)	$u^+ = y^+$	$\alpha = \nu + D_m$
508	4-7 (Nunner)	4-11 (Nunner)	4-2 (Von Karman)	4-11 (Nunner)	$u^+ = y^+$	$\alpha = \nu + D_m$
110	4-7 (Nunner)	4-11 (Nunner)	4-2 (Von Karman)	4-14 (Lin)	$u^+ = y^+$	4-15 (Lin)
111	4-7 (Nunner)	4-29 (Seagrave)	4-2 (Von Karman)	4-14 (Lin)	$u^+ = y^+$	4-15 (Lin)

This can not be true since in the extreme case of plug flow, axial mixing is positive and finite because of axial and radial eddy diffusion. One has to attribute this result to the fact that axial eddy diffusion is not accounted for in these computations. This means that the effect of axial eddy diffusion and its contribution to overall axial mixing is at least equal to the lowest (-SUMSZ) value shown in Figures 25 to 29. It also suggests that the axial eddy diffusivity effect is larger than Tichacek et al. estimated (91). Recent work indicates that axial eddy diffusivity is considerably larger than radial eddy diffusivity (76).

The Boundary Layer

It is clear from the plotted results that the boundary layer makes the greatest contribution to axial mixing. The very sharp increase in (-SUMSZ) near the wall suggests that axial mixing is critically determined by the boundary layer. This can be explained by the appearance of α in the denominator in Equation (5-10); as α becomes very small, SZ becomes very large.

One may argue that the very sharp increase in (-SUMSZ) near the wall may be caused by the assumption of constant $\frac{\partial C}{\partial x}$. In other words, it is conceivable that a very sharp decrease in $\frac{\partial C}{\partial x}$ near the wall could offset a sharp decrease in α. This point is examined below where it is shown that for sufficiently long pipes, variations in $\frac{\partial C}{\partial x}$ with radial position are not responsible for the computed steep gradient

at the wall.

Diffusion in the sublaminar layer was assumed molecular in some of the earlier computational runs. This gave extremely large and unreal values of E because D_m is very small, especially for liquids. The results obtained here refute the assumption of laminar flow at the wall. Lin, Moulton and Putnam (52) pointed out that the concept of the existence of a sublaminar layer for molecular diffusion may not be true. There are evidences that the fluctuating velocities do not cease to exist before the wall and that the flow is intermittently laminar and turbulent at the wall.

In series 500, turbulent viscosity in the sublaminar was arbitrarily assumed to have the same magnitude as the kinematic viscosity. Lin et al. proposed two equations for the turbulent viscosity in the buffer and sublaminar regions which have been discussed before. These equations were used for the boundary layer in programs 110 and 111. The computed turbulent viscosities (Figure 18) were lower than ν throughout the sublaminar layer and part of the buffer zone, which gave higher contributions to E as shown in Figure 29.

Diffusivity and Velocity Correlations

It is not possible to make any conclusive evaluation of the various diffusivity and velocity correlations used in the computations. The assumption that $\alpha_t = \nu$ in the sublaminar layer gave reasonable axial mixing results for

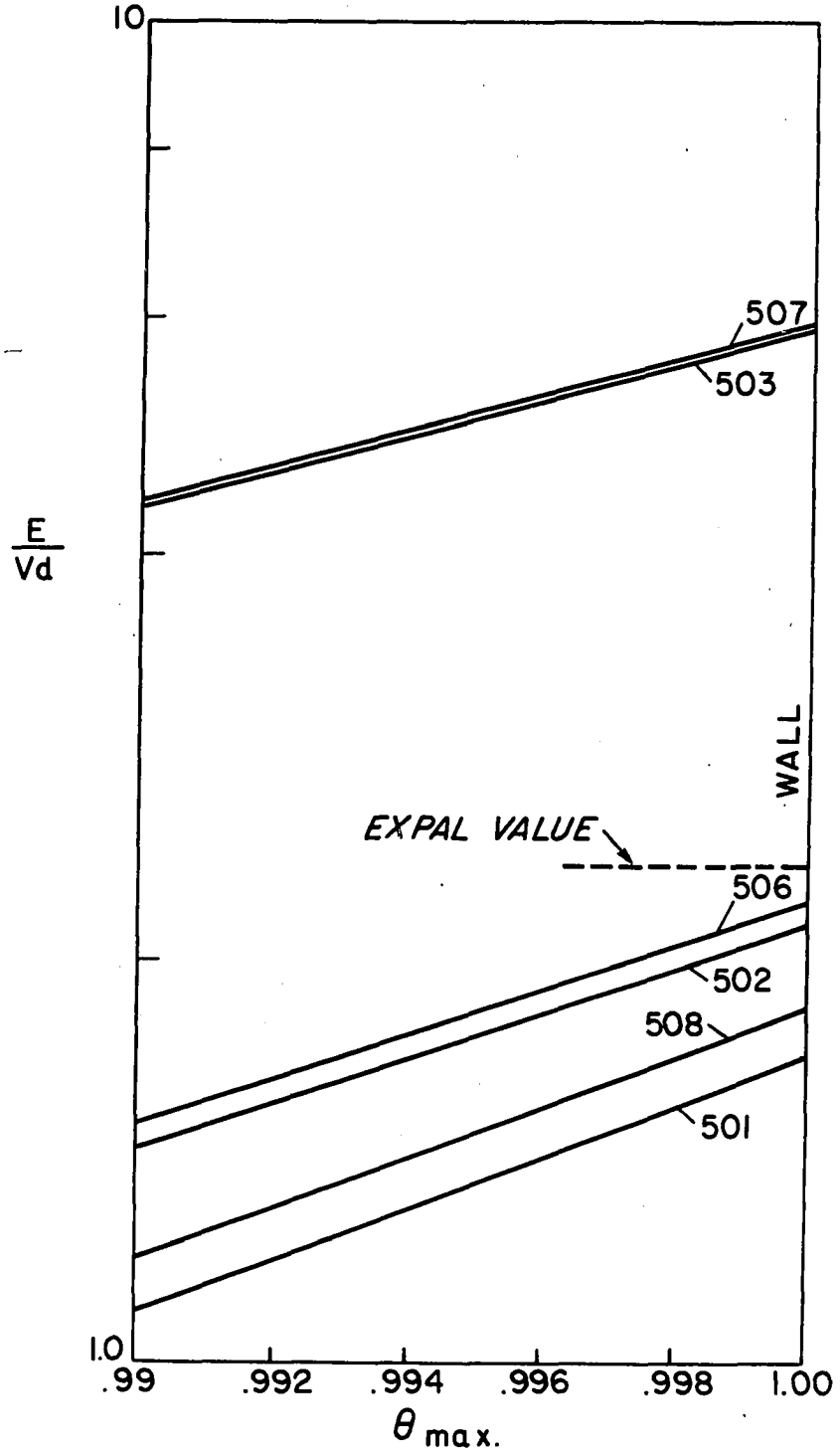


Fig. 24 COMPUTED LONGITUDINAL DISPERSION NUMBER FOR WATER FLOW AT Re=3770

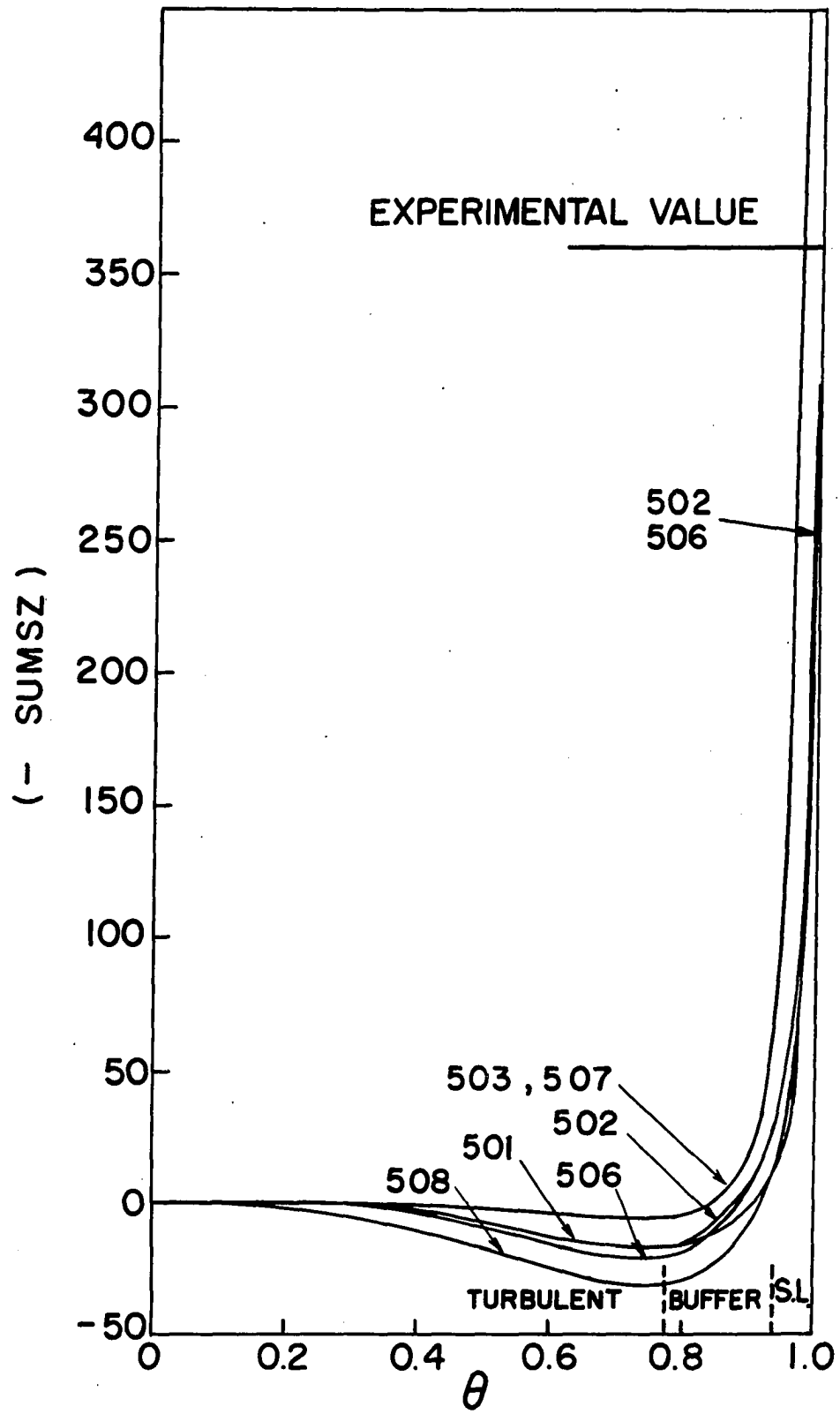


Fig. 25 RADIAL CONTRIBUTIONS TO AXIAL MIXING @ Re = 3770

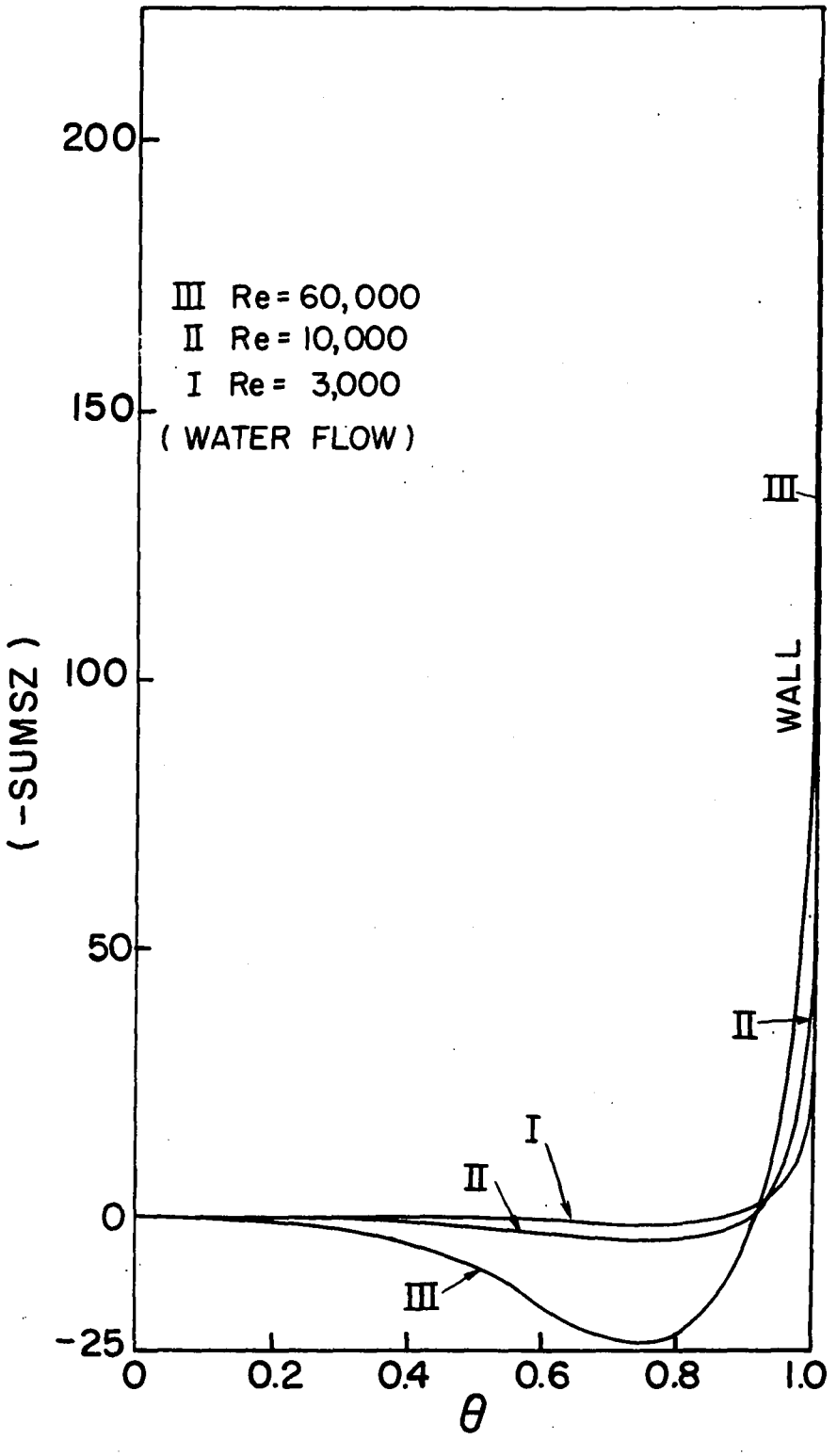


Fig. 26 RADIAL CONTRIBUTIONS TO AXIAL MIXING AT DIFFERENT REYNOLDS NUMBERS (PROGRAM 506)

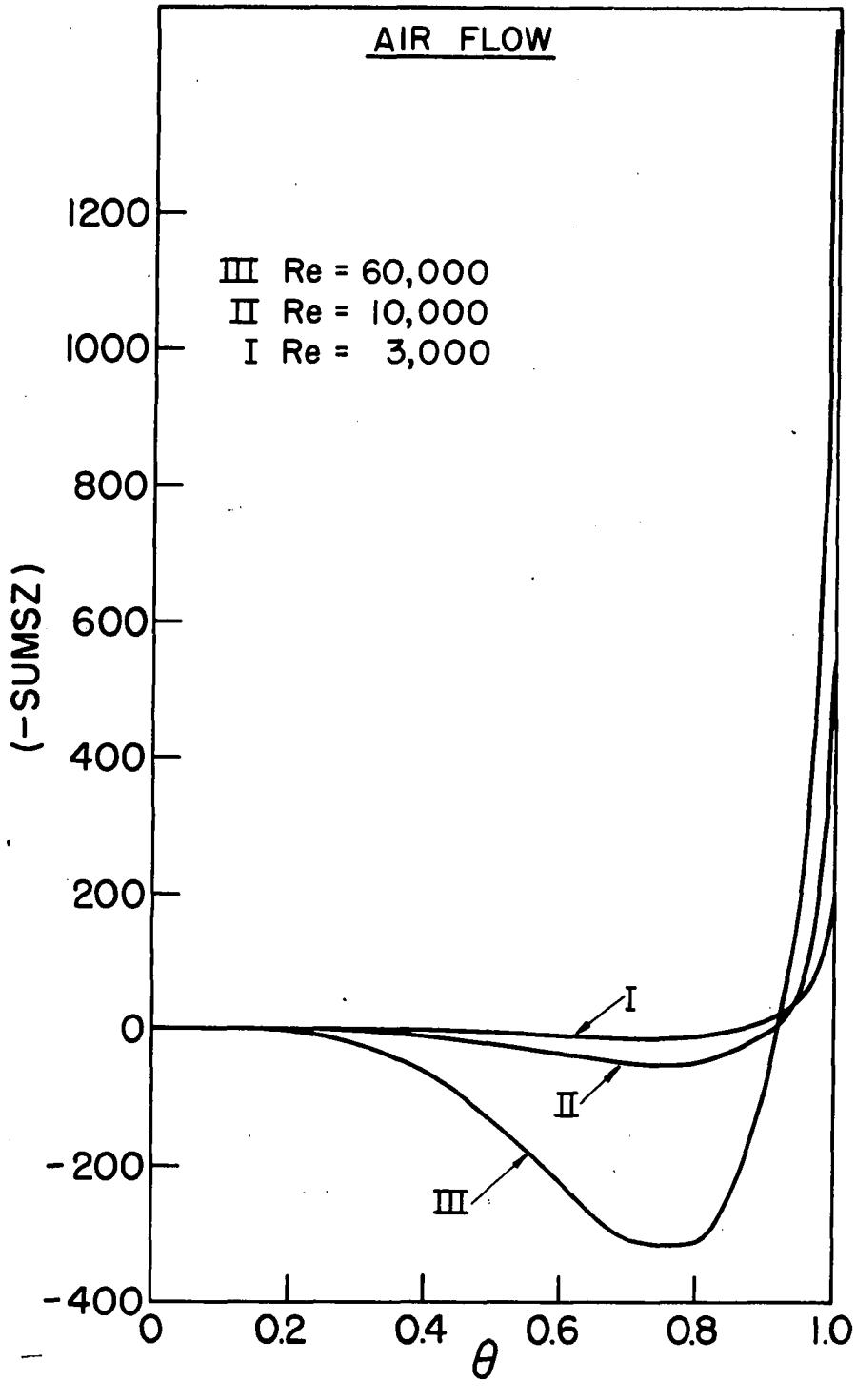


Fig.27 RADIAL CONTRIBUTIONS TO AXIAL MIXING AT DIFFERENT REYNOLDS NUMBERS (PROGRAM 506)

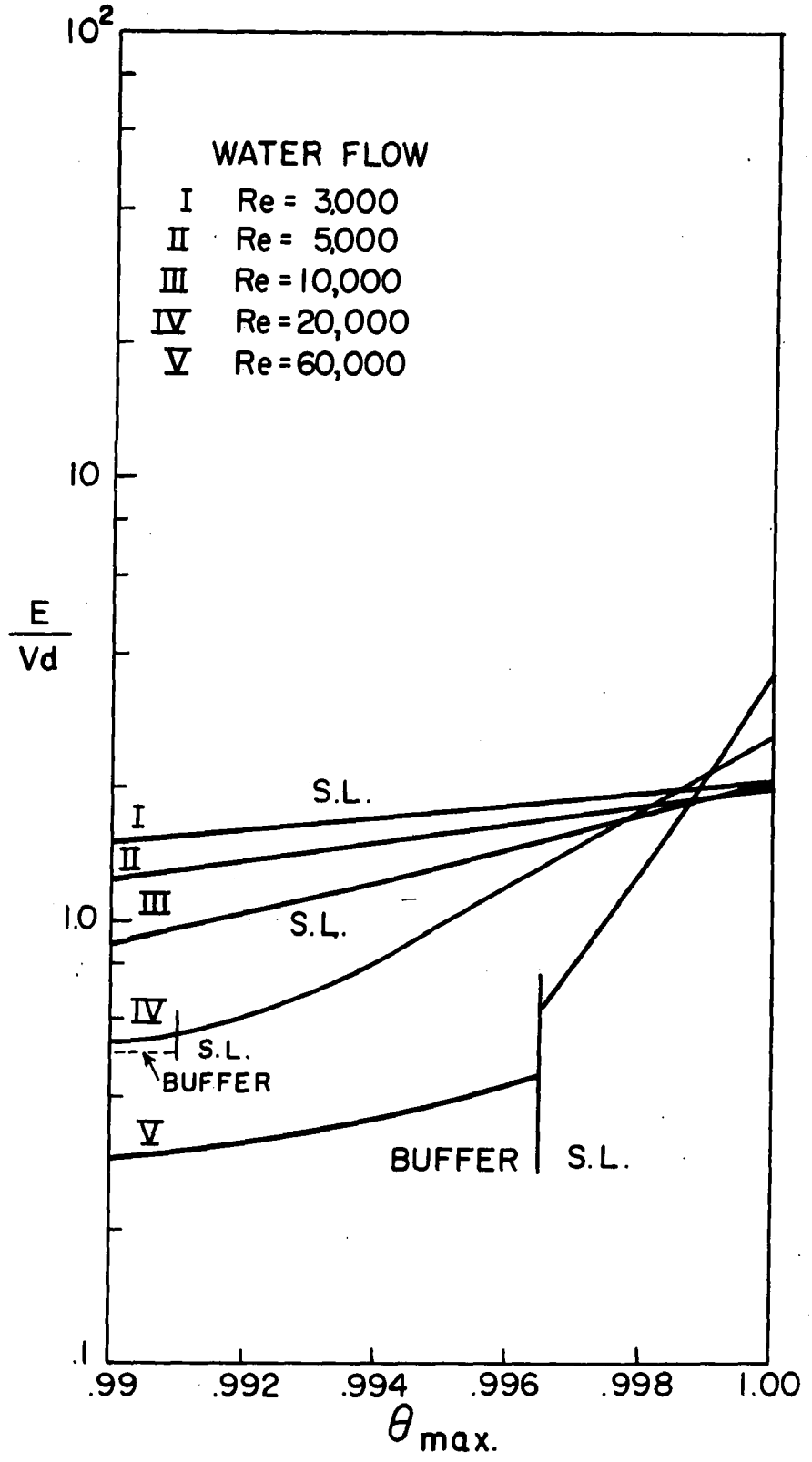


Fig. 28 COMPUTED LONGITUDINAL DISPERSION NUMBER AT DIFFERENT REYNOLDS NUMBERS

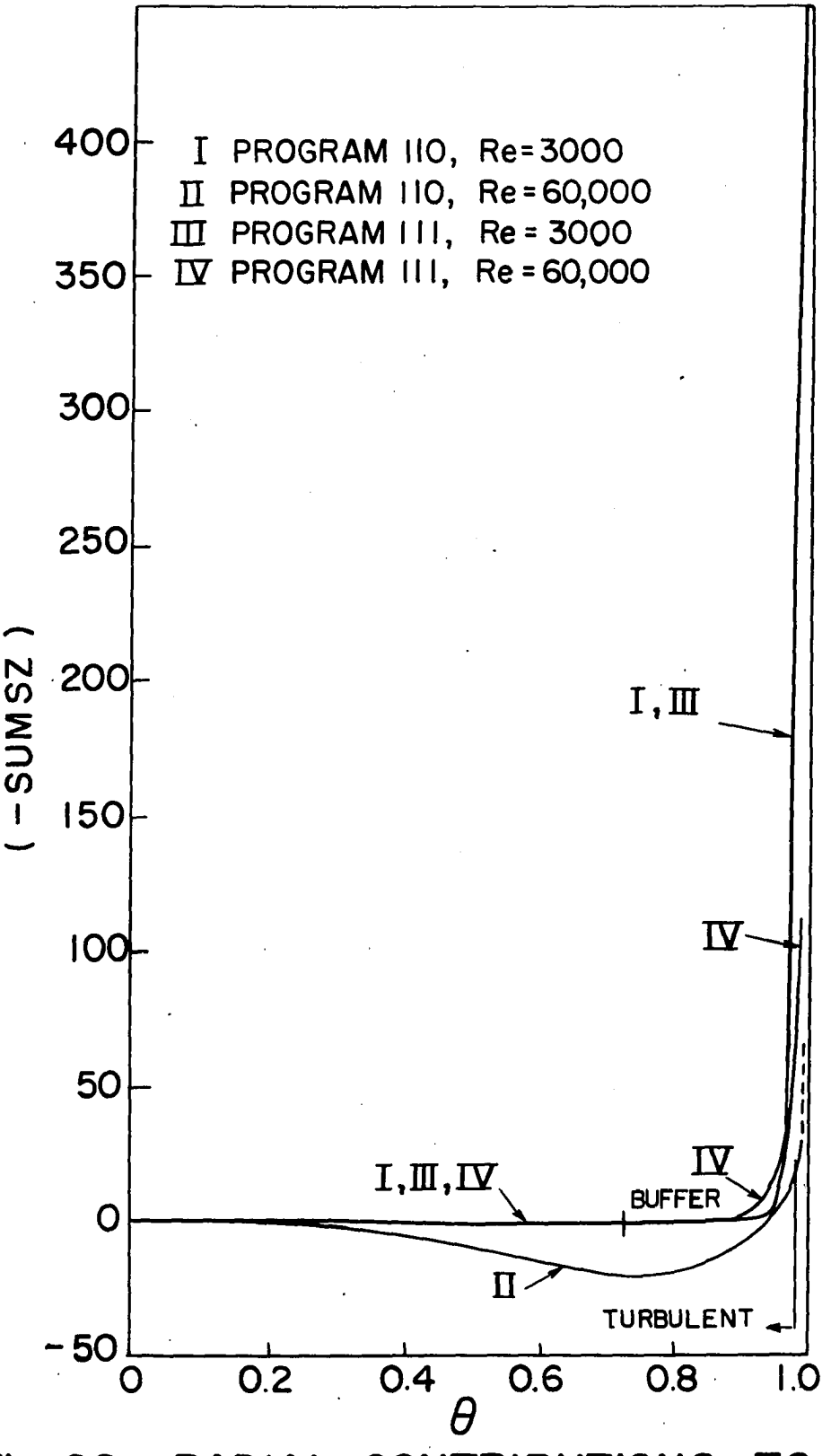


Fig. 29 RADIAL CONTRIBUTIONS TO AXIAL MIXING - LIN'S EQNS.

transition flow (Reynolds number between 3000 and 8000). At higher Re, E was found to go through a minimum which means that α_t must exceed ν. The proposed eddy diffusivity equation (Equation 4-27) gave results that are in good agreement with the mixing data reported in Appendix B (Re = 3770).

Variation of $\frac{\partial C}{\partial x}$ with Radial Position

Tichacek et al. (91) used a first order approximation to evaluate the validity of the assumption of constant $\frac{\partial C}{\partial x}$. They concluded that for most applications where the contaminated length is of the order of 50 to 100 pipe diameters, the error introduced in E due to this assumption is less than 25 %, or less than the usual scatter of mixing data. Their error analysis may not have picked up the effect of the steep wall gradients reported here, since their last interval was θ = 0.975 - 1.0.

Variations in $\frac{\partial C}{\partial x}$ are calculated here using Tichacek's method and the results obtained here. The object of this examination is to determine if variations in $\frac{\partial C}{\partial x}$ could account for the phenomenal rapid increase in SUMSZ near the wall.

By integrating the x partial derivative of Equation (5-1) twice with respect to r, we get:

$$\frac{1}{r}\ \frac{\partial}{\partial r}\left(\alpha\ r \frac{\partial C}{\partial r}\right) = (U-V)\ \frac{\partial C}{\partial x} + \frac{\partial C}{\partial t} \qquad (5\text{-}1)$$

$$\frac{\partial^2 C}{\partial t \partial x} = \frac{1}{r}\frac{\partial}{\partial r}\left(\alpha r \frac{\partial^2 C}{\partial r \partial x}\right) - (U-V)\frac{\partial^2 C}{\partial x^2} \tag{5-18}$$

$$\int_0^r \frac{1}{\alpha r'}\, dr' \int_0^{r'} (U-V)\frac{\partial^2 C}{\partial x^2}\, r''\, dr'' +$$

$$\int_0^r \frac{1}{\alpha r'}\, dr' \int_0^{r'} \frac{\partial^2 C}{\partial t\, \partial x}\, r''\, dr'' =$$

$$\int_0^r \frac{\partial^2 C}{\partial r\, \partial x} = \left.\frac{\partial C}{\partial x}\right|_r - \left.\frac{\partial C}{\partial x}\right|_0 \tag{5-19}$$

For a first order approximation, assume:

$$\frac{\partial^2 C}{\partial x^2} = \frac{\partial^2 C_m}{\partial x^2}\,, \quad \frac{\partial^2 C_m}{\partial t\, \partial x} = \frac{\partial^2 C}{\partial t\, \partial x}\,, \quad \frac{\partial C}{\partial t} = \frac{\partial C_m}{\partial t} \tag{5-20}$$

From the diffusion-type equation:

$$\frac{\partial}{\partial x}\frac{\partial C_m}{\partial t} = \frac{\partial}{\partial x}\left(E\frac{\partial^2 C_m}{\partial x^2}\right) \tag{5-21}$$

Substitute for $\frac{\partial^2 C}{\partial t\, \partial x}$ in (5-19) by $\frac{\partial}{\partial x} E \frac{\partial^2 C_m}{\partial x^2}$:

$$\left.\frac{\partial C}{\partial x}\right|_r - \left.\frac{\partial C}{\partial x}\right|_0 = \frac{\partial^2 C_m}{\partial x^2}\int_0^r \frac{1}{\alpha r'}\, dr' \int_0^r (U-V)\, r''\, dr'' +$$

$$E\frac{\partial^3 C_m}{\partial x^3}\int_0^r \frac{r'}{2\alpha}\, dr' \tag{5-22}$$

which can be written as:

$$\left.\frac{\partial C}{\partial x}\right|_\theta - \left.\frac{\partial C}{\partial x}\right|_0 = \frac{\partial^2 C_m}{\partial x^2}\int_0^\theta \frac{a^2}{\alpha\theta'}\int_0^\theta (U-V)\,\theta''\, d\theta'' +$$

$$a^2 E\frac{\partial^3 C_m}{\partial x^3}\int_0^\theta \frac{\theta'}{2\alpha}\, d\theta' \tag{5-23}$$

which is:

$$\left.\frac{\partial C}{\partial x}\right|_{\theta} - \left.\frac{\partial C}{\partial x}\right|_{o} = a^2 \frac{\partial^2 C_m}{\partial x^2} \text{SUMSY} + \frac{a^2 E}{2} \frac{\partial^3 C_m}{\partial x^3} \int_o^{\theta} \frac{\theta'}{\alpha} d\theta \quad (5\text{-}24)$$

Successive flow in pipe lines is a typical step-function imput which spreads into an integrated Gaussian function; C_m can be expressed in terms of x and t (19):

$$\frac{C_m}{C_o} = \frac{1}{2}\left[1 - \text{erf}\left(\frac{X}{2\sqrt{Et}}\right)\right] \quad (5\text{-}25)$$

One can therefore obtain the first, second and third x derivatives:

$$\frac{\partial C_m}{\partial x} = \frac{-C_o}{2\sqrt{\pi Et}} \exp - \frac{(x - Vt)^2}{4Et} \quad (5\text{-}26)$$

$$\frac{\partial^2 C_m}{\partial x^2} = - \frac{(x - Vt)}{2Et} \frac{\partial C_m}{\partial x} \quad (5\text{-}27)$$

$$\frac{\partial^3 C_m}{\partial x^3} = \frac{- (x - Vt)}{2Et} \frac{\partial^2 C_m}{\partial x^2} - \frac{1}{2Et} \frac{\partial C_m}{\partial x} \quad (5\text{-}28)$$

$$\text{let } \bar{x} = tV \quad (5\text{-}29)$$

$$\text{and } \eta = \frac{\bar{x}}{d} \text{ ratio} \quad (5\text{-}30)$$

also writing $x = \sigma \bar{x}$ where σ is a dimensionless factor. One could then evaluate $\left.\frac{\partial C}{\partial x}\right|_{\theta} - \left.\frac{\partial C}{\partial x}\right|_{o}$ from Equation (5-24) for water flow at Re = 60000 using computed SUMSY and evaluated $\int_o^{\theta} \frac{\theta'}{\alpha}$ (Program 506). Pipe diameter is taken as one inch, and E is read from estimated smooth pipe data as 0.156 $ft^2/sec.$, for a sudden switch from one pure liquid to another $C_o = 1$. The results plotted in

Figure 30 show that $\frac{\partial C}{\partial x}$ could vary appreciably over the pipe cross section at low length-diameter ratios ($\eta < 500$). The 50-100 diameters mentioned by Tichacek et al. is apparently too low. For very large η values (around 5000), the assumption of constant $\frac{\partial C}{\partial x}$ is quite good (Figure 30).

Summary of Conclusions

1. The axial mixing coefficient, E, is critically determined by the boundary layer which makes the greatest and most decisive contribution.
2. Diffusion in the "sublaminar" layer is turbulent rather than molecular.
3. For high Reynolds numbers (>10000), turbulent diffusivity (α_t) in the sublaminar is larger than the kinematic viscosity ν.
4. The axial eddy diffusivity effect on axial mixing was found to be more than 10% in some cases. This is considerably higher than estimates given in earlier work ($< 4\%$).
5. The assumption of constant $\frac{\partial C}{\partial x}$ is satisfactory for very large "contaminated" length - diameter ratios (>500).
6. Because the contribution of the turbulent core to axial mixing is negligibly small compared to that of the boundary layer, errors due to the Reynolds analogy assumption could not be determined until a reliable

boundary layer diffusivity equation is available.

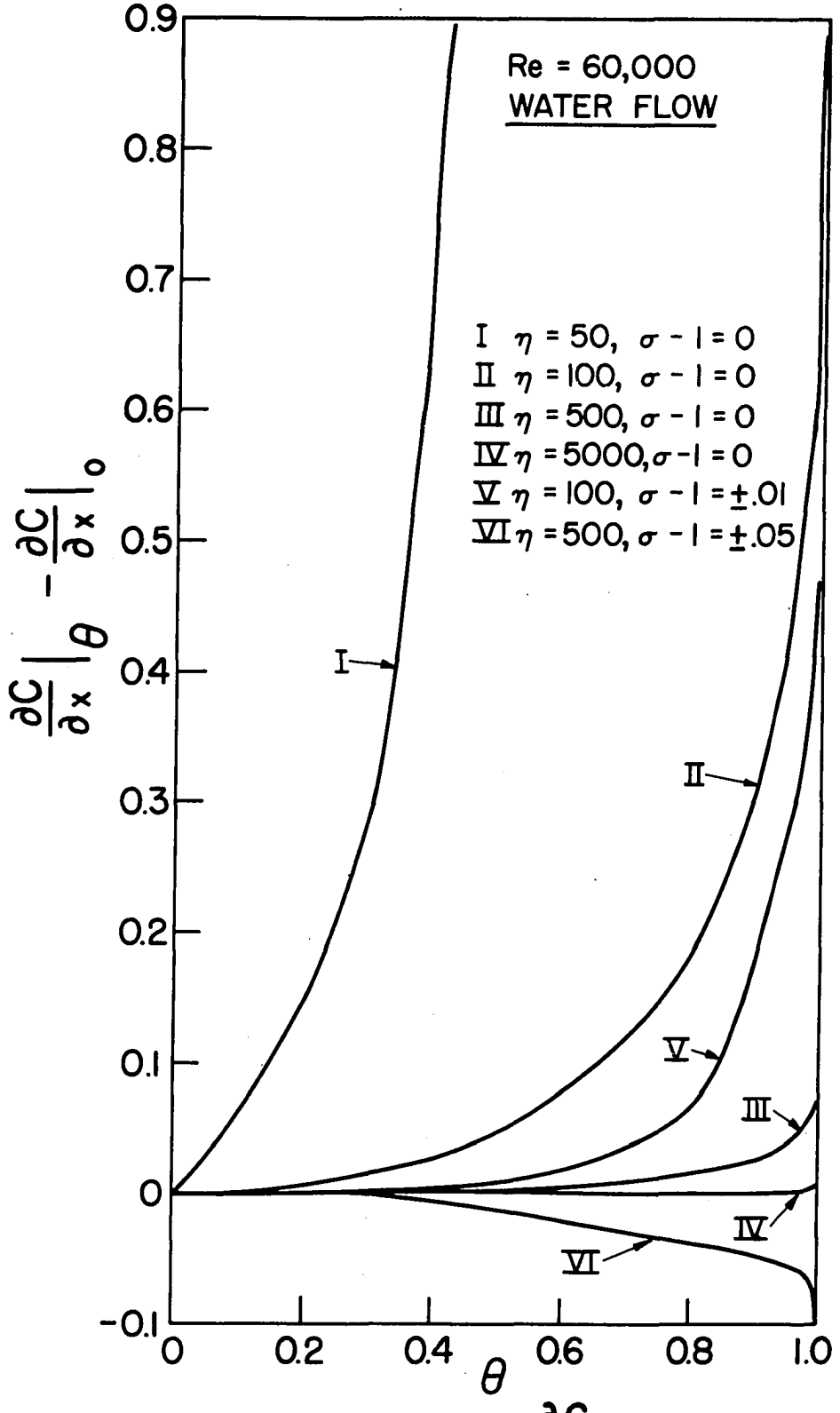


Fig. 30 VARIATION OF $\frac{\partial C}{\partial x}$ WITH RADIAL POSITION

CHAPTER VI

CONCLUSIONS

The following conclusions resulted from this study:

1. Turbulent diffusion in the "isotropic" core is related to the deformation rate tensor, pipe diameter, and the kinematic viscosity. Turbulent diffusion is therefore related to Eulerian turbulence quantities measured by hot wire anemometry (Chapter III).

2. A "microscopic deformation" model is postulated to describe the mechanism of turbulent diffusion. It is presented here as an extension of Prandtl's "Mixing Length Theory." Large eddies or lumps are assumed to deform and strain under the effect of permanent and fluctuating stresses until they break down into smaller and smaller eddies that disperse. Large eddies are considered anisotropic, enlongated in the axial direction and to have a diameter proportional to pipe diameter. The smallest eddies are considered isotropic and independent of pipe geometry as would be expected from the Theory of Local Isotropy (Chapter III).

3. An excellent correlation of core eddy diffusivity data was obtained by plotting $\frac{\alpha_c}{\nu}$ as a function of Reynolds

number. A generalized correlation is given that applies to mass or heat transfer for gas and liquid flow in pipes or between parallel plates at Reynolds numbers between 5000 and 684000 (Chapter II).

4. For long diffusion times in fully developed nondecaying turbulent pipe flow, turbulent diffusion was found to be independent of molecular diffusivity; treated data were for gaseous, aqueous, and liquid metal systems, Sc = 0.63-2341 (Chapter II).

5. Empirical relationships are given in this work for the Lagrangian integral scale (or Taylor's mixing length), eddy viscosity, turbulent Schmidt and Prandtl numbers in the "isotropic" central core. The material mixing length was found to be roughly 0.077 the pipe diameter (Chapter II).

6. An equation is proposed for the calculation of nonisotropic point eddy diffusivity across the entire pipe cross section. It is based on the premise that the positional eddy diffusivity is a function of core eddy diffusivity and the degree of isotropy (Chapter IV).

7. The overall axial mixing coefficient in pipe flow was found to be critically determined by the boundary layer which made the greatest and most decisive contribution. The synthetic numerical analysis used here showed that diffusion in the "sublaminar" layer must be turbulent rather than molecular. The relative effect of axial eddy

diffusivity on axial mixing was found to be more than ten per cent which is higher than earlier estimates (4%). The assumption of constant $\frac{\partial C}{\partial x}$ was found acceptable at length-diameter ratios greater than five hundred (Chapter V).

8. The overall axial mixing coefficient was determined experimentally for transitional water flow in a straight tube by the pulse response method. The result agreed with earlier data by Fowler and Brown (26), (Appendix-B).

BIBLIOGRAPHY

1. Allen, C. M. and E. A. Taylor. "The Salt Velocity Method of Water Measurement," Trans. ASME, 45 (December, 1923), 285-341.

2. Arnold, J. H. "Studies in Diffusion: Part II. A Kinetic Theory of Diffusion in Liquid Systems," J. Am. Chem. Soc., 52 (October, 1930), 3937-3955.

3. Baldwin, L. V. "Turbulent Diffusion in the Core of Fully Developed Pipe Flow," Ph.D. Thesis in Chemical Engineering, Case Institute of Technology, Cleveland, Ohio, (1959).

4. Baldwin, L. V. and T. J. Walsh. "Turbulent Diffusion in the Core of Fully Developed Pipe Flow," A. I. Ch. E. Journal, 7, No. 1 (March, 1961), 53-61.

5. Batchelor, G. K. "Small-scale Variation of Convected Quantities Like Temperature in Turbulent Fluid: Part I. General Discussion and the Case of Small Conductivity," J. Fluid Mech., 5 (January, 1959), 113-133.

6. _____. "Kolmogoroff's Theory of Locally Isotropic Turbulence," Proc. Camb. Phil. Soc., 43 (1947), 533-559.

7. Batchelor, G. K. and A. A. Townsend. Surveys in Mechanics. Cambridge: Cambridge University Press, 1956, 367.

8. Becker, H. A., R. E. Rosensweig and J. R. Gwozdz. Turbulent Dispersion in a Pipe Flow. Paper presented at the fifty-seventh annual A.I.Ch.E. meeting, Boston, Massachusetts, 1964.

9. Bosworth, R. C. L. "Distribution of Reaction Times for Laminar Flow in Cylindrical Reactors," Phil. Mag., 39 (1948), 847-858.

10. Boussinesq, J. Mem. Pres. par Div. Savants a l'Acad. Sci. Paris. 23 (1877), 46.

11. Brookshire, W. A. "A Study of the Structure of Turbulent Shear Flow in Pipes," Ph.D. Thesis in Chemical Engineering, Louisiana State University, Baton Rouge, Louisiana, (1961).

12. Carter, D. and W. G. Bir. "Axial Mixing in a Tubular High Pressure Reactor," Chem. Eng. Progr., 58, No. 3 (March, 1962), 40-43.

13. Cohen, M. F., M. S. Thesis in Chemical Engineering, The Ohio State University, Columbus, Ohio, (1962).

14. Connell, W. R., W. G. Schlinger and B. H. Sage. American Documentation Institute, Washington, D. C., Doc. 3657 (1952).

15. Corcoran, W. H., J. B. Opfell and B. H. Sage. Momentum Transfer in Fluids. New York: Academic Press Inc., 1956, 201-206.

16. Corrsin, Stanley. "The Isotropic Turbulent Mixer: Part II. Arbitrary Schmidt Number," A.I.Ch.E. Journal, 10, No.6 (November, 1964), 870-877.

17. _____. "On the Spectrum of Isotropic Temperature Fluctuations in an Isotropic Turbulence," J. Appl. Phys., 22 (April, 1951), 469-473.

18. _____. "Further Generalization of Onsager's Cascade Model for Turbulent Spectra," The Physics of Fluids, 7, No. 8 (August, 1964), 1156-1159.

19. Danckwerts, P. V. "Continuous Flow Systems: Distribution of Residence Times," Chem. Eng. Sci., 2, No. 1 (February, 1953), 1-13.

20. Deissler, R. G. Analytical and Experimental Investigation of Adiabatic Turbulent Flow in Smooth Pipes. National Advisory Committee for Aeronautics, Technical Note 2138, (July, 1950).

21. Ebach, E. A. Private Communication.

22. Emmert, R. E. and R. L. Pigford. Chemical Engineer's Handbook. 4th ed. New York: McGraw-Hill Book Co. Inc., 1963, 14-14.

23. Fage, A. and H. C. H. Townend. "An Examination of Turbulent Flow with an Ultramicroscope," Proc. Roy. Soc. (London), 135A (1932), 656.

24. Farrell, M. A. and E. F. Leonard. "Dispersion in Laminar Flow by Simultaneous Convection and Diffusion," A.I.Ch.E. Journal, 9 (March, 1963), 190-195.

25. Flint, D. L., H. Kada and T. J. Hanratty. "Point Source Turbulent Diffusion in a Pipe," A.I.Ch.E. Journal, 6, No. 2 (June, 1960), 325-331.

26. Fowler, C. F. and G. G. Brown. "Contamination by Successive Flow in Pipe Lines," Trans. A.I.Ch.E., 39 (1943), 491-516.

27. Frandolig, J. E. and R. W. Fahlen. Mass Transfer in Low Velocity Gas Streams. U. S. Atomic Energy Commission Report No. ISC-908, (1957).

28. Friedlander-Topper. Turbulence--Classical Papers on Statistical Theory. New York: Interscience Publishers, Inc., 1961, 151-156, 159-162. (Translations of 44 and 45).

29. Gibson, C. H. "Scalar Mixing in Turbulent Flow," Ph.D. Thesis, Stanford University, Palo Alto, California, (1962).

30. Goldstein, S. Modern Developments in Fluid Dynamics. Oxford: The Clarendon Press, 1938, 331-356.

31. Hinze, J. O. Turbulence. New York: McGraw-Hill Book Company, Inc., 1959, 15.

32. _____. 154.

33. _____. 181-190.

34. _____. 467-487, 514-520.

35. _____. 525.

36. _____. 526-537.

37. Hull, E. D. and J. W. Kent. "Radioactive Tracers to Mark Interfaces and Measure Intermixing in Pipelines," Ind. Eng. Chem., 44, No. 11 (November, 1952), 867.

38. Isakoff, Sheldon. "Heat and Momentum Transfer in Turbulent Flow of Mercury," Ph.D. Thesis in Chemical Engineering, Columbia University, New York, New York, (1952).

39. Johnk, R. E. and T. J. Hanratty. "Temperature Profiles for Turbulent Flow of Air in a Pipe: I. The Fully Developed Heat Transfer Region," Chem. Eng. Sci., 17 (November, 1962), 867-879.

40. Kalinske, A. A. and E. R. Van Driest. Fifth International Congress for Applied Mechanics Proceedings. New York: John Wiley and Sons, 1939.

41. Keeler, R. N., E. E. Petersen and J. M. Prausnitz. "Mixing and Chemical Reaction in Turbulent Flow Reactors," A.I.Ch.E. Journal, 11 (March 1965), 221-224.

42. Keyes, J. J. "Diffusional Film Characteristics in Turbulent Flow: Dynamic Response Method," A.I.Ch.E. Journal, 1, No. 3 (September, 1955), 305-311.

43. Knudsen, J. G. and D. L. Katz. Fluid Dynamics and Heat Transfer. New York: McGraw-Hill Book Company, Inc., 1958, 224.

44. Kolmogoroff, A. N. "Dissipation of Energy in the Locally Isotropic Turbulence," Comptes Rendus (Doklady) de l'Academie des Sciences de l'U.R.S.S., 30 (1941), 301-305.

45. _____. 32 (1941), 16-18.

46. Laufer, J. The Structure of Turbulence in Fully Developed Pipe Flow. National Advisory Committee for Aeronautics, Technical Report 1174, (1954).

47. _____. Private Communication.

48. Lee, J. "Turbulent Motion and Mixing," Ph.D. Thesis in Chemical Engineering, The Ohio State University, Columbus, Ohio, (1962).

49. Lee, J. and Robert S. Brodkey. Turbulent Motion and Mixing in a Pipe. Paper presented at the A.I.Ch.E. National Meeting, Chicago, Illinois, 1962.

50. Levenspiel, O. and W. K. Smith. "Notes on the Diffusion-Type Model for the Longitudinal Mixing of Fluids in Flow," Chem. Eng. Sci., 6 (April-May, 1957), 227-33.

51. Lin, C. C. "On Taylor's Hypothesis and the Acceleration Terms in the Navier-Stokes Equations," Quart. Appl. Math., 10 (1953), 295-306.

52. Lin, C. S., P. W. Moulton and G. L. Putnam. "Mass Transfer Between Solid Wall and Fluid Streams," Ind. Eng. Chem., 45, No. 3 (March, 1953), 636-640.

53. Liepmann, H. W., J. Laufer and K. Liepmann. On the Spectrum of Isotropic Turbulence. National Advisory Committee for Aeronautics, Technical Note 2473, (November, 1951).

54. Lynn, Scott, W. H. Corcoran and B. H. Sage. "Material Transport in Turbulent Gas Streams: Radial Diffusion in a Circular Conduit," A.I.Ch.E. Journal, 3, No. 1 (March, 1957), 11-15.

55. Martin, G. Q. "An Investigation into the Turbulence Characteristics of Fluids in Pipe Flow," Ph.D. Thesis in Chemical Engineering, University of Washington, Seattle, Washington, (1963).

56. McCarter, R. J., L. F. Stutzman and H. A. Koch, Jr. "Temperature Gradients and Eddy Diffusivities in Turbulent Fluid Flow " Ind. Eng. Chem., 41, No. 6 (June, 1949), 1290-1295.

57. McMaster, L. P. "Flash Photolysis Tracer Studies," B. S. Thesis in Chemical Engineering, University of Delaware, Newark, Delaware, (1964).

58. Mickelsen, W. R. An Experimental Comparison of the Lagrangian and Eulerian Correlation Coefficients in Homogeneous Isotropic Turbulence. National Advisory Committee for Aeronautics, Technical Note 3570, (October, 1955).

59. _____. "Measurements of the Effect of Molecular Diffusivity in Turbulent Diffusion," J. Fluid Mech., 7, part 3 (March, 1960), 397-400.

60. Nikuradse, J. VDI - Forschungsheft No. 356, (1932).

61. Nunner, W. "Wärmeübergang and Druckabfall in Rauhen Rohren," VDI - Forschungsheft No. 455, (1956).

62. Page, F., Jr., W. G. Schlinger, D. K. Breaux and B. H. Sage. "Point Values of Eddy Conductivity and Viscosity in Uniform Flow Between Parallel Plates," Ind. Eng. Chem., 44, No. 2 (February, 1952) 424-430.

63. Page, F., Jr., W. H. Corcoran, W. G. Schlinger and B. H. Sage. "Temperature and Velocity Distributions in Uniform Flow Between Parallel Plates," Ind. Eng. Chem., 44, No. 2 (February, 1952), 419-423.

64. Reid, R. C. and T. K. Sherwood. The Properties of Gases and Liquids. New York: McGraw-Hill Book Company, Inc., 1958, 268.

65. Reiss, L. P. and T. J. Hanratty. "Measurement of Instantaneous Rates of Mass Transfer to a Small Sink on a Wall," A.I.Ch.E. Journal, 8, No. 2 (May, 1962), 245-247.

66. Rice, S. O. "Mathematical Analysis of Random Noise," The Bell System Tech. J., 24 (1945), 46-108.

67. Roley, G. and R. W. Fahien. Gaseous Diffusion at Moderate Flow Rates in Circular Conduits. U. S. Atomic Energy Commission Report No. IS 330, (1960).

68. Rothfus, R. R. and C. C. Monrad. "Correlation of Turbulent Velocities for Tubes and Parallel Plates," Ind. Eng. Chem., 47, No. 6 (June, 1955), 1144-1149.

69. Saffman, P. G. "On the Effect of the Molecular Diffusivity in Turbulent Diffusion," J. Fluid Mech., 8, part 2 (June, 1960), 273-283.

70. Sandborn, V. A. Experimental Evaluation of Momentum Terms in Turbulent Pipe Flow. National Advisory Committee for Aeronautics, Technical Note 3266, (January, 1955).

71. _____. Private Communication.

72. Schlichting, H. Boundary Layer Theory. 4th ed. New York: McGraw-Hill Book Company, Inc., 1960, 487-492 and 502-514.

73. Schlinger, W. G., V. J. Berry, J. L. Mason and B. H. Sage. "Temperature Gradients in Turbulent Gas Streams: Nonuniform Flow," Ind. Eng. Chem., 45, No. 3 (March, 1953), 662-666.

74. Seagrave, R. C. "Turbulent Mass Transfer in Liquid Streams," Ph.D. Thesis in Chemical Engineering, Iowa State University, Ames, Iowa, (1961).

75. Seagrave, R. C. and R. W. Fahien. Turbulent Mass Transfer in Liquid Streams. Paper presented at the A.I.Ch.E. National Meeting, New Orleans, Louisiana, 1961.

76. _____. Turbulent Mass Transport in Liquid Streams - Radial and Axial Mass Diffusivities. Preprint.

77. Senecal, Vance E. "Fluid Flow in the Transition Zone," Ph.D. Thesis in Chemical Engineering, Carnegie Institute of Technology, Pittsburgh, Pennsylvania, (1951).

78. Sherwood, T. K. and B. B. Woertz. "The Role of Eddy Diffusion in Mass Transfer Between Phases," Trans. A.I.Ch.E., 35 (1939), 517-540.

79. Simmons, L. F. G. and C. Salter. "Velocity Variations in Turbulent Flow," Proc. Roy. Soc. (London), Ser. A., 145 (1934), 212-234.

80. _____. "An Experimental Determination of the Spectrum of Turbulence," Proc. Roy. Soc. (London), Ser. A., 165 (1938), 73-89.

81. Sjenitzer, F. "How Much Do Products Mix in a Pipeline?", Petroleum Engineer, 30, No. 13 (December, 1958), D31-D34.

82. Smith, S. S. and R. K. Schulze. "Interfacial Mixing Characteristics of Products in Products Pipe Lines," Petroleum Engineer, 20 (September, 1948), 330.

83. Tatarski, V. I. Wave Propagation in a Turbulent Medium. New York: McGraw-Hill Book Company, Inc., 1961, 44-49. (Translated from Russian).

84. Taylor, G. I. "Diffusion by Continuous Movements," Proc. Lond. Math. Soc., 20 (1921), 196-212.

85. _____. "Statistical Theory of Turbulence," Proc. Roy. Soc. (London), Ser. A., 151 (1935), 421-478.

86. _____. "The Spectrum of Turbulence," Proc. Roy. Soc. (London), Ser. A., 164 (1938), 476-490.

87. _____. "Dispersion of Soluble Matter in Solvent Flowing Slowly Through a Tube," Proc. Roy. Soc. (London), Ser. A., 219 (1953), 186-203.

88. _____. "The Dispersion of Matter in Turbulent Flow Through a Pipe," Proc. Roy. Soc. (London), Ser. A., 223 (1954), 446-468.

89. _____. "Conditions Under Which Dispersion of a Solute in a Stream of Solvent Can Be Used to Measure Molecular Diffusion," Proc. Roy. Soc. (London), Ser. A., 225 (1954), 473-477.

90. _____. "The Present Position in the Theory of Turbulent Diffusion," Advances in Geophysics, 6 (1959), 101-111.

91. Tichacek, L. J., C. H. Barkelew and Thomas Baron. "Axial Mixing in Pipes," A.I.Ch.E. Journal, 3, No. 4 (December, 1957), 439-442.

92. Towle, W. L. and T. K. Sherwood. "Eddy Diffusion: Mass Transfer in the Central Portion of a Turbulent Air Stream," Ind. Eng. Chem., 31, No. 4 (April, 1939), 457-462.

93. Townend, H. C. H. "Turbulence in the Flow of Air Through a Pipe," Proc. Roy. Soc. (London), Ser. A., 145 (1934), 180-211.

94. Townsend, A. A. Proc. Camb. Phil. Soc., 43 (1947), 560-570.

95. _____. "The Diffusion Behind a Line Source in Homogeneous Turbulence," Proc. Roy. Soc. (London), Ser. A., 224 (1954), 487.

96. _____. The Structure of Turbulent Shear Flow. Cambridge: Cambridge University Press, 1956, 202-219.

97. Van de Vusse, J. G. "A New Model for the Stirred Tank Reactor," Chem. Eng. Sci., 17 (July, 1962), 507-521.

98. Von Karman, T. J. Aeronaut. Sci., 1 (1934), 1.

99. Von Karman, T. and L. Howarth. "On the Statistical Theory of Isotropic Turbulence," Proc. Roy. Soc. (London), Ser. A., 164, (1938), 192-215.

100. Wasan, D. T., C. L. Tien and C. R. Wilke. "Theoretical Correlation of Velocity and Eddy Viscosity for Flow Close to a Pipe Wall," A.I.Ch.E. Journal, 9, No. 4 (July, 1963), 567-569.

101. Wilke, C. R. "Estimation of Liquid Diffusion Coefficients," Chem. Eng. Progr. 45, No. 3 (March, 1949), 218-224.

NOMENCLATURE

a	pipe radius
A	area of tube cross section
a_o	spacing between parallel plates or width of rectangular duct
b	a scalar constant in Equation (3-45)
B	numerical factor in Equation (3-33)
C	concentration at a point
C_a	concentration at pipe axis
C_o	concentration of tracer in a pulse slug
C_m	average concentration across the cross section
d	pipe diameter
D_m	molecular diffusivity
D_{12}^m	molecular diffusivity of fluid 1 into fluid 2
$\overline{D'_{xy}}$	root mean square turbulent deformation
$\overline{D^2_{xy}}$	mean square turbulent deformation
$D_{xy}(t)$	total instantaneous deformation
E	axial mixing coefficient
$F(n)$	the one dimensional spectrum function
G	degree of isotropy $= \frac{v'}{u'}$
h	a constant in Equation (3-25)
H	height of tracer paraboloid within the slit
I	intensity of emerging light beam

I_i	intensity of incident light beam (on the flow tube)
$\underline{J}$	rate of mass flux in vectorial notations
k	Baldwin's empirical factor, Equation (3-43)
K	Von Karman's constant in Equation (3-27)
ℓ	Prandtl mixing length
ℓ_L	Lagrangian integral scale or Taylor's mixing length for the turbulent diffusion of mass or heat
L	tube length
L_{yv}, L_{xu}, etc.	Eulerian scales of turbulence
m	dimensionless slit thickness $= \frac{\delta}{L}$
n	frequency in the energy spectrum
$\overline{n^2}$	$= \int_0^\infty n^2 F(n)\, dn$
n	Nunner velocity distribution exponent $= 1/\sqrt{\lambda}$
N_v	expected number of zero v velocities per second
N_u	expected number of zero u velocities per second
p	fluctuating pressure at a point
q	dimensionless pulse thickness $= \frac{X}{L}$
Q	flow rate of injected point-source tracer
r	radial distance
R_{xu}	Eulerian correlation coefficient for u velocities at points spaced x apart
R_{yv}	Eulerian correlation coefficient for v velocities at points spaced y apart

R_{uv}	Eulerian cross correlation coefficient between u and v at a point
R_L	Lagrangian correlation coefficient
s	distance between the source and a point at a radial distance r from the axis ($s = \sqrt{r^2 + x^2}$
t	time
t_o	time elapsed from the introduction of a pulse to the first appearance of its response
T_1	time limit in Equation (3-1)
T	Lagrangian integral time scale $T = \int_o^\infty R_L \, d\xi$
u	fluctuating velocity in the x direction
u'	root mean square fluctuating u velocity
u^+	dimensionless velocity parameter $= \frac{U}{U_*}$
U(t)	instantaneous velocity
U	mean velocity in the x direction at point r
U_o	maximum mean velocity at the pipe axis
U_*	friction velocity $= \sqrt{\frac{\tau_w}{\rho}}$
v	fluctuating velocity in the y direction
v_L	fluctuating Lagrangian particle velocity in the y direction
v_L'	$= \sqrt{\overline{v_L^2}}$
V	average bulk velocity
w	fluctuating velocity in the z direction
x	direction of main flow
$\overline{x}$	= tV for a step imput
X	pulse thickness

y lateral direction

y' distance from the wall

y^+ dimensionless distance parameter $= \frac{y' U_*}{\nu}$

Y_i the integral obtained after the second sequential integration in Equation (5-11)

$\overline{Y^2}$ variance of the concentration distribution at any point x downstream from a point source

z z direction in a cartesian coordinate system

Z_i the final integral obtained after three sequential integrations, Equation (5-13)

Dimensionless Numbers

Pe Peclet number $= \frac{Vd}{\alpha_c}$

$(Pr)_t$ turbulent Prandtl number in the core $= \frac{\epsilon_c}{\alpha_c}$

Re Reynolds number $= \frac{Vd}{\nu}$

Re_c axial Reynolds number $= \frac{U_o d}{\nu}$

Re_λ = microscale Reynolds number $= \frac{u' \lambda_g}{\nu}$

Sc molecular Schmidt number $= \frac{\mu}{\rho D_m}$

$(Sc)_t$ turbulent Schmidt number in the core $= \frac{\epsilon_c}{\alpha_c}$

Greek Letters

α eddy diffusivity at any point r

α_c average eddy diffusivity across the core

α_r radial eddy diffusivity computed when the term $\alpha_x \frac{\partial^2 C}{\partial x^2}$ is not ignored

α_x axial eddy diffusivity

α_y	eddy diffusivity in the y direction
α_t	turbulent diffusivity = $\alpha - D_m$
γ	amount of tracer introduced in the slug = C_o X A
δ	slit thickness
ϵ	eddy viscosity
ϵ_c	average eddy viscosity across the core
ϵ_t	turbulent diffusivity for momentum transfer = $\epsilon - \nu$
η	length (or position) - diameter ratio, η = $\bar{x}/d$
θ	relative distance variable = r/a
λ	Moody friction factor
λ_f	Longitudinal microscale of turbulence
λ_g	Taylor's microscale of turbulence
ξ	time variable
ξ'	local rate of energy dissipation per unit mass per unit time
μ	dynamic viscosity
ν	kinematic viscosity
ρ	density
σ	a numerical factor indicating relative position from the mean, $x = \sigma\bar{x}$
τ_{yx}	shear stress in the x direction on a fluid surface of constant y

τ_w axial shear stress at the wall

ϕ rate of material transport in the axial direction across a reference plane moving with velocity V

ω vorticity

ω_f Lagrangian spreading coefficient

ω_f Eulerian spreading coefficient

Arabic Letters

$\forall$ volume of test section of the tube = LA

Subscripts

t indicates the contribution of the turbulent effect

m indicates the contribution of the molecular effect

APPENDIX A

DETERMINATION OF TURBULENT DEFORMATION FROM TURBULENCE MEASUREMENTS

The mean square deformation or the dissipation terms $\overline{\left(\frac{\partial u}{\partial y}\right)^2}$, etc. can be determined from any of these four different types of experimental turbulence data:

(a) The microscale of turbulence (correlation coefficient data).

(b) By electronically differentiating a hot wire velocity signal.

(c) The energy spectrum.

(d) The frequency of occurrence of zero velocities per second as determined by zero counts.

The microscale of turbulence which is also called the dissipation length has been defined by Equations (3-6), (3-7) and (3-16). The determination of the microscale from the correlation coefficient requires that the shape of the correlation curve be accurately known at its vertex. Accurate measurement of R_{xu} becomes increasingly difficult as its value approaches unity. Because of this, this method is considered less preferable and less accurate than other alternative methods for determining turbulent dissipative terms. Equation (3-17) relates λ_f and $\overline{\left(\frac{\partial u}{\partial x}\right)^2}$:

$$\frac{1}{\lambda_f^2} = \frac{1}{2\,\overline{u^2}} \overline{\left(\frac{\partial u}{\partial x}\right)^2} \qquad (3\text{-}17)$$

Another method for determining $\overline{\left(\frac{\partial u}{\partial x}\right)^2}$ is by electronically differentiating a hot wire velocity signal, thus determining $\overline{\left(\frac{\partial u}{\partial t}\right)^2}$ directly (94). Taylor's transformation for homogeneous turbulence may be then applied

$$\frac{\partial}{\partial t} = - U \frac{\partial}{\partial x} \qquad (A\text{-}1)$$

and

$$\overline{\left(\frac{\partial u}{\partial x}\right)^2} = \frac{1}{U^2} \overline{\left(\frac{\partial u}{\partial t}\right)^2} \qquad (A\text{-}2)$$

Lin (51) showed that this assumption is valid if no mean velocity gradient exists and if $(\frac{u}{U})^2 << 1$. Both conditions are well satisfied across the turbulent core. This direct method is considered one of the most accurate and reliable.

The intensity of deformation could be also determined from energy spectrum data. The method is comparable in its accuracy to the direct velocity differentiation method. By making use of the fact that the energy spectrum and the correlation coefficient are related by Fourier transforms, and also by taking into consideration Equation (3-16) which relates the microscale to the second derivative of the correlation coefficient, the following equation was obtained:

$$\frac{1}{\lambda_f^2} = \frac{2\pi^2}{U^2} \int_0^\infty n^2 F(n)\, dn \qquad (A\text{-}3)$$

That is, the microscale is related to the integral of the second moment of the energy spectrum function which is normally written as $\overline{n^2}$ and could be determined by graphical integration.

From Equations (3-17) and (A-3) it follows that

$$\overline{\left(\frac{\partial u}{\partial x}\right)^2} = \frac{4\pi^2\, \overline{u^2}}{U^2} \int_0^\infty n^2 F(n)\, dn \qquad (A\text{-}4)$$

It can be also shown that the intensity of deformation, D'_{xy}, is related to the frequency of occurrence of zero velocities per second, N_u, and the intensity of turbulence, $\frac{u'}{U}$. This is a very interesting relationship since both parameters describe the velocity spectrum and can be obtained from it. It bears resemblance to the simpler case of a sinusoidal wave that is characterized by its frequency and amplitude. In a Lagrangian sense, the frequency of occurrence of zero velocities is analogous to the number of times a particle changes direction per unit time. It was intuitively felt early in this work that some sort of relationship should exist between the turbulent diffusion coefficient and the Eulerian parameters N_u and $\frac{u'}{U}$. The intensity of deformation is shown below to be approximately a linear function of the

product of these two quantities.

Rice (66) related the expected number of passages through zero per unit time to the energy spectrum function of any linear stationary random process such as electrical noise. The condition of linearity is an approximation in case of turbulence since the equations of motion are nonlinear. As a result of this, the distribution of $\frac{\partial u}{\partial t}$ is in general slightly skewed rather than truly Gaussian. The error introduced due to this approximation was tested by Liepmann et al. (53) by comparing the microscale values calculated from actual zero counts with those obtained by velocity differentiation or from the energy spectrum. The absolute values of λ_g^2 calculated from zero counts were somewhat larger than those obtained by other methods. The deviation, however, does not appear to be significant. The frequency of occurrence of zero velocities could be easily counted over a long period of time from an oscilloscope signal and used for calculating the intensity of deformation.

Rice showed that:

$$N_u = 2\left[\int_0^\infty n^2\, F(n)\, dn\right]^{\frac{1}{2}} \qquad (A\text{-}5)$$

$$= 2\sqrt{\overline{n^2}}$$

Where N_u is the expected number of occurrences of zero u

velocities per second. Equations (A-3) and (A-4) show that N_u can be readily related to λ_f and $\overline{(\frac{\partial u}{\partial x})^2}$

$$\frac{1}{\lambda_f^2} = \frac{2\pi^2 \overline{n^2}}{U^2} \tag{A-3}$$

$$\overline{\left(\frac{\partial u}{\partial x}\right)^2} = \frac{4\pi^2 \overline{u^2}\ \overline{n^2}}{U^2} \tag{A-4}$$

and since

$$\overline{\left(\frac{\partial v}{\partial x}\right)^2} = 2\ \overline{\left(\frac{\partial u}{\partial x}\right)^2} \tag{3-10}$$

Then

$$N_v = \sqrt{2}\ N_u \tag{A-6}$$

Where N_v is the expected number of occurrences of zero v velocities per second.

It can be easily seen from Equations (3-58), (3-9), (A-4), (3-68) and (A-6) that:

$$D'_{xy} = \pi\sqrt{\frac{3}{2}}\ (\frac{v'}{U})\ N_v$$

$$= 3.846\ (\frac{v'}{U})\ N_v \tag{A-7}$$

and

$$\xi' = (73.95)\ \nu\ (\frac{v'}{U})^2\ N_v^2 \tag{A-8}$$

where ξ' is the rate of energy dissipation per unit mass per unit time.

Other equations relating N_v and other isotropic turbulence parameters are:

$$N_v = \frac{U}{\pi v'} \left[\overline{\left(\frac{\partial v}{\partial x} \right)^2} \right]^{\frac{1}{2}} \qquad \text{(A-9)}$$

$$N_v = \frac{2U}{\pi \lambda_f} \qquad \text{(A-10)}$$

U here is the mean velocity for the pipe core which is approximately equal to the maximum mean velocity U_o.

APPENDIX B

EXPERIMENTAL DETERMINATION OF AXIAL MIXING IN TRANSITION FLOW

Problem Review

The scope of this experimental investigation is limited to the determination of the axial mixing coefficient in case of transitional or low turbulence flow in a straight smooth tube at a Reynolds number of 3770 and a high Moody friction factor λ of 0.04.

One of the well-known methods for studying transfer characteristics of packed beds as well as open pipes is transient response to a pulse function. The response curve is a recording of the concentration of the tracer at the end of the test section as a function of t. This C-t curve represents the residence time distribution and provides useful information that can be interpreted in terms of mixing or reactor efficiency. Theoretically, a uniform slug of tracer is assumed to appear instantly in the moving stream at the beginning of the test section. The rapid introduction of a tracer slug by means of pulse injection normally results in some flow disturbances due to the fact that the flow is interrupted or brought to rest momentarily during the injection. Following the injection,

the fluid goes through a period during which both turbulence and velocity profile are not fully developed. The complete development of a steady flow pattern occurs at some distance from the injector. For short tubes, the length of the unsteady section could be appreciable compared to the total length of the test section which may introduce sizeable errors in the results. Disturbances due to the injection effect may not be noticeable in case of packed beds since the bed acts as a filter that damps out these disturbances. On the other hand, slight disturbances are likely to be readily transmitted through the test section of an open pipe.

It is rather surprising that this injection effect has been neglected in the past which makes one wonder about the accuracy of the experimental data obtained from open tubes of low L/d ratios. Ebach (21) communicated to the writer that he encountered considerable difficulties in packed bed investigation due to the nonuniformity of the velocity profile after injection and the lack of uniformity of the tracer within the tube cross section. Some of the runs in his work gave irregular or wavy response traces that were discarded and not reported.

Several authors reported axial mixing data in open pipe flow (1, 12, 26, 37, 42, 50, 81, 82, 87, 88). The only smooth pipe data available on axial mixing in the unstable transition flow at large values of λ are those

of Fowler and Brown (26) which were reported some twenty years ago in which stationary step function technique was applied by switching the flow using a three-way valve. Samples were collected from the end of the tube in a series of beakers contained in a motor driven moving cart. According to the authors, spillage in flowing into the beakers was the major source of error. It is now known that a true step function can not be produced by this technique since the switching of streams takes place in a finite rather than infinitesimal time.

The experiment reported here differs from Fowler's work in that a pulse function input is used rather than a step function. The concentration of the tracer at the end of the test section is determined photometrically, using a highly sensitive detecting device, and recorded on a recorder of about 10 milliseconds resolution time.

Apparatus and Procedure

The set-up consisted of a constant head water tank, a 0.276 inch I.D. straight pyrex glass tube, a pulse injector, a device for the photometric determination of tracer concentration, and a recorder. A needle valve was used for regulating the flow rate followed by a 100 diameter entry length for the full development of the flow pattern, and the pulse injector which was located right before the test section. The tube passed through the photometer or colorimeter which was at the other end of the test section.

The building's tap water was fed to the constant head feed tank.

Figure 31 depicts the pulse injection device used for obtaining the data reported here. The flow tube was aligned and supported by lucite blocks A and B and fitted flush against C. Part C was also a lucite parallelpiped with two one-half inch long cylindrical conduits bored in it that were of the same diameter as the I.D. of the flow tube. All B blocks were fixed to a heavy steel frame; blocks A were pressed tight against C by the shown springs. In order to minimize mechanical vibrations caused by the strong impact of a stroke, the supporting frame was firmly bolted to a heavy concrete filled 10 inch pipe pedestal which in turn was bolted to the ground.

The procedure followed for injecting a tracer slug was to charge the tracer chamber with $KMnO_4$ solution using a syringe. After plugging the holes with the three screws, the pulse was quickly placed in the main stream in less than 200 milliseconds by pulling the lever L which forced part C downward to the injection position, thus making the tracer slug part of the flow stream.

Figure 32 shows a piston-type pulse injector that did not perform satisfactorily due to mechanical problems and was discarded. The injector was made out of solid aluminum except for the plunger which was "Teflon" lined brass. The main difficulty was that minute particles

of solid deposits or sediments from the water were trapped in the clearance between the moving plunger and the stationary body, thus hindering the free motion of the inner plunger or preventing it from completing a stroke. Also, slight scratches developed in the "Teflon" lining causing leakage from the tracer chamber.

A photometer or colorimeter was constructed for determining the concentration of $KMnO_4$ tracer in the flow at the end of the test section. The light source was an 85 watts, G.E. -H85-C3 mercury arc lamp that emits a predominantly green light beam which was passed through a collimating lens, an Iris diaphragm, an interference filter, and a 7 x 3.2 mms slit followed by the flow tube. Part of the light was absorbed by the $KMnO_4$ solution, another small portion was reflected and refracted by the glass tube wall and the rest was transmitted to a condensing lens which focused the outcoming beam on the surface of the photomultiplier tube. A green glass filter was found to be inadequate in its filtering selectivity and was replaced by a Bausch and Lomb interference filter of a 527 mμ maximum spectrum line and 12 mμ half band width. Its range at 50 per cent of peak transmission was 521-533 mμ, and its transmission factor was 48 per cent. The idea here is to get maximum detection sensitivity by filtering out all wavelengths except for a narrow band corresponding to the maximum absorption range of potassium permang-

anate solution. Sizeable and measurable changes in transmittance could then be obtained from slight changes in tracer concentration. Dilute $KMnO_4$ solution has a maximum absorption at a wavelength of 525 mμ which is close to the 527 mμ maximum transmission line of the filter. Also, the width of the band transmitted by the interference filter is very narrow so that it approximates monochromatic light and, therefore, permits applying Beer's law.

The circuit diagram is given in Figure 33. The photomultiplier tube was a DuMont 6291 of S-11 response and 90 per cent relative sensitivity in the range 430 ± 50 mμ. It had a sensitivity of about 60 amperes per lumen and a current amplification of up to one million depending on the total voltage applied. Five dry batteries were used for a power source; any number of batteries could be connected in the circuit providing a maximum voltage of 1590 volts. The actual voltages of the different batteries were checked before the run and are indicated in Figure 33. The output signal was taken across a 5100Ω resistor and fed to a Sanborn recorder. A small capacitor was connected between the recorder's leads in order to eliminate a.c. background noise. The signal was recorded instantly by the recorder which had a full scale rise-time of 13 milliseconds and attained 80 per cent of the final full deflection in 10 milliseconds.

According to Beer's law which holds rigorously

in case of monochromatic light transmitting through dilute nonionizable solutions, the logarithm of the transmittance is directly proportional to the concentration of the solution and its thickness or depth. That is at a constant tube traverse dimension,

$$\ln\left(\frac{I}{I_i}\right) = - \text{(Constant)}\ C_m \qquad \text{(B-1)}$$

where

I_i = intensity of incident beam

I = intensity of emergent beam

$\frac{I}{I_i}$ = transmittance

C_m = average tracer concentration across the cross section

Since I_i is constant, the logarithm of the intensity, I, or the recorded voltage should be linearly related to the concentration provided that Beer's law applies and that the applied voltage remains constant. The calibration curves of Figure 34 show satisfactory agreement with Beer's law for dilute solutions of concentrations less than 0.1 per cent (by weight). They were determined using standard solutions in the tube with three, four, or five batteries in circuit. This was done immediately before recording the pulse response to avoid errors caused by battery decay. A very sensitive electrometer was used for checking the recorded voltage output; the maximum deviation between the readings of the two instruments was less than 4 per cent.

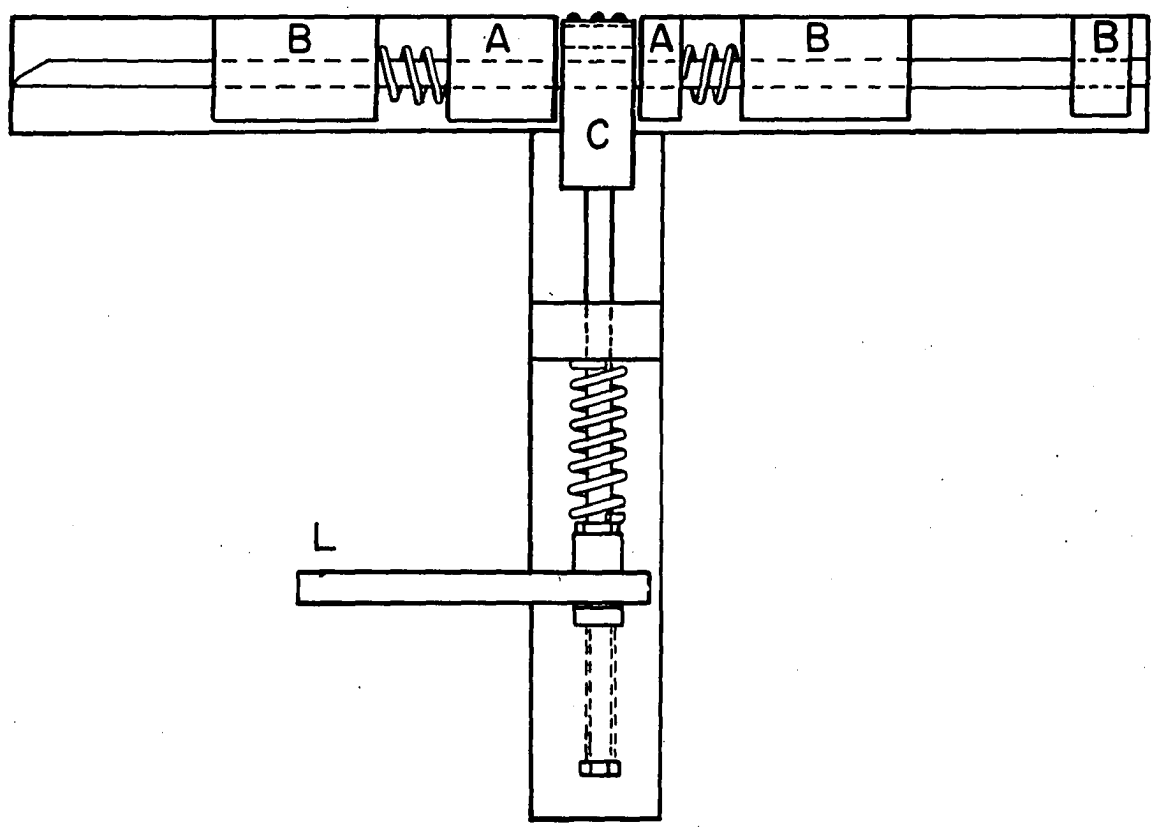


Fig. 31 IMPROVED PULSE INJECTION DEVICE

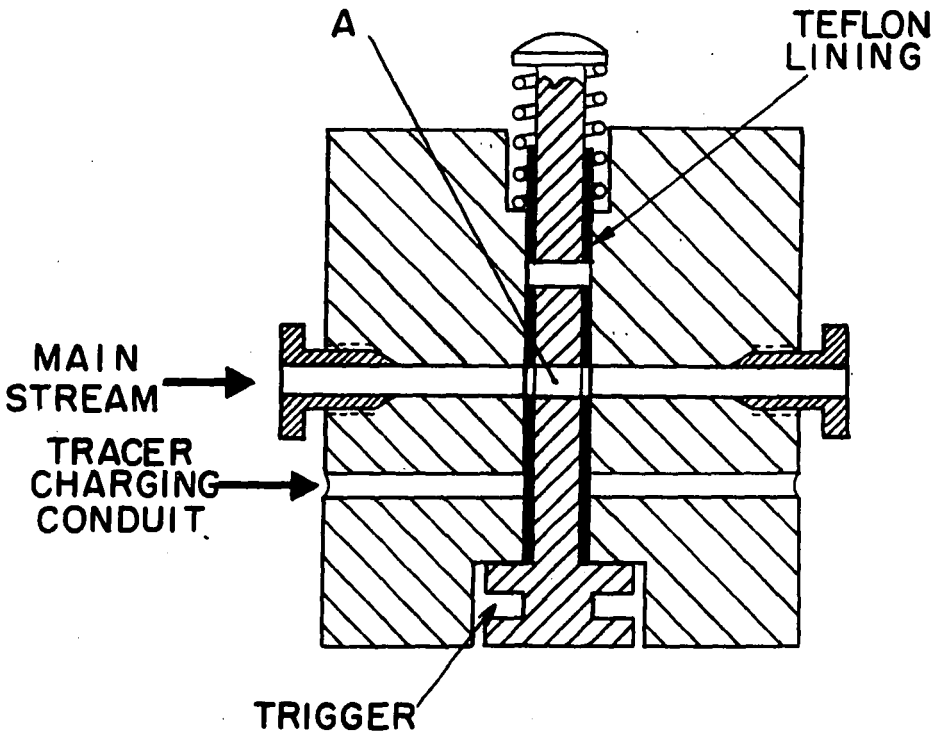


Fig. 32 PISTON-TYPE PULSE INJECTOR

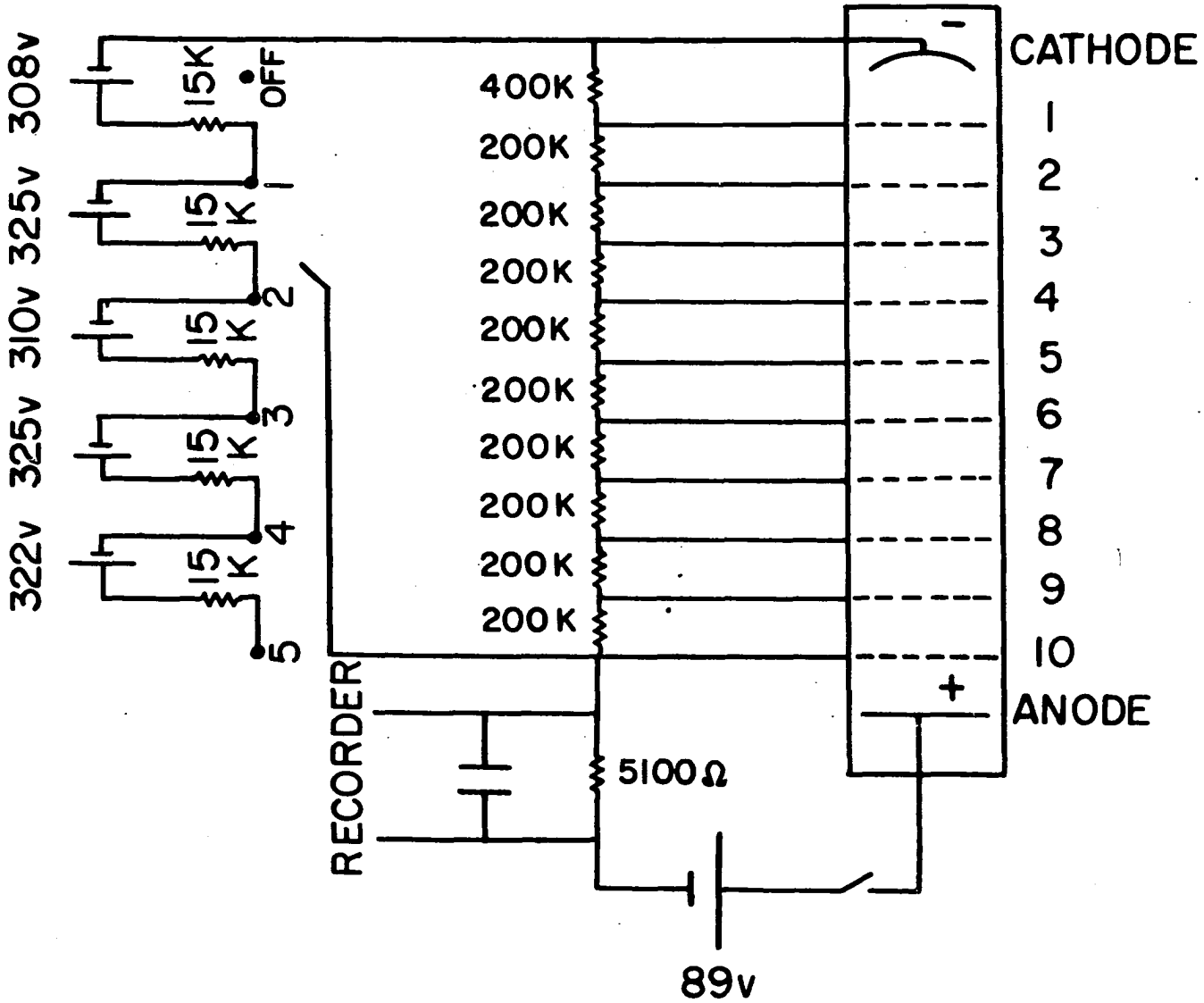


Figure 33: PHOTOMULTIPLIER CIRCUIT

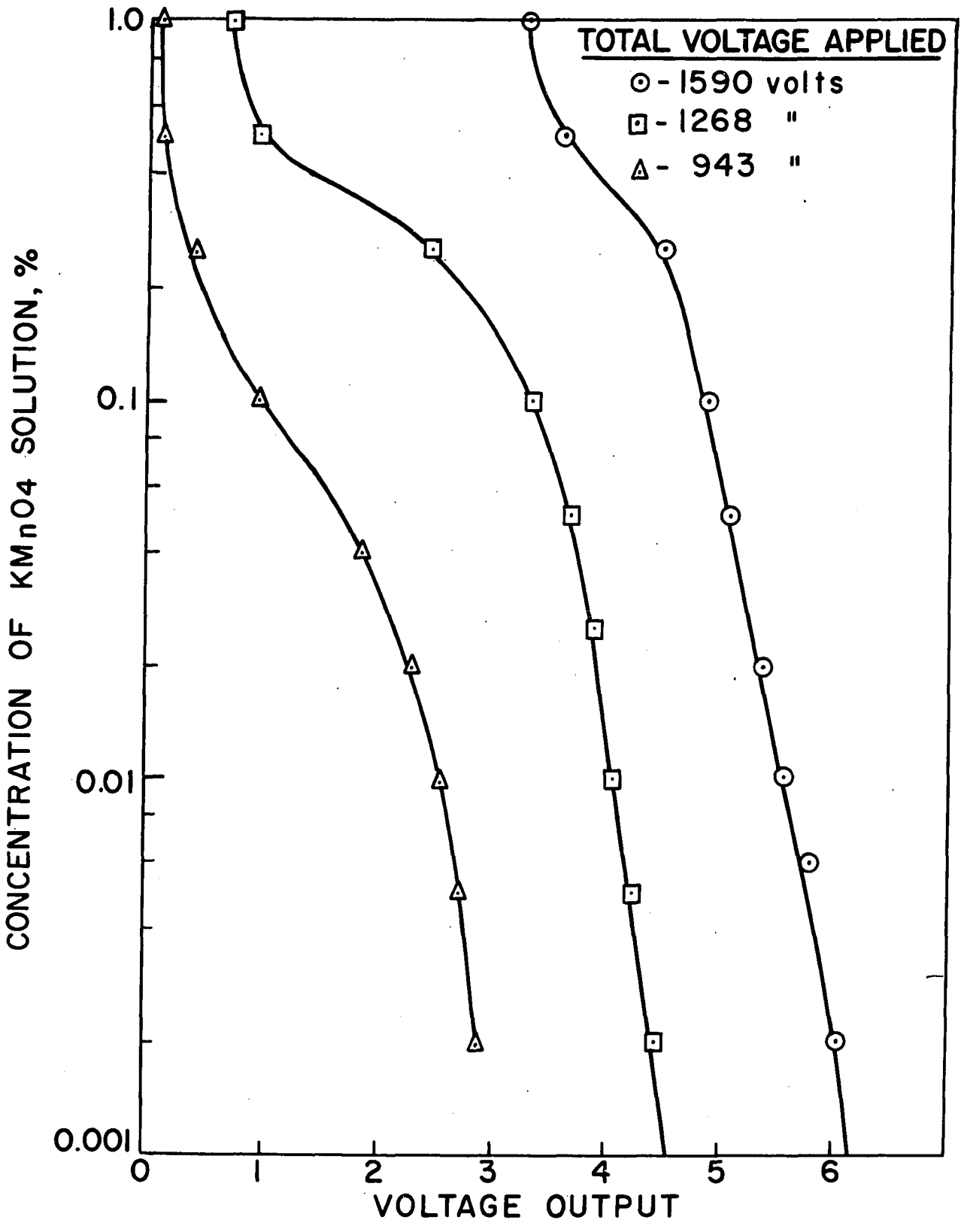


Fig. 34 PHOTOMETER CALIBRATION CURVES

Water flow rate was determined by collecting the water in a graduated vessel over a certain period of time. Sufficient time was allowed to develop a steady flow that is free of air. After charging the pulse injector with a slug of 2 per cent $KMnO_4$ solution, the lever, L, was pulled and a recording of the pulse was immediately obtained.

Results

The experimental pulse response curve (Figure 35) was obtained from the voltage pulse output tracing for Re = 3770, and the calibration curves of Figure 34. The peak relative concentration, $(C_m/C_o)_{max}$, of Table XIV was read off Figure 35.

Since it is difficult to determine accurately (to a fraction of a second) the time elapsed, t_o, between the introduction of a pulse and the first appearance of its response on the recorder's chart, C_m/C_o data are reported in Table XV as a function of $t-t_o$ rather than t, where $t-t_o$ is the time elapsed from the first appearance of a response signal.

It should be more accurate to calculate t_o by determining the mean axial velocity U_o:

$$t_o = \frac{L}{U_o} \qquad \text{(B-2)}$$

Experimental data on the ratio $\frac{V}{U_o}$ for transition flow were reported by Senecal (77) (Figure 16). One can also

compute U_o from Nunner's power law, Equation (4-7), or by the analytical integration of Von Karman logarithmic velocity distribution Equations (4-3) and (4-4) for the boundary layer section and Nunner's equation over the turbulent core. Different U_o values obtained by these different methods are compared below:

	U_o fps.
From Senecal's data	2.416
Based on Von Karman logarithmic distribution law for the boundary layer and Nunner equation for the turbulent region	2.355
Based on Nunner equation for the entire cross section	2.342

Using Senecal's actual data, t_o was calculated as 1.207 seconds which is the value used for determining the time coordinate in Figure 35.

Treatment and Discussion of Experimental Mixing Results

The axial mixing coefficient, E, can be calculated from the pulse response data given in Figure 35. A Fick's type equation is used for defining E:

$$\frac{\partial C_m}{\partial t} = E \frac{\partial^2 C_m}{\partial x^2} \qquad \text{(B-3)}$$

The solution of this equation is well known. Levenspiel and Smith (50) showed that it can be readily deduced from the solution that at $\frac{Vt}{L} = 1.0$,

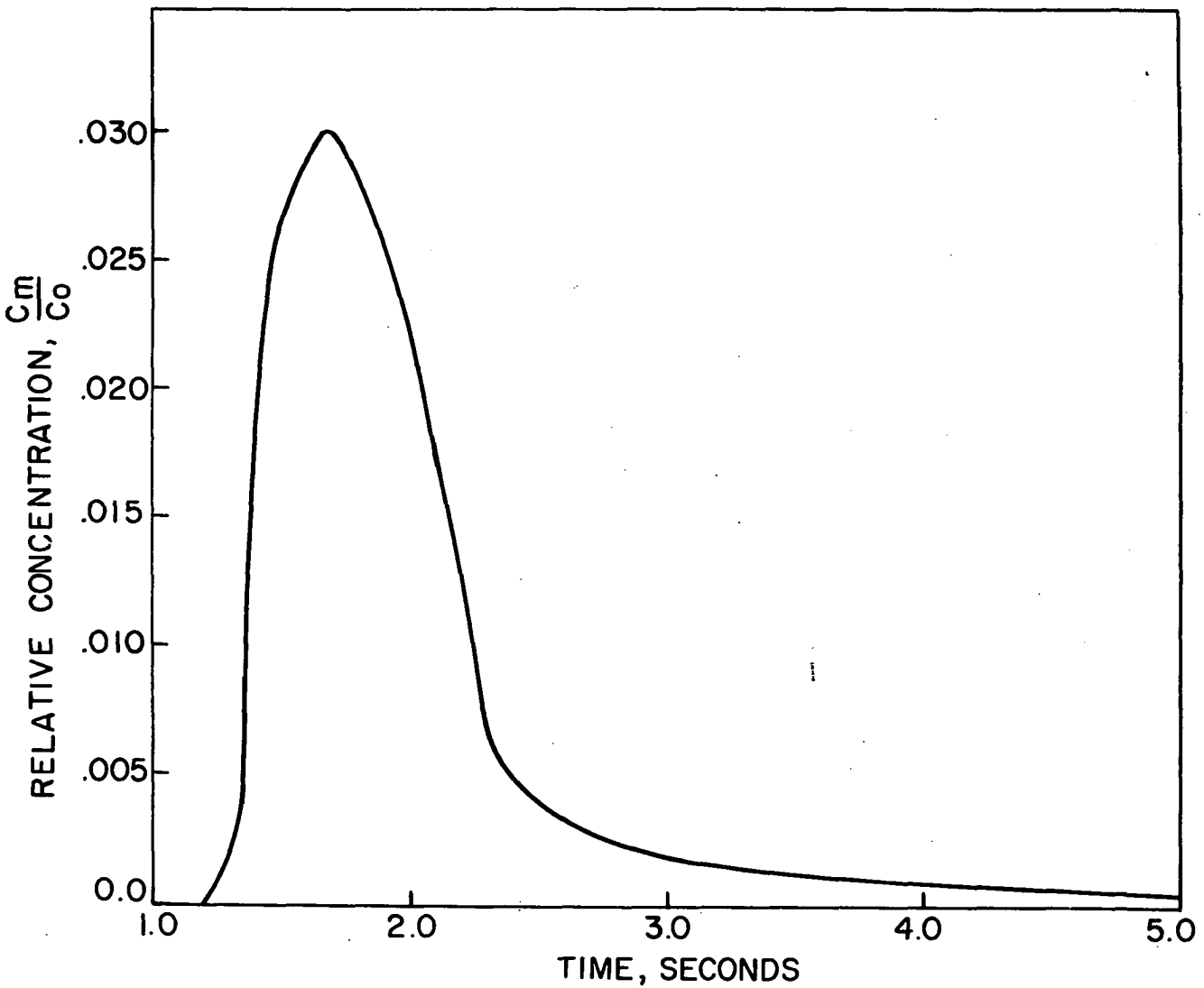


Fig. 35 PULSE RESPONSE DATA

TABLE XIV

SUMMARY OF EXPERIMENTAL CONDITIONS

Reynolds number, Re	3770	
Moody friction factor, λ	0.0402	
Bulk average velocity, V	1.773	f.p.s.
Temperature	70°F	
Inside diameter of tube, d	0.0230	ft.
Length of test section, L	2.917	ft.
L/d ratio	127	
Pulse thickness, X	0.0417	ft.
Slit thickness, δ	0.0105	ft.
Total voltage applied	1268	volts
Concentration of tracer solution, C_o	2.0	%
$(C_m/C_o)_{max}$	0.030	

TABLE XV

PULSE RESPONSE DATA

$t-t_o$ Seconds	Voltage Output	$\frac{C_m}{C_o}$
0	4.50	0
0.08	4.35	0.0015
0.12	4.20	0.0030
0.16	3.85	0.0130
0.20	3.75	0.0195
0.28	3.68	0.0260
0.48	3.60	0.0300
0.60	3.65	0.0275
0.76	3.70	0.0230
1.00	3.88	0.0115
1.08	4.00	0.0070
1.24	4.10	0.0045
1.56	4.25	0.0025
2.00	4.35	0.0016
2.60	4.40	0.0013
3.20	4.45	0.0010
4.00	4.46	0.0005

$$\left[\left(\frac{C_m}{C_o}\right)\left(\frac{L}{X}\right)\right]_{\frac{Vt}{L}=1} = \frac{1}{2\sqrt{\pi}}\left(\frac{E}{VL}\right)^{-\frac{1}{2}} \qquad \text{(B-4)}$$

where C_m = average concentration of tracer across the cross section

C_o = initial tracer concentration in the slug

X = pulse thickness

V = bulk average velocity

L = length of test section

t = elapsed time measured from time of tracer injection into the main stream

From the results given in Figure 35 one may calculate E using Equation (B-4),

at $\frac{Vt}{L} = 1$, t = 1.645 seconds

$$\frac{C_m}{C_o} = 0.02975$$

Therefore $\frac{E}{VL} = 0.0184$

$E = 0.0953 \text{ ft}^2/\text{sec}$

$\frac{E}{Vd} = 2.333$

As pointed out by Levenspiel, $\frac{C_m}{C_o}$ at $\frac{Vt}{L} = 1$ is practically equal to $(C_m/C_o)_{max}$ for values of $\frac{E}{VL}$ smaller than 0.1. The axial mixing coefficient calculated from $(C_m/C_o)_{max}$ is 0.094 ft.^{2}/sec which is very close to the above value. The skewness of the C-t curve of Figure 35 is what would be expected at large values of $\frac{E}{VL}$.

Axial mixing data for liquid flow in straight smooth pipes are plotted against the friction factor, λ, in Figure 36. It is evident that the present result agrees very well with earlier data due to Fowler and Brown (26). Tichacek, Baron and Barkelew (91) computed $\frac{E}{Vd}$ from known velocity profile and eddy viscosity data; their results for the turbulent flow of liquids of Schmidt numbers larger than 100 are also plotted in Figure 36.

The effect of injection disturbances was more dramatic when the author attempted to use the pulse response technique in laminar flor. The response curve was very irregular and wavy. Taylor's capillary flow method (87) is evidently more suitable for laminar flow studies.

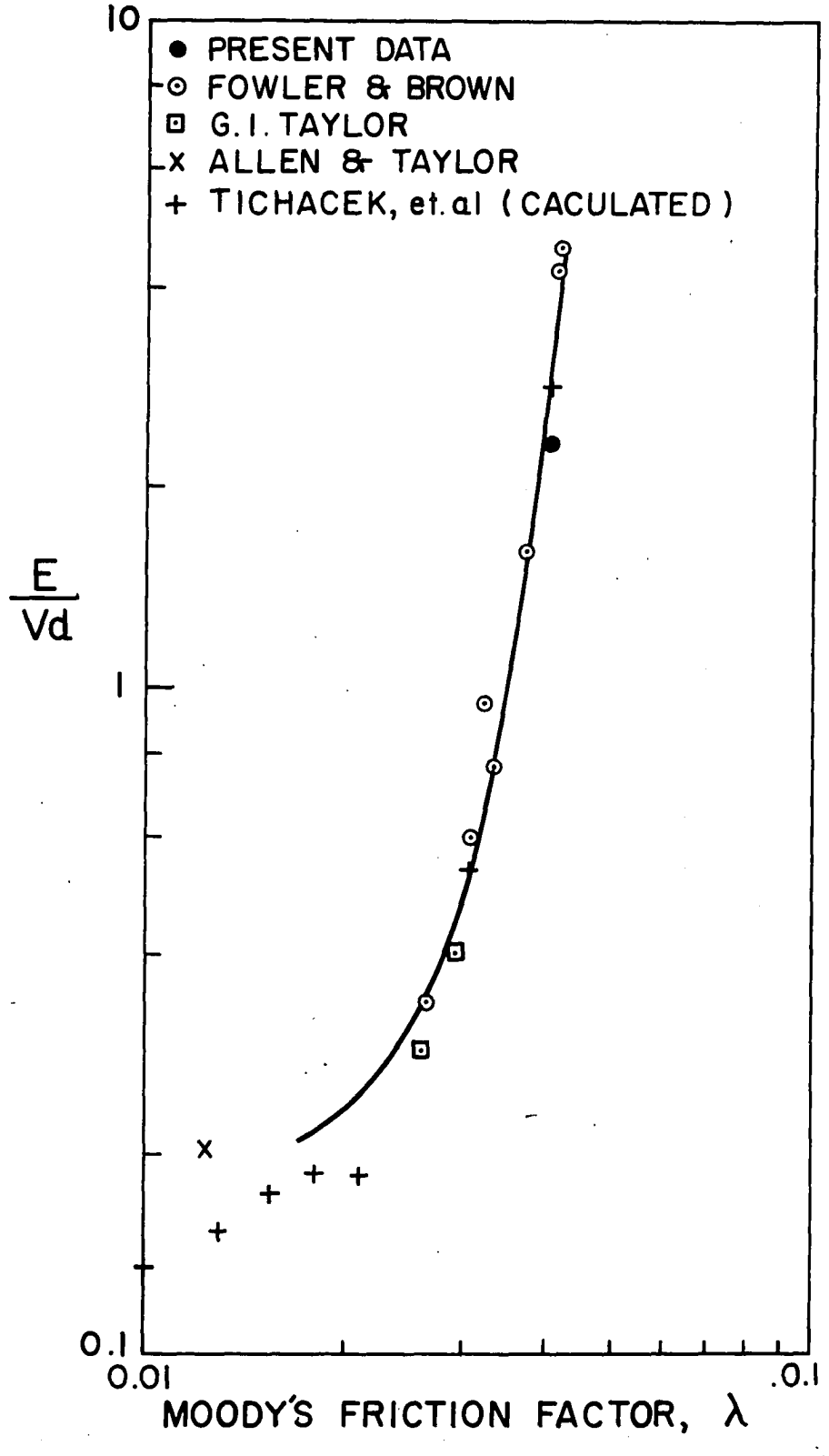


Fig.36 AXIAL MIXING DATA FOR LIQUID FLOW IN STRAIGHT SMOOTH PIPES

APPENDIX C

EFFECTS OF PULSE THICKNESS AND SLIT THICKNESS ON PULSE RESPONSE IN LAMINAR FLOW

Review and Statement of Problem

The main objective of this appendix is to determine the dependence of the pulse response curve on pulse and slit thicknesses in case of laminar flow. The effects of Reynolds number, length-diameter ratio, and Schmidt numbers are also investigated.

Tube length and diffusion time are assumed short enough that molecular diffusion may be considered to have a negligible effect on the response curve. In other words, convective effects only are considered here.

Taylor (87) suggested that molecular diffusion effect should not be neglected if $\frac{L}{U_o}$ is larger than the time necessary for radial concentration variations to die down to 1/e of their initial value. This condition is:

$$\frac{L}{V} \gg \frac{d^2}{28.8 D_m} \qquad \text{(C-1)}$$

L = Tube length,

D_m = Molecular diffusivity of tracer material in the main stream

V = Average bulk velocity

d = Pipe diameter

He also proposed that for extremely long dispersion times satisfying Equation C-1, the overall axial mixing coefficient for laminar flow is:

$$E = \frac{a^2 V^2}{48 D_m} \qquad (C\text{-}2)$$

In a later paper (89), Taylor pointed out that longitudinal molecular diffusion may be negligible compared to E, if

$$\frac{aV}{D_m} >> 6.9 \qquad (C\text{-}3)$$

Farrel and Leonard (24) showed that the axial molecular diffusion effect could be considered negligible when Schmidt number is greater than 0.434. This condition is satisfied in most liquids and gases.

Fowler and Brown (26) studied contamination by successive flow in laminar pipe flow. They derived the following expression for the contaminated portion as a fraction of pipe volume <u>assuming negligible molecular diffusion effect</u>:

$$= \frac{1}{2}\left[\frac{1}{\sqrt{(C_m)_2}} - \frac{1}{\sqrt{(C_m)_1}}\right] \qquad (C\text{-}4)$$

where $(C_m)_2$ and $(C_m)_1$ are the mean concentrations at the boundaries of this contaminated length. This was a step function study that did not deal with slit or pulse thick-

ness. McMaster (57) studied the effect of pulse shape on the response curve assuming negligible diffusion effect. He dealt with disc, bullet (paraboloid) and pencil shaped imputs. Slit and pulse thicknesses were assumed the same in case of the disc or square pulse imput. One of McMaster's findings was that none of the imputs gave a response that agrees with Bosworth's analytical result for residence time distribution in laminar flow of negligible molecular diffusion effect (9).

Developments and Computations

Derivations

A uniform slug of tracer of thickness X is introduced in laminar flow of maximum axial velocity U_o and average bulk velocity V. Tracer concentration is measured through a slit hole of thickness δ. This may be accomplished by means of a photometric or radioactive detecting device that determines continuously the average tracer concentration in the slit section of the tube.

In absence of molecular diffusion, the tracer slug should spread itself in the form of a paraboloid shaped envelope. The first detection of any tracer in the slit is when the apex of the outer paraboloid reaches the slit. This is followed by other stages as the tracer slug progresses through the tube as illustrated in Figure 37.

One may express the pulse thickness, X, and slit

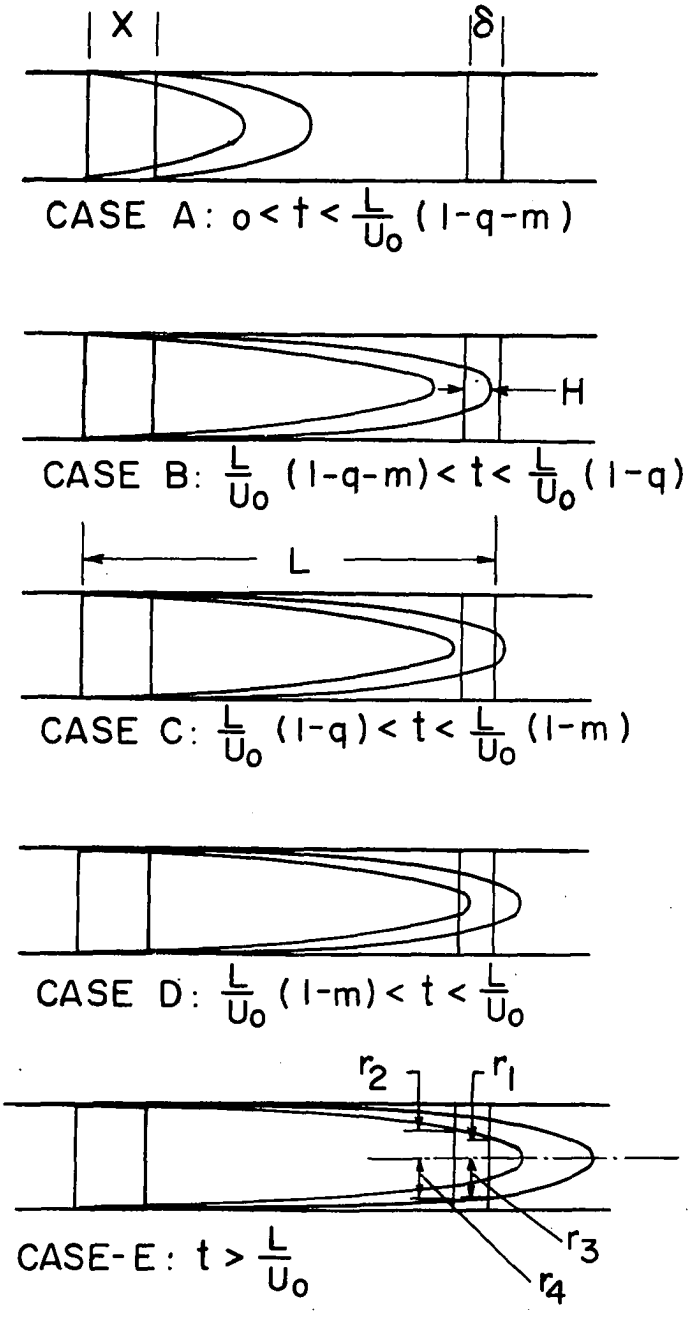


Fig. 37 ILLUSTRATION OF SLUG PASSAGE THROUGH THE SLIT AT DIFFERENT STAGES

thickness, δ, in dimensionless form:

$$q = \frac{X}{L} \tag{C-5}$$

$$m = \frac{\delta}{L} \tag{C-6}$$

It can be readily seen that the time boundaries of the different cases illustrated in Figure 37 are

$$\text{CASE A:} \quad 0 < t < \frac{L}{U_o}(1-q-m) \tag{C-7}$$

$$\text{CASE B:} \quad \frac{L}{U_o}(1-q-m) < t < \frac{L}{U_o}(1-q) \tag{C-8}$$

$$\text{CASE C:} \quad \frac{L}{U_o}(1-q) < t < \frac{L}{U_o}(1-m) \tag{C-9}$$

$$\text{CASE D:} \quad \frac{L}{U_o}(1-m) < t < \frac{L}{U_o} \tag{C-10}$$

$$\text{CASE E:} \quad t > \frac{L}{U_o} \tag{C-11}$$

The assumptions made here are:

(a) The effect of molecular diffusivity, D_m, on the C-t diagram is negligible.

(b) $X \geq \delta$, $L >> X$

One may proceed now to determine the volume and concentration of tracer in the slit at any time by expressing the paraboloid's volume in terms of fluid velocity and elapsed time.

CASE A:

$$t < \frac{L}{U_o}(1-q-m) \qquad \text{(C-7)}$$

$$\frac{C_m}{C_o} = 0 \tag{C-12}$$

where C_m is the average concentration of tracer in the slit section, C_o is the initial tracer concentration in the slug.

CASE B:

For laminar flow,

$$x = Ut = U_o t \left(1 - \frac{r^2}{a^2}\right) \qquad \text{(C-13)}$$

$$x = L - \delta - X \qquad \text{(C-14)}$$

$$r^2 = a^2 \left[1 - \frac{(L- -X)}{U_o t}\right] \qquad \text{(C-15)}$$

where r is the radius of intersection of the inner slit plane with the solid paraboloid surface and a is the radius of the tube.

The volume of the tracer paraboloid contained within the slit is $\frac{1}{2}\pi r^2 H$ where H is the height of the paraboloid.

$$H = U_o t - L + X + \delta \qquad \text{(C-16)}$$

The average concentration of tracer within the slit can then be expressed as follows

$$C_m = \frac{\pi a^2}{2\pi a^2 \delta}\left[1 - \frac{L-\delta-X}{U_o t}\right]\left[U_o t - L + X + \delta\right] C_o \qquad \text{(C-17)}$$

and considering that $q = \frac{X}{L}$ and $m = \frac{\delta}{L}$, then,

$$\frac{C_m}{C_o} = \frac{1}{2m}\left[\frac{U_o t}{L} + q + m - 1\right]\left[1 - \frac{L}{U_o t}(1-m-q)\right] \qquad \text{(C-18)}$$

for

$$\frac{L}{U_o}(1-q-m) < t < \frac{L}{U_o}(1-q) \qquad (C-8)$$

CASE C:

The tracer volume in this case is a truncated paraboloid whose volume is $\frac{1}{2}\pi\delta(r_1^2 + r_2^2)$ where r_1 and r_2 are the radii of intersection with the inside and outside planes of the slit section respectively.

$$r_1^2 = a^2\left[1 - \frac{(L-\delta-X)}{U_o t}\right] \qquad (C-19)$$

$$r_2^2 = a^2\left[1 - \left(\frac{L-X}{U_o t}\right)\right] \qquad (C-20)$$

$$C_m = \frac{1}{2U_o t}(2U_o t - 2L + 2X + \delta)\, C_o \qquad (C-21)$$

$$\frac{C_m}{C_o} = \frac{L}{2U_o t}\left(\frac{2U_o t}{L} + 2q + m - 2\right) \qquad (C-22)$$

for the period

$$\frac{L}{U_o}(1-q) < t < \frac{L}{U_o}(1-m) \qquad (C-9)$$

CASE D:

The volume of tracer contained within the slit compartment is the difference between a paraboloid segment and a smaller paraboloid. A dimensionless concentration C_m/C_o can be derived following a procedure similar to that described above

$$\frac{C_m}{C_o} = \frac{1}{2U_o t}\left[2\,U_o t - 2L + 2X + \delta\right] - \frac{1}{2\delta}\left[1 - \frac{(L-\delta)}{U_o t}\right]\left[U_o t - L + \delta\right] \qquad \text{(C-23)}$$

$$\frac{C_m}{C_o} = \frac{L}{2U_o t}\left[\frac{2U_o t}{L} + 2q + m - 2\right] - \frac{1}{2m}\left[\frac{U_o t}{L} + m - 1\right]\left[1 - \frac{L(1-m)}{U_o t}\right] \qquad \text{(C-24)}$$

where

$$\frac{L}{U_o}(1-m) < t < \frac{L}{U_o} \qquad \text{(C-10)}$$

CASE E:

In this case the tracer volume within the slit is the difference between two paraboloid segments which equals

$$\frac{1}{2}\pi\delta\left[(r_3^2 + r_4^2) - (r_1^2 + r_2^2)\right] \qquad \text{(C-25)}$$

r_1, r_2, r_3 and r_4 can be expressed as follows

$$L = U_o t\left(1 - \frac{r_1^2}{a^2}\right) \qquad \text{(C-26)}$$

$$L - \delta = U_o t\left(1 - \frac{r_2^2}{a^2}\right) \qquad \text{(C-27)}$$

$$L - X = U_o t\left(1 - \frac{r_3^2}{a^2}\right) \qquad \text{(C-28)}$$

$$L - X - \delta = U_o t\left(1 - \frac{r_4^2}{a^2}\right) \qquad \text{(C-29)}$$

It follows that

$$\frac{C_m}{C_o} = \frac{1}{2}\left[1 - \frac{L(1-q)}{U_o t} + 1 - \frac{L(1-q-m)}{U_o t}\right] - \left[1 - \frac{L}{U_o t} + 1 - \frac{L(1-m)}{U_o t}\right] \qquad \text{(C-30)}$$

which reduces to

$$\frac{C_m}{C_o} = \frac{Lq}{U_o t} \qquad \text{(C-31)}$$

where

$$t > \frac{L}{U_o} \qquad \text{(C-11)}$$

Since the actual amount of injected tracer increases as X increases, C_m/C_o should be corrected for such variations in the total amount of tracer injected, γ. A preferred dimensionless concentration is $\frac{C_m \forall}{\gamma}$.

where

C_m = the average concentration of tracer in the slit

$\gamma = C_o XA$ = total amount of trace introduced regardless of the magnitude of X.

A = area of the tube cross section

$\forall = LA$ = volume of tube test section

$$\frac{C_m \forall}{\gamma} = \frac{C_m}{C_o q} \qquad \text{(C-32)}$$

Equation (C-31) for Case E can be written as follows:

$$\frac{C_m \forall}{\gamma} = \frac{C_m}{C_o q} = \frac{1}{2}\left(\frac{Vt}{L}\right)^{-1} \qquad \text{(C-33)}$$

In other words, at constant γ, the dimensionless concen-

tration $\frac{C_m}{\gamma}$ is independent of pulse or slit dimensions for all values of $t > \frac{L}{U_o}$.

Computational Results

The equations derived above for the relative concentration C_m/C_o were programmed for digital computer computation at different values of V, L, X and δ. Table XVI lists the different computational runs made. Reynolds number varied from 10 to 1000 for air and water flow. Tube diameter was held-at 2" in all runs. Run number 603 is the control run with which other runs may be compared. According to Taylor (87), axial mixing in laminar flow should not be considered purely convective if:

$$\frac{L}{V} \gg \frac{d^2}{28.8 D_m} \qquad \text{(C-1)}$$

which can be written as

$$\frac{L}{d} \gg \left(\frac{1}{28.8}\right) \text{Re Sc} \qquad \text{(C-34)}$$

A typical value of Schmidt number for liquids is 1000; for gases it can be taken roughly equal to 1. Therefore, for liquids:

$$\frac{L}{d} \gg 35 \text{ Re} \qquad \text{(C-35)}$$

and for gases

$$\frac{L}{d} \gg 0.035 \text{ Re} \qquad \text{(C-36)}$$

TABLE XVI

VALUES OF PARAMETERS USED IN DIFFERENT COMPUTATIONAL RUNS

Run Number	Fluid	Re	d in.	L ft.	V f.p.s.	X in.	$\frac{X}{L}$	δ in.	$\frac{\delta}{L}$	$\frac{L}{d}$	.035 Re Sc
601	Air	10	2	5	0.01	1	0.01667	1/4	.004167	30	0.35
602	Air	100	2	5	0.1	1	0.01667	1/4	.004167	30	3.5
603	Air	1000	2	5	1.0	1	0.01667	1/4	.004167	30	35
604	Water	10	2	5	$(6.5)(10^{-4})$	1	0.01667	1/4	.004167	30	350
605	Water	100	2	5	0.0065	1	0.01667	1/4	.004167	30	3500
606	Water	1000	2	5	0.065	1	0.01667	1/4	.004167	30	35000
701	Air	1000	2	100	1.0	1	$(8.33)(10^{-4})$	1/4	$(2.08)(10^{-4})$	600	35
702	Air	1000	2	10^4	1.0	1	$(8.33)(10^{-6})$	1/4	$(2.08)(10^{-6})$	60000	35
801	Air	1000	2	5	1.0	1	0.01667	1/32	$(5.21)(10^{-4})$	30	35
802	Air	1000	2	5	1.0	1	0.01667	1/2	$(8.33)(10^{-3})$	30	35
901	Air	1000	2	5	1.0	1/2	$(8.33)(10^{-3})$	1/4	.004167	30	35
902	Air	1000	2	5	1.0	2	$(3.333)(10^{-2})$	1/4	.004167	30	35
903	Air	1000	2	5	1.0	0.25	0.004167	1/4	.004167	30	35

As shown in Table XVI the assumption of negligible molecular diffusion effect is valid for all computational runs except runs number 601, 602, 701 and 702.

The computed response data are presented in Figures 38, 39, and 40. The results are plotted as $\left(\frac{C_m}{C_o}\right)_{equiv.}$ versus $\frac{Vt}{L}$; where

$$\left(\frac{C_m}{C_o}\right)_{equiv.} = \left(\frac{C_m}{C_o}\right)\left(\frac{X_{603}}{X}\right) \qquad (C\text{-}37)$$

X_{603} = the pulse thickness in case of the control run (1 inch)

The purpose of plotting $\left(\frac{C_m}{C_o}\right)_{equiv.}$ rather than $\frac{C_m}{C_o}$ is to be able to compare the different runs at a fixed total amount of tracer introduced

$$\gamma = C_o \, A \, X_{603} \qquad (C\text{-}38)$$

Including the slit and pulse thicknesses as part of the test section results in a negligible time translation of the ascending portion of the response curves but has no effect on their shape.

Discussion of Results

The response curve, plotted on dimensionless coordinates, rises almost instantly to sharp peak and then declines slowly (Figure 38). The height of the peak depends on slit and pulse thicknesses which have a negli-

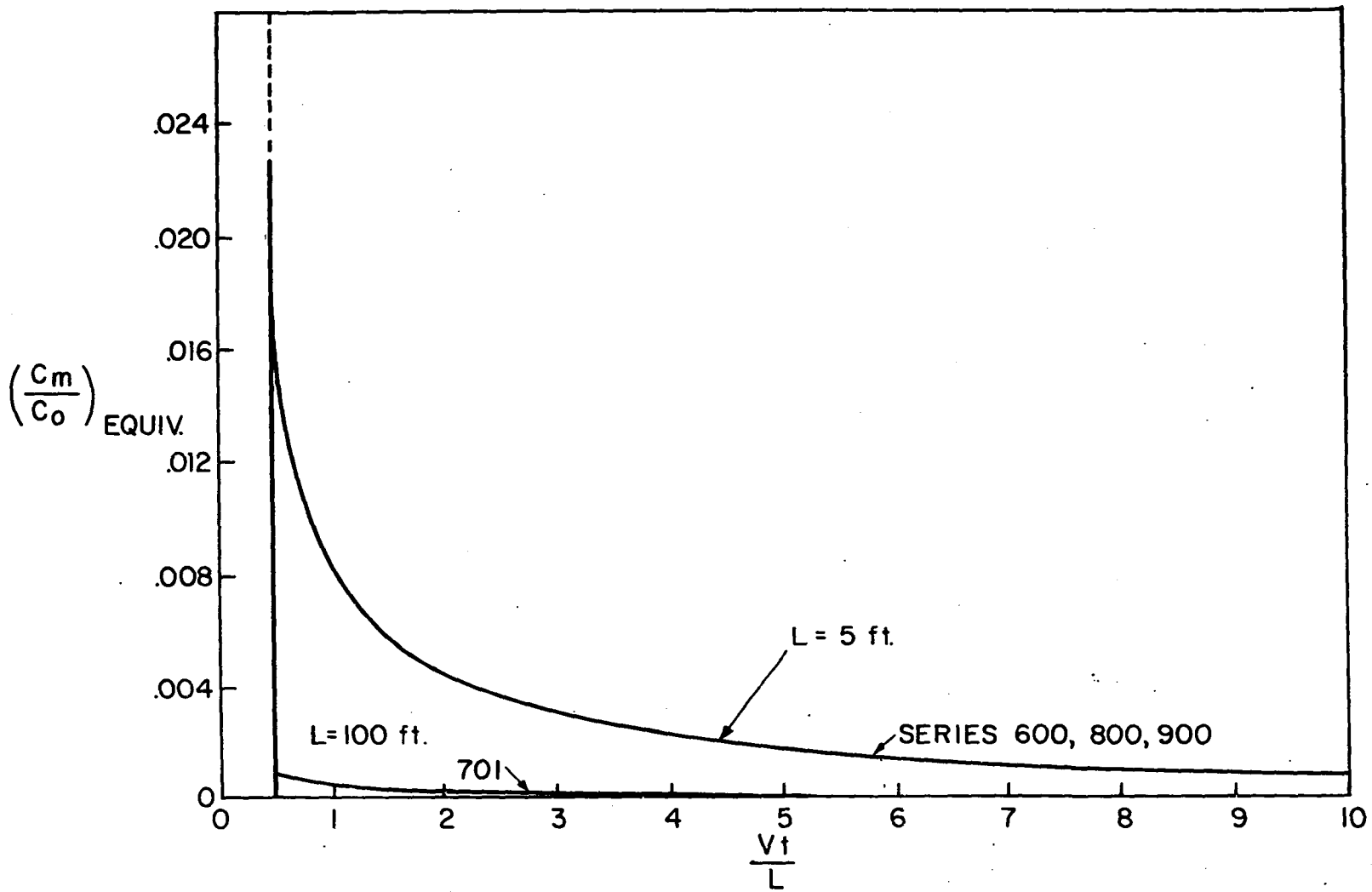


Fig.38 COMPUTED PULSE RESPONSE DIAGRAMS

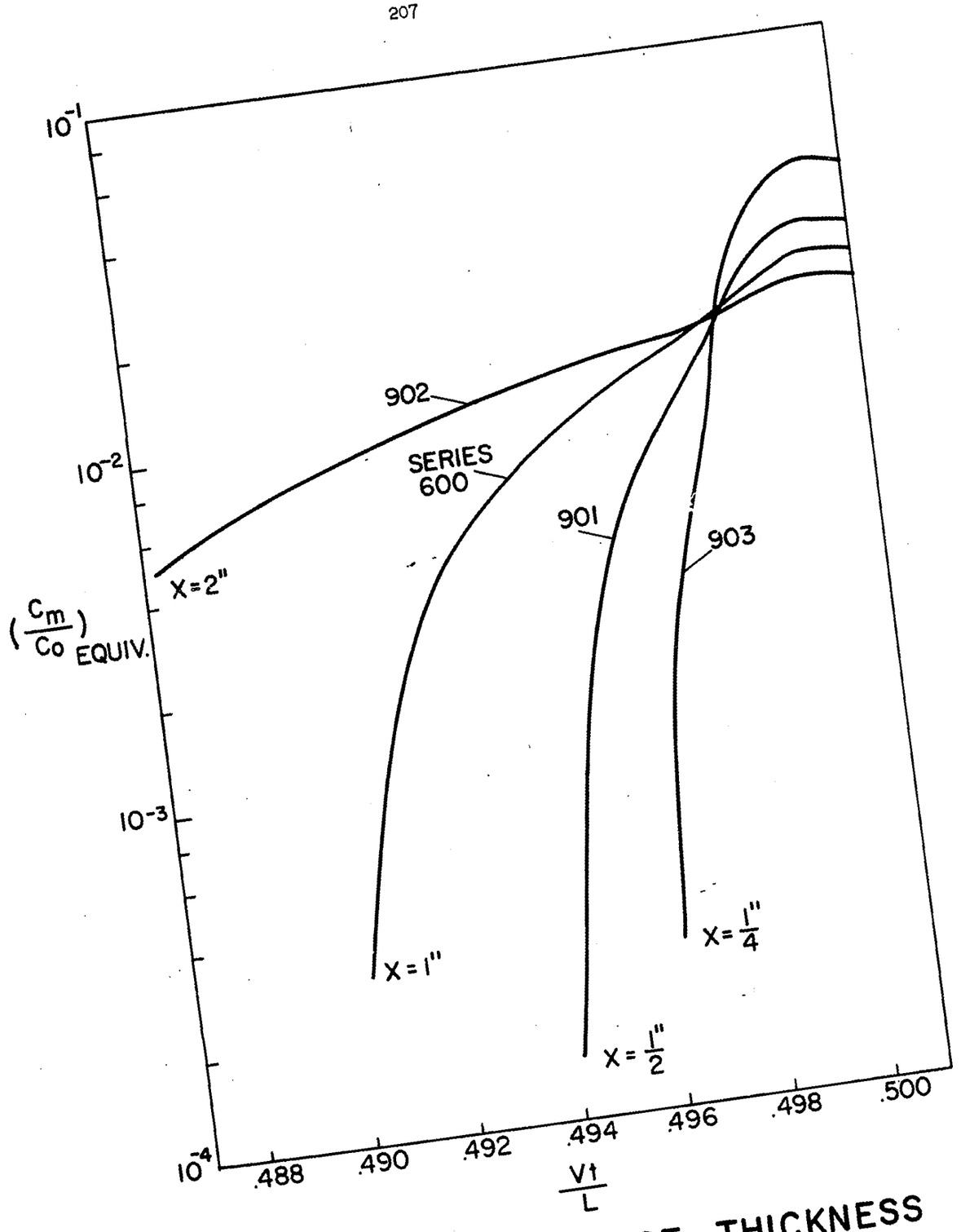


Fig. 39 EFFECT OF PULSE THICKNESS ON PULSE RESPONSE

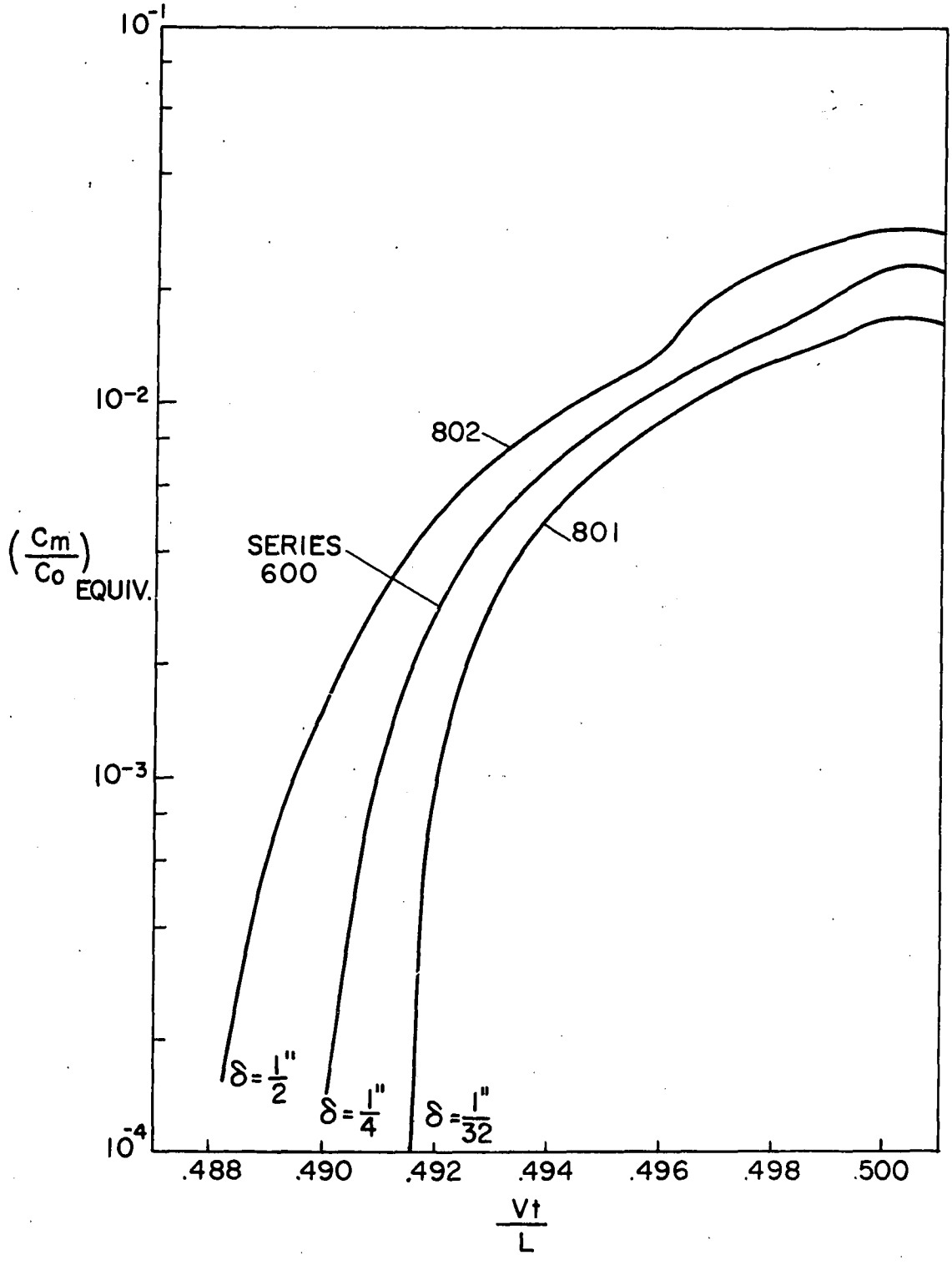


Fig. 40 EFFECT OF SLIT THICKNESS ON PULSE RESPONSE

gible effect on the rest of the curve. The declining portion is also independent of Reynolds number and type of fluid. Tube length is by far the most important variable affecting the response curve (Run # 701).

This result obtained for a parabolic velocity distribution could be expected to apply in general to turbulent flow. It may suggest that for turbulent flow in short pipes one may use the deviation or the variance rather than the peak of the concentration distribution curve to obtain axial mixing and residence time distribution data to eliminate the effects of pulse and slit thicknesses on the results.

The effects of slit and pulse thicknesses on the rising portion of the response curve are shown in Figures 39 and 40 which are semilogarithmic plots of expanded time scale. For the same amount of injected tracer, a decrease in pulse thickness results into a higher peak concentration. Increasing the slit thickness has the same effect.

One should bear in mind that the C-t response curve obtained from an injected slug is not the same as the residence time distribution, for the latter could be only obtained in the hypothetical case of fluid particles turning into tracer over an infinitesimal time at the reactor inlet. Another way of saying this is that a plane of tracer appears instantly at the reactor inlet; each

radial element of this plane travels with the local mean velocity. In turbulent flow, the usual pulse response seems to approximate the residence time distribution because of the effects of turbulent randomness and eddy diffusion.

Another important point here is that it is not permissible to apply a Fickian diffusion-type model to axial mixing in short pipes of negligible molecular diffusion effect because the concentration distribution with respect to x is neither Gaussian nor symmetrical. Therefore, one could no longer use the overall axial mixing coefficient. Axial mixing should be expressed by a contaminated length as proposed by Fowler and Brown (26). The results reported here (Figure 38) are still a true representation of axial mixing due to the convective effect. They show that the degree of mixing in laminar flow is independent of Reynolds number and proportional to pipe length; both results were arrived at by Fowler and Brown.

Since the diffusion-type model does not apply here, one should obtain an invalid result by attempting to obtain an axial mixing coefficient using an expression due to Levenspiel and Smith (50):

$$\left(\frac{C_m}{\gamma}\right)_{\frac{Vt}{L}=1} = \frac{1}{2\sqrt{\pi}}\left(\frac{E}{VL}\right)^{\frac{1}{2}} \qquad \text{(C-39)}$$

and from Equation (C-33), for negligible diffusion effect,

$$\frac{1}{2} = \frac{1}{2\sqrt{\pi}}\left(\frac{E}{VL}\right)^{-\frac{1}{2}} \qquad \text{(C-40)}$$

or:

$$\frac{E}{VL} = \frac{1}{\pi} \qquad \text{(C-41)}$$

$$\frac{E}{Vd} = \frac{1}{\pi}\frac{L}{d} \qquad \text{(C-42)}$$

Equation (C-42) shows the longitudinal dispersion number independent of all flow variables and solely a function of the length-diameter ratio

$$E = \frac{VL}{\pi} \qquad \text{(C-43)}$$

As expected, applying the Fickian model to compute an axial mixing coefficient gives exceedingly large and unreal values.

APPENDIX D

TEST OF DEPENDENCE OF TURBULENT DIFFUSIVITY ON MOLECULAR DIFFUSIVITY

In Chapter II the dependence of turbulent diffusivity on molecular diffusivity was tested by showing that $\frac{\alpha_c}{\nu}$ correlates well with Reynolds number for all the systems examined despite a variation in D_m by a factor of 10^5. It was also shown that the introduction of the molecular diffusivity as a variable produces no correlation.

The test is based on the following analysis. Equation (D-1) is a general equation for the case when α_c and D_m are correlated:

$$\overline{Y^2} = \overline{Y_t^2} + \overline{Y_m^2} + 2\,\overline{Y_m\, Y_t} \qquad \text{(D-1)}$$

where $\overline{Y^2}$ = the total lateral dispersion or the observed variance of the concentration distribution; $2\,\overline{Y_m\, Y_t}$ is a term that accounts for possible dependence of turbulent diffusivity on molecular diffusivity.

In Chapter II, it was shown that $\overline{Y_t^2}$ as obtained from Equation (D-2) is the same at the same Re and for all the systems examined regardless of their molecular

diffusivity.

$$\overline{Y_t^2} = \overline{Y^2} - \overline{Y_m^2} \qquad \text{(D-2)}$$

The use of α_c here rather than $\overline{Y^2}$ is permissible because the turbulence is nondecaying

i.e., $$\alpha_c = \frac{U_o}{2} \frac{d\,\overline{Y^2}}{dx} \qquad \text{(3-38)}$$

Equation (3-38) applies when x is large enough that $R_L = o$.

For all systems where D_m was less than 3 per cent of α_c, $\overline{Y^2}$ and $\overline{Y_t^2}$ were assumed equal since the data are normally in error by more than 3 per cent. A correction for $\overline{Y_m^2}$ was made for all systems of higher molecular diffusivities. The result supports Equation (D-2); that is, no interaction between turbulent and molecular diffusivities over D_{12}^m ranging from 4.6×10^{-9} to 9.6×10^{-4} ft.^{2}/sec. and Schmidt numbers ranging from 0.72 to 2341.